ABSTRACT

Using Microgravity and Passive Seismic Methods Jointly to Explore the Brazos River Alluvium Aquifer

Wynne M. Casteel III, M.S.

Mentor: Joe C. Yelderman Jr., Ph.D.

This study used a combined passive seismic (HVSR) and microgravity method to estimate depth to bedrock, alluvial composition, and saturated thickness throughout the Northern Segment of the Brazos River Alluvium Aquifer. Previous borings and confirmation borings drilled in this study suggest this method was able to estimate depth to bedrock with an average error of 21% throughout the study area and was able to indicate trends in changing alluvial composition along each transect. Surveys were completed over eight transects at five sites within the Brazos River Alluvium aquifer in McLennan and Falls County, TX. In all, 202 passive seismic and 342 microgravity measurements were obtained. The combined passive seismic (HVSR) and microgravity method can be used to estimate depth to bedrock and alluvial composition with medium resolution (several meters) over transects of medium spatial extent (hundreds of meters to several kilometers).

Using Microgravity and Passive Seismic Methods Jointly to Explore the Brazos River Alluvium Aquifer

by

Wynne M. Casteel III, B.S., B.B.A.

A Thesis

Approved by the Department of Geosciences

_____

Steven G. Driese, Ph.D., Chairperson

Submitted to the Graduate Faculty of
Baylor University in Partial Fulfillment of the
Requirements for the Degree
of

Master of Science

Approved by the Thesis Committee

_____

Joe C. Yelderman Jr., Ph.D., Chairperson

_____

Peter B. James, Ph.D.

_____

Ron Morgan, Ph.D.

Accepted by the Graduate School

August 2020

_____

J. Larry Lyon, Ph.D., Dean

Page bearing signatures is kept on file in the Graduate School.

TABLE OF CONTENTS

LIST OF FIGURES

LIST OF TABLES

ACKNOWLEDGMENTS

Many individuals and organizations helped make this thesis possible. First, I would like to thank Dr. Joe Yelderman for the initial inspiration, constant guidance, and unfailing support in completing this project. I would also like to thank Dr. Peter James for assistance acquiring, modeling, and interpreting gravity data. Another thanks goes to Wayne Hamilton for your support and for introducing me to passive seismic, HVSR methodology. Furthermore, thank you to Scooter Radcliffe at Southern Trinity GCD for all of the wisdom you imparted to me during my tenure at the district.

I would also like to thank landowners Lewis Hirsch, MCC Highlander Ranch, and Arcosa, Inc for permission to do research on your property. To Wayne Hamilton, Will Brewer, Christopher Mitchell, and Mason Frucci, thank you tremendously for assisting with fieldwork during this project. And to Dr. Scott James and Stephanie Wong, thank you for your help interpreting and displaying results. Additionally, I'd like to thank Scott Langerman for providing access to helpful data used in this study and Dennis Mills from Exploration Instruments, LLC for helping with my use of the Tromino Zero seismograph.

Finally, I would like to thank my sponsors for financial assistance completing this project: Southern Trinity GCD, the Elan Allen Memorial Foundation, the National Ground Water Foundation, and the Graduate School at Baylor University.

CHAPTER ONE

Introduction

Background

The Brazos River Alluvium Aquifer (BRAA) is a 90,000 acre-foot capacity rechargeable resource in the Waco, Texas vicinity that may play an important water supply role in the coming decades. McLennan County water supply is sourced primarily from Lake Waco, a 189,773 acre-foot capacity reservoir (Solis and others, 2012), and secondarily from the productive Trinity Aquifer, a confined, slowly recharging aquifer underlying the entire county. High pumping volumes exceeding the Trinity Aquifer's effective recharge has caused hundreds of feet of historic drawdowns versus pre-1900 levels (Cronin and Wilson, 1967). Currently, the Trinity is experiencing yearly water level declines of approximately 3 m (10 ft)/year in much of McLennan County, making Trinity water more expensive to produce (STGCD, 2015). Because of these drawdowns, at some future date the aquifer may be a less preferable water resource or even incapable of meeting water supply needs. Alternative water resources, such as the Brazos River Alluvium Aquifer (BRAA) are being investigated today along with conjunctive use plans for maximizing surface water resources from Lake Waco and Lake Belton. While the BRAA will never overtake Lake Waco as the area's primary water source, it could be a valuable asset as an emergency water supply—especially during droughts, when reservoirs are most stressed.

According to the Texas Water Development Board (TWDB) water availability model of the Brazos River Alluvium Aquifer, McLennan county has 15,023 acre-feet of managed available groundwater (MAG) per year (modeled to ensure 82% conservation after 50 years), and an estimated average of 14,448 acre-feet of recharge per year (Bradley, 2008). The estimated total recoverable storage for the BRAA by county is displayed in Table 1.1 showing 90,000 acre-feet for McLennan County(Shi and others, 2014). While these amounts of water seem vast, all of the recoverable BRAA water in McLennan County could only fill Lake Waco Reservoir about half-way. Furthermore, every year, potentially usable volumes are reduced as the aquifer is mined for sand and gravel, polluted, or pumped (if pumping exceeds recharge). These external pressures indicate a need for more data so that the aquifer can be effectively managed to meet future water supply needs.

Table 1.1. Estimated recoverable storage in the Northern Segment of the Brazos River Alluvium Aquifer (Shi and others, 2014).

County	Total Storage (acre-feet)
Bosque	9,600
Hill	6,600
McLennan	90,000
Falls	160,000

Texas's alluvial aquifers have often been overlooked as water supply resources for two reasons: size and treatment. Alluvial aquifers in Texas (excluding the Ogallala) generally hold far less water than large surface reservoirs, deep confined aquifers, or many karst aquifers. Compounding the size problem is that near-surface groundwater needs more treatment than deeper aquifer water as shallow groundwater has more contamination risks. Despite these weaknesses, an alluvial aquifer is one of the most

efficient reservoirs of water—losing much less water to evapotranspiration than surface reservoirs and having recharge rates often many times higher than deep, confined aquifers (like the Trinity). The current explosive population growth in central Texas, an area that receives significantly less rainfall than the eastern U.S., will inevitably lead to the need for expanding the water supply. The Brazos River Alluvium Aquifer is a likely candidate for being developed in a future water supply project.

Location

The study area is the Northern Segment of the Brazos River Alluvium Aquifer which includes portions of Bosque, Hill, McLennan, and Falls counties from Whitney Dam to the Falls County border with Milam and Robertson Counties. The straight-line distance from the study area's northern to southern edges is roughly 60 miles or 100 km (Figure 1.1).

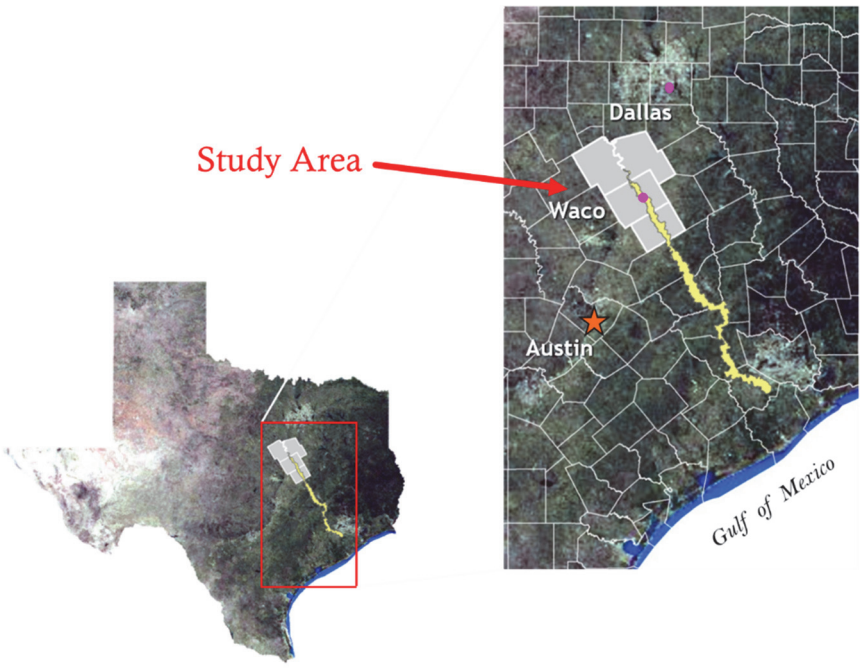

Figure 1.1. Index map showing the study area and areal extent of the Brazos River Alluvium Aquifer. Bosque, Hill, McLennan and Falls counties are highlighted in grey. Modified from Wong (2012).

Purpose

Previous studies of the Northern Segment of the Brazos River Alluvium Aquifer fall into two general categories: low resolution, large spatial-extent or high resolution, small spatial-extent. While aquifer-wide geospatial maps of alluvial thickness produced by Ewing and others (2016) or Wong (2012) are helpful, data are too sparse in many areas of the BRAA to make confident estimations of depth to bedrock (DTB). To the other extreme, boreholes provide excellent information on depth to bedrock and alluvial type distribution. However, boreholes have miniscule spatial resolution. The MC-5 cores collected by Jarvis (2019) and in this study are only 5.7 cm (2.25 in.) wide. This study attempts to be a middle ground by estimating depth to bedrock and alluvial composition with medium resolution (a few meters) and medium spatial extent (hundreds of meters to several kilometers). This intermediate resolution is applicable for assessing sustainable water well production and evaluating aggregate resources within the natural heterogeneity of the alluvial sediments (Figure 1.2).

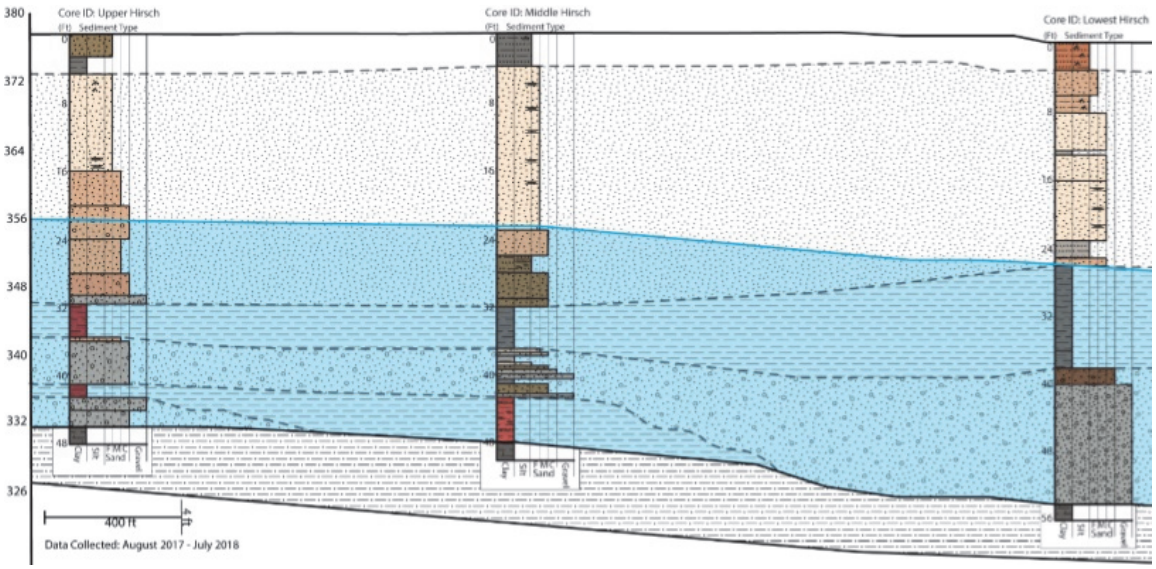

Figure 1.2. Stratigraphic cross-section of the BRAA at Hirsch Dairy from three cores displaying changing alluvial composition over 800 meters. Modified from Jarvis (2019).

Regardless of resolution and/or spatial extent, nearly every previous study has confirmed the heterogeneity of the BRAA caused by the alluvial deposition system. While most transmissivity (T) and hydraulic conductivity (K) values are high enough to support productive wells (Ewing and others, 2016), data are biased as test holes that do not find productive areas of the aquifer are not recorded. In reality, many areas of the BRAA have T and K values too low to support much pumping. It is easy to predict that saturated sediments exist at any given location in the BRAA; however, it is difficult to predict if the alluvium will be primarily a channel (coarse-grained), bank (medium-grained), or overbank (fine-grained) deposit. Though less variable than alluvial composition, it is also important to know the approximate depth to bedrock, which defines the lower bound of saturated section thickness. Having a general idea of anticipated depth to bedrock and alluvial heterogeneity before drilling a well could be more efficient than using resources for numerous test holes. The purpose of this study was to meet these needs by fulfilling the following goals:

1. Estimate depth to bedrock (DTB) with an error < 10%
2. Approximate alluvial distribution (clay, sand, and/or gravel)
3. Estimate saturated section of the aquifer using estimated depth to bedrock
4. Evaluate geophysical results against boreholes in a central Texas alluvial setting. It is hypothesized that the gravity/passive seismic method will have a higher chance of succeeding when at least one calibration boring is nearby.

Few previous investigations have attempted to study the Brazos River Alluvium Aquifer using geophysical methods. This may be because the aquifer is generally shallow enough that test borings are less expensive than in other settings. In this study, five

combined microgravity and passive seismic, horizontal-to-vertical spectral ratio (HVSR) surveys were undertaken to explore the BRAA (goals 1-3). Each survey location was chosen due to previously known information (boreholes, wells etc.), ease of land access, and spatial variability. An overarching goal was to find productive areas in the alluvium that can be tapped by water wells (e.g. gravel-filled buried nickpoints or buried channels). Though many geophysical methods were considered, including electrical resistivity, seismic reflection/refraction, and ground-penetrating radar, the microgravity and passive seismic combination was chosen due to the non-invasiveness, ease of use, and complementary nature of the two methods. Gravity measurements reflect *relative* changes in subsurface densities, while passive seismic (HVSR) methods produce *absolute* depth to bedrock estimates based on presumed seismic velocities. Typically, gravity data are difficult to model as small changes in gravity could be the result many different subsurface variations (nonunique solutions). However, bedrock depth estimations from passive seismic provide a convenient starting point for constraining and modeling the gravity data. Similarly gravity data can help verify or refute a passive seismic depth to bedrock estimation. The combined method, if proven to be viable, would be an improvement over expensive and highly labor-intensive exploration techniques such as direct-push drilling, augering, seismic refraction, or electrical resistivity surveys.

Previous Works

The following relevant previous works are subdivided into three categories and discussed in chronological order. First, studies of the Brazos River Alluvium Aquifer itself are discussed with an emphasis on studies of the Northern Segment of the aquifer. Next, previous studies that used passive seismic, HVSR methods to estimate depth to

bedrock under unconsolidated sediments are discussed, followed by studies that used microgravity methods to map depth to bedrock under unconsolidated sediments.

Brazos River Alluvium Aquifer

Several large-scope studies have been published on the Brazos River and its deposits or the Brazos River Alluvium Aquifer itself. Stricklin (1961) investigated the geomorphology of the interior Brazos River from Knox City, TX to Waco, TX. He found that the channel gradient of the Brazos River decreases from 3.5 ft/mile upstream of Graham to 3.5 – 2 ft/mile between Graham and Waco to 2 – 1.5 ft/mile downstream of Waco. These changes in channel gradient reflect changes in lithologic units that the river crosses—sandy Pennsylvanian red beds, resistant Cretaceous strata, and weaker Cretaceous/Paleogene strata. Downstream of Waco, the weak Cretaceous and Paleogene units allow broad floodplain meandering and allowed development of terraces. Cronin and Wilson (1967) performed the most comprehensive study of the Brazos River Alluvium Aquifer to date by drilling test holes (many of these sites were used as HVSR calibration locations in this study), performing aquifer tests, monitoring water levels, and compiling existing information to achieve a holistic picture of the aquifer. The results of their study, including water-level, water-quality, and aquifer properties, have been considered baseline values by later researchers. Epps (1973) studied the geomorphology of the Brazos River basin in depth and concluded that the present Brazos River is an underfit stream and an ancestral Brazos River had a discharge 5 to 9 times present discharge. He also identified three levels of varying Pleistocene-aged terraces deposited by an ancestral Brazos River. Shah and others (2007) compiled geologic and hydrologic data from public records, previous investigations, and universities and generated a

database that was used to create the groundwater availability model (GAM) for the BRAA. Finally, Ewing and others (2016) developed the conceptual model used for the BRAA's groundwater availability model (GAM). Their report compiles data from previous studies in order to generate model inputs for recharge, discharge, K, water levels, aquifer geometry, water quality, and water use.

Other smaller scale studies added to various sections of the broader knowledge of the Brazos River Alluvium Aquifer. Harlan (1985, 1990) investigated the aquifer from Waco, TX to Marlin, TX and found that some aquifer water may be transmitted through the Lower Taylor Marl (Ozan) Fm, recharging the BRAA. He also found that aquifer water in his study area is predominately a calcium bicarbonate type (with significant variation). Finally, he developed a 2D flow model and found that water in the aquifer flows toward the river or nearest tributary and slightly down valley. Pinkus (1987) studied the impact of several solid waste disposal sites on the BRAA. He also produced an alluvium thickness map for a roughly 30 square mile segment of the aquifer and terraces directly southeast of Waco finding that alluvium thickness ranged from a few ft to over 40 ft. Cannata (1987) performed a seismic refraction survey at the Hirsch Dairy site. He found that soils, dry alluvium, and saturated alluvium had average seismic velocities of 60 m/s, 172 m/s, and 289 m/s respectively. Goforth and Hayward (1992) performed a p-wave and s-wave seismic reflection survey in the BRAA near Baylor University. They attained an average v_s value of 204.2 m/s for a 49 ft thick section of alluvium.

More recently, Wong (2012) and Wong and others (2013) performed a geospatial investigation of the Brazos River Alluvium Aquifer by compiling and analyzing data

using GIS. She found that in the Northern Segment of the BRAA, well depths can be used to approximate alluvium thickness when stratigraphic data are unavailable and demonstrated the sizable gravel pit footprint on the aquifer. Ju (2014) investigated the effect that open gravel pits have on the aquifer through the use of a MODFLOW model, a water budget, K measurements, chemical analyses, and electrical resistivity surveys over undisturbed aquifer and a filled-in gravel pit. He found that open gravel pits likely lead to a net loss in aquifer water—evaporating10% of average annual recharge. Jarvis (2019) performed an extensive borehole coring campaign in the northern segment of the BRAA and found that the aquifer is compartmentalized into many discrete flow systems that are hydraulically disconnected due to hydrologic boundaries. Finally, Noonan (2019) investigated trends in salinity in the northern segment of the BRAA (which has high salinity risk according to Ewing and others (2016)). She also investigated surface water / groundwater interaction between the Brazos river and the aquifer during high flow and low flow events.

Passive Seismic Method

The passive seismic, horizontal-to-vertical spectral ratio method is the first geophysical tool used in this study. Several previous works are outlined with emphasis on findings relevant to this study. Nakamura (1989) is the pioneer of the horizontal-to-vertical spectral ratio (HVSR) method. He found that the characteristics of surface layers (thickness) could be calculated based on the assumption that the horizontal and vertical spectra of microtremors can be approximated as an empirically derived transfer function. This requires that microtremor seismic data are simultaneously collected at the site of interest in each of the three orthogonal directions (two horizontal, one vertical).

Ibs-von Seht and Wohlenberg (1999) used Nakamura's technique to map the thickness of soft sediments over bedrock in the Lower Rhine Embayment (Germany). They made over 100 passive seismic measurements and determined soft Tertiary cover thicknesses between 25 and over 1000 m. They also realized that depth to bedrock and site resonance frequency (peak frequency) could be correlated using a power-law regression calibration curve – this relationship was used by many later studies including this study.

The Site Effects assessment using Ambient Excitations (SESAME) is a European Commission project with 85 participants from 14 universities, labs, and governmental agencies across Europe. The 2004 report outlines guidelines for measuring, processing, and interpreting HVSR data. Of importance is the data quality test which states nine statistical criteria that the commission suggests an H/V curve should meet to be considered reliable with a clear peak frequency. Data collected in this study were tested against these criteria.

Mucciarelli and others (2005) investigated the influence of wind on passive seismic measurements using physical experiments and numerical modeling. They found that windy conditions increase the amplitude of all three seismic components but do not affect HVSR measurements. However, they do recommend using all-in-one units, such as the Tromino 3G+ used in this study, and that sensors be well protected from direct wind.

Chandler and Lively (2014) accomplished a large scale HVSR data collection effort throughout Minnesota, estimating depths to bedrock ranging from a few meters to 300 meters. Their depth to bedrock estimates were based on 280 passive seismic measurements made at control points where bedrock depth was known. They generated

multiple HVSR calibration curves distinguished by geologic setting, investigated a buried valley, and found problems when bedrock type was the soft saprolith found in certain areas of Minnesota. They recommend that the impedance contrast between the bedrock and the overlying sediment cover (caused by the difference in shear wave seismic velocity) be at least 2.5:1. They found bedrock estimates to have 15-25% error in most of the state, but only 13% in the Twin Cities metro area. Finally, they concluded that the HVSR method is less accurate than the <10% error attainable with seismic refraction. Nonetheless, HVSR is quicker, lower cost, and easier to apply compared to seismic refraction.

Johnson and Lane (2016) analyzed data from 176 HVSR measurements acquired on alluvium and drift overlying gneissic bedrock near Tylerville, CT. They found that 156 of the 176 measurements had well defined peaks and contrasted depth to bedrock interpretations using various calibration curves, finding that interpreted depth varied up to 8 m depending on the calibration curve used. They recommend an acoustic impedance ratio of at least 2:1 between the bedrock and overlying sediment cover.

Bignardi (2017) used numerical simulations to evaluate the Ibs-von Seht and Wohlenberg calibration curve approach to estimating depth to bedrock. Bignardi also reviewed the work of several HVSR studies and found that an error of at most 20% is typical when using the method developed by Ibs-von Seht and Wohlenberg.

Several other authors including Delgado and others (2000), Haefner and others (2010), and Blake and Nash (2018) also used the HVSR method, finding the thickness of softer rock/sediments over harder rock with depths of 11 m to over 200 m with 14%-20% error.

Microgravity Method

Microgravity is the other geophysical tool used in this study; several previous works are outlined with emphasis on how they influenced the field, post-processing, and modeling methods used in this project.

Montgomery (1970) used microgravity to estimate the storage coefficient of a water table aquifer near Tucson, AZ. He found that the method could succeed if an aquifer had a relatively high coefficient of storage and a change in water level of 20 ft (~6 m) or more. As water levels in the Brazos River Alluvium Aquifer infrequently fluctuate to that magnitude, this thesis refrained from attempting to estimate storage coefficients using gravity surveys. He also provided helpful guidelines for post processing gravity data using the Bouguer correction and demonstrated the insignificance of a water-table slope correction.

Ibrahim and Hinze (1972) used microgravity in order to map depth to bedrock buried under unconsolidated glacial sediments. Their method was successful—measuring gravity to a precision of 20 μGals (1 m/s^2 = 1 x 10^8 μGals) and generating a bedrock topographic map with a contour interval of 25 ft. Depths to bedrock had a much larger range (350 to 850 ft) in their study than bedrock depths in the BRAA (0-100 ft). Also, their spatial extent was much larger, covering a ~600 mi^2 area of Michigan with approximately 4000 gravity measurements at 500 ft spacing. Hence, their study has only loose similarities with this thesis.

Carmichael and Henry (1977) used microgravity to identify channels buried under glacial drift in Indiana and Michigan that are likely to contain productive groundwater resources. A gravity anomaly greater than 140 μGal can be distinguished with their

method assuming elevation measurements accurate to ± 2 inches (~5 cm). While this anomaly is much higher than the expected gravity anomalies in the BRAA, the gravimeter and elevation measuring system used in this study are much more sensitive than those used by Carmichael and Henry.

Pool and Eychaner (1995) were able to estimate the specific yield of an Arizona aquifer with a temporal-gravity survey over a two-year period. The change in measured gravity (up to 158 μgals) reflected the change in the water level of the aquifer (up to 58 ft). Their result, an improvement on Montgomery (1970), showed the gravity method is a viable way to measure aquifer storage if the aquifer has variations in water levels that have gravity anomalies significantly higher than measurement standard deviations.

Bohidar and others (2001) used microgravity to determine depth to bedrock in a shallow (30 m), unconfined aquifer setting with a confidence interval of 1.8 m. They used a wide spacing, averaging 160 m (over five times the depth to bedrock), and modeled their data to fit known bedrock depths at five boreholes along the transect with a vertical sheet model. Their study showed that choosing a wider station spacing than the expected depth to bedrock can still provide reliable results at lower spatial resolution.

Finally, Feldpausch (2017) mapped depth to bedrock under glacial drift (28-145 m depth) using a combined passive seismic (HVSR) and microgravity method somewhat similar to this study. Making measurements with wide, 0.4 to 0.8 km spacing, he found that HVSR methods were more useful than gravity for mapping bedrock depths beneath the glacial drift and was able to calculate drift thickness with errors of 14% or less.

In short, previous studies suggest that the Brazos River Alluvium Aquifer is heterogeneous in composition and has varying underlying depth to bedrock throughout

the Brazos River alluvial valley. Many previous studies have used passive seismic (HVSR) methods or microgravity methods to map depth to bedrock; however, few previous researchers have used a combination of the two methods together like Feldpausch (2017) or have attempted to discern differing alluvial composition using the two methods. No known previous works have used this combined passive seismic and gravity method in a Central Texas, alluvial aquifer setting. Since the Brazos River Alluvium Aquifer is the largest alluvial aquifer in the state (excluding the Ogallala), this method could have broad applications to other, smaller alluvial groundwater systems around Texas.

Geologic Setting

The geology of the study area ranges from the Lower Cretaceous Edwards Limestone at Lake Whitney to Holocene present-day fluvial Brazos River deposits. Underlying bedrock ranges from Lower Cretaceous to Eocene in age and includes limestones, marls, chalks, sands, clays and shales. All bedrock units dip southeast at low angles, with the Brazos River flowing up section through the study area. The units from oldest to youngest are the Edwards, Georgetown, Del Rio, Buda, Woodbine, Eagle Ford, Austin, Ozan, Wolfe City, Pecan Gap, Kemp and Nacatoch and Neylandville, Willis Point, and Kincaid formations (Barnes, 1979). Since the Pleistocene, the ancestral Brazos River has deposited sediments and subsequently eroded through them leaving behind several terraces above the current floodplain valley floor. The terraces have decreasing height with decreasing age (i.e. the oldest are highest) (Epps, 1973). While some terraces are laterally and hydraulically connected to the current valley alluvium (Pinkus, 1987), many are ‘stranded’—isolated by differential erosion (Harlan, 1990). The current

floodplain alluvium consists of a generally fining-upward, but heterogeneous sequence of clay, silt, sand, and gravel. These deposits are the youngest of the fluvial system. The bedrock geology appears to have a noticeable effect on the width of the Brazos floodplain and amount of alluvium therein (Stricklin, 1961). From Whitney Dam to Waco, the alluvium is narrow and shallow—underlain by more resistant limestones and chalk bedrock formations. Southeast of Waco, the floodplain broadens as the less-resistant shales and clays allowed the lower-gradient river to cut a wide, meandering course. Wide alluvial sections are present in this portion of the Brazos River valley, making up most of the yellow, Quaternary alluvium displayed in Figure 1.3.

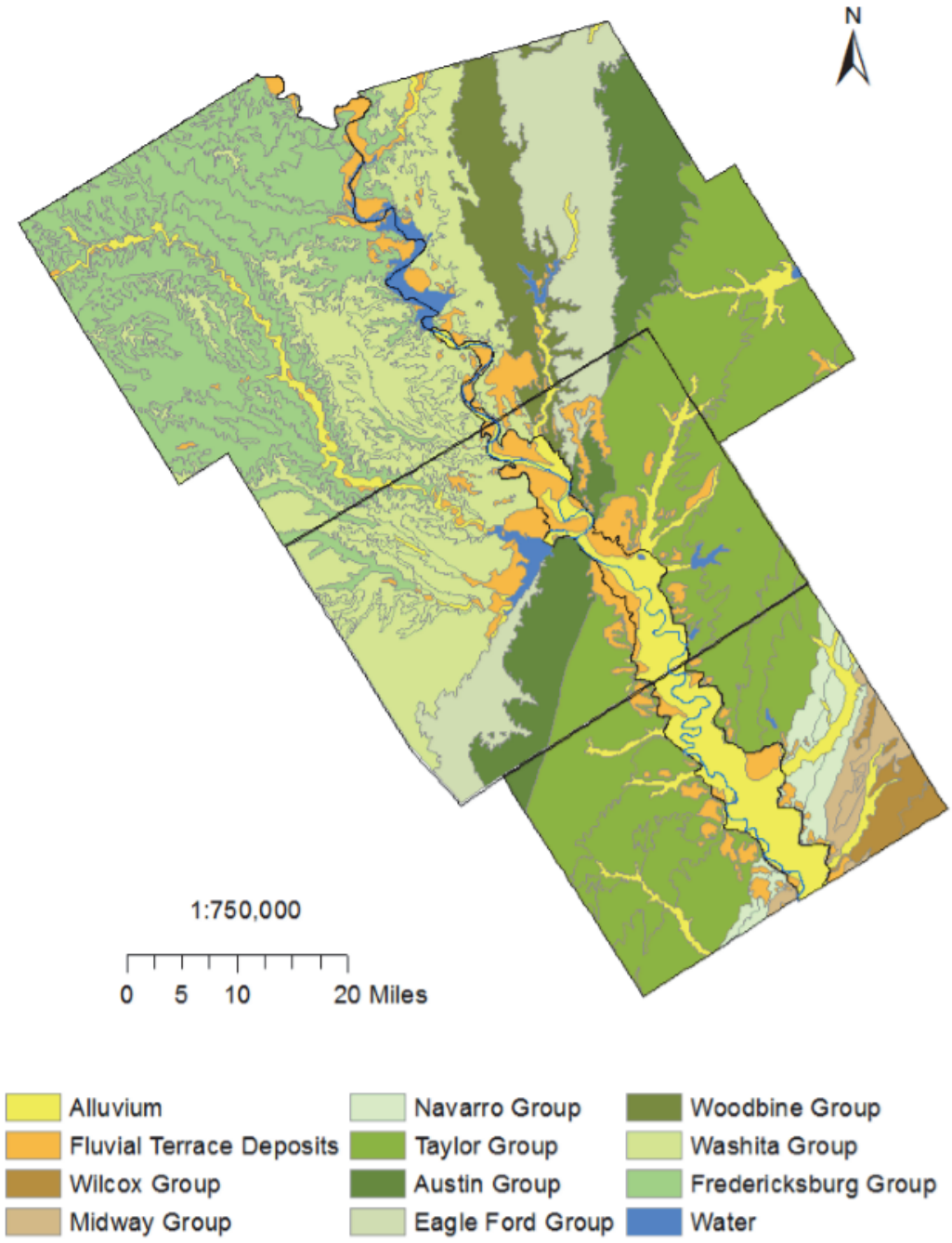

Figure 1.3. Geologic map of the study area (Noonan, 2019), originally modified from Barnes (1979). Note the connected or 'stranded' orange terrace deposits adjacent to the younger yellow alluvium. All bedrock formations are Cretaceous except for the Midway and Wilcox groups which are Eocene age.

Hydrogeologic Setting

The Brazos River Alluvium Aquifer covers over 1050 square miles and is one of twenty-one minor aquifers in Texas. The aquifer is generally unconfined, though locally confined conditions exist, caused by the presence of clay lenses (Cronin and Wilson, 1967). Alluvium thickness ranges from a few feet up to 127 ft, increasing from north to south (Ewing and others, 2016). In the northern segment of the BRAA, thickness ranges from a few feet to 69 feet with an average of 40 feet. An interpolation of alluvium thickness from 62 wells in the study area is shown in Figure 1.4. The BRAA primarily receives recharge from precipitation that infiltrates down to the water-table and generally discharges water to Brazos River (a gaining stream). Other sources of recharge include runoff from adjacent higher ground, underflow from higher terrace alluvium, lateral flow from bedrock, and flood events. Recharge estimates range from 0.11 to 5 inches per year (Cronin and Wilson, 1967; Ewing and others, 2016). Besides flow into the Brazos River, other sources of discharge include transpiration, pumping from wells and/or open pits, and evaporation through soil or from open gravel pit lakes. Flow direction is generally toward the river and slightly downstream depending on the local gradient (Cronin and Wilson, 1967; Harlan, 1990). Aquifer properties vary widely due to the heterogeneity of fluvial deposits with horizontal hydraulic conductivity (K) ranging from 0.26 to 890 ft/day with a mean of 59 ft/day (Ewing and others, 2016). Transmissivity similarly ranges from 100 ft^2/day to 46,000 ft^2/day. Specific Capacity ranges from 1.44 gallons per minute per ft (gpm/ft) to 134 gpm/ft with a median of 23.5 gpm/ft (Shah and others, 2007). Terrace alluvium, which stores smaller amounts of groundwater, typically has lower transmissivity than younger, floodplain alluvium (Cronin and Wilson, 1967).

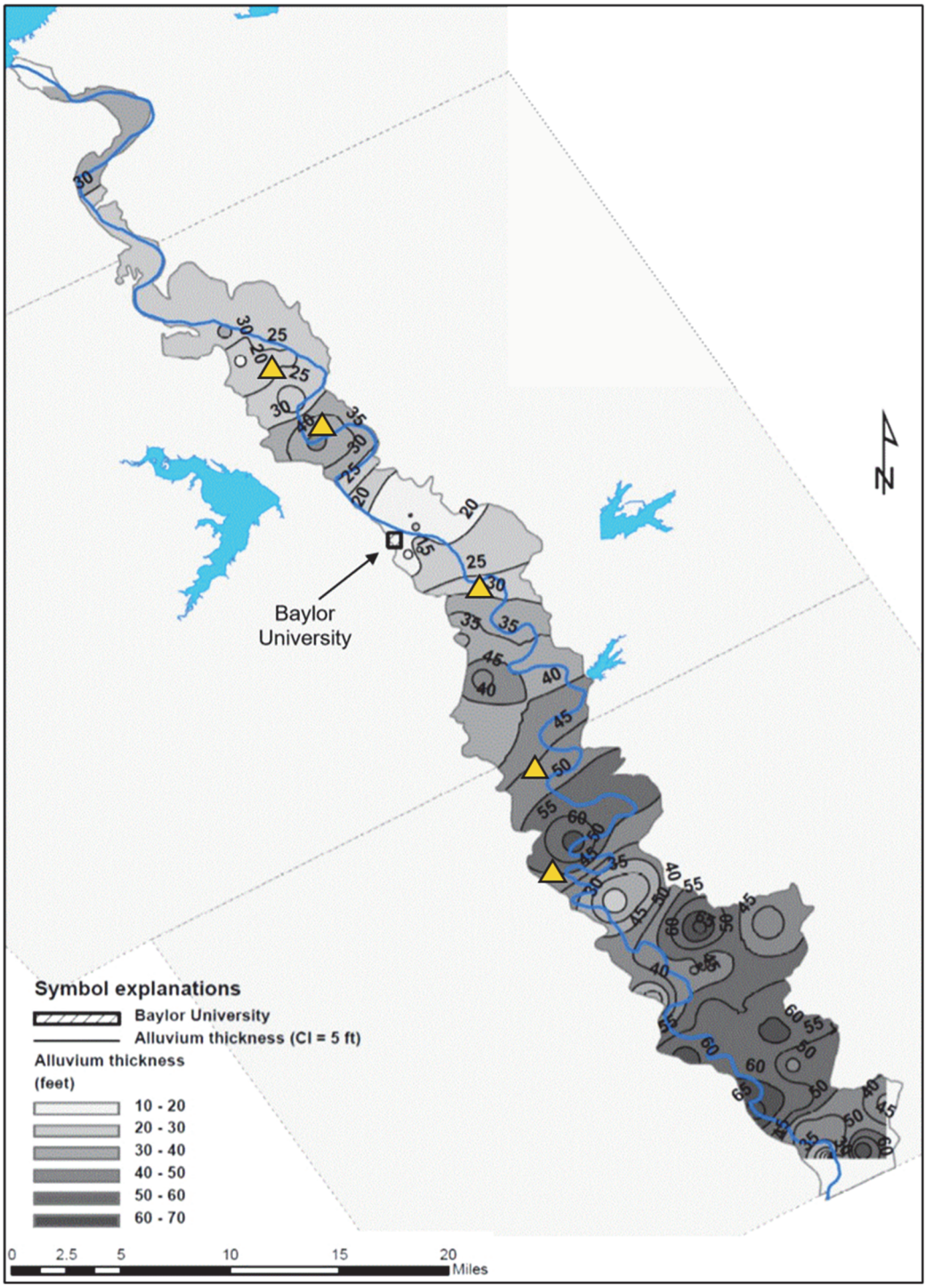

Figure 1.4. Contoured alluvium thickness in the Northern Segment of the BRAA. The contoured result is interpolated from just 62 wells throughout the study area. Gold triangles mark the locations of the gravity and passive seismic surveys completed in this study. Modified from Wong (2012).

CHAPTER TWO

Methodology

This study used a combined passive seismic and microgravity approach. The two complementary methods are detailed sequentially in this chapter. Modeled results of bedrock elevation and sand and gravel thickness were produced by comparing measured Bouguer gravity anomalies to passive seismic depth to bedrock estimates. Then, a modeled thickness of a bedrock slab that roughly mirrors the bedrock elevation profile from passive seismic was determined. Finally, a modeled sand and gravel thickness was determined so that each modeled result precisely equals the measured Bouguer gravity anomaly. Sediment cores were drilled to bedrock at sites without previous borehole information to assess the geophysical results.

Passive Seismic HVSR Method

Theoretical Overview

The passive seismic, horizontal-to-vertical spectral ratio (HVSR) method relies on the collection and processing of natural and anthropogenic ambient seismic noise (sometimes referred to as microtremors) using a 3-component (2 horizontal, 1 vertical) seismograph. Collected seismic data are Fourier transformed and horizontal traces are divided by the vertical trace to attain an H/V curve. The peak H/V frequency is known as the site resonance frequency and can be used to approximate depth to bedrock under an

unconsolidated overburden using the following empirically based formula (Nakamura, 1989):

$$f_0 = \frac{(n*v_s)}{4Z} \quad (1)$$

where f_0 is the fundamental site resonance frequency in Hz, n is the number of layers above the impedance contrast (one in most cases), v_s is the shear wave seismic velocity for the layer above bedrock (m/s), and Z is the depth to bedrock in meters. The empirical basis for this formula is robust and has been confirmed by many publications (Bignardi, 2017); however, the theoretical basis explaining this relationship has not been fully determined, and controversy continues over which type of seismic wave(s) (shear, Rayleigh, and/or Love) cause this relationship (Van der Baan, 2009). A value for the shear-wave velocity variable, v_s, is required to approximate depth to bedrock along with the measured site resonance frequency. The v_s, can be estimated and assumed to stay constant over the survey area, or preferably, the necessity to estimate v_s can be bypassed by using a power-law regression calibration curve that relates measured peak resonance frequency to known depth to bedrock. Ibs-von Seht and Wohlenberg (1999) developed this simple relationship:

$$Z = \mathrm{a}(f_0)^{\mathrm{b}} \quad (2)$$

where a and b are coefficients determined from the regression. Many authors have found that using such a calibration curve is a vast improvement over assuming a singular v_s value for a survey area (Haefner and others, 2010; Johnson and Lane, 2016). Seismic refraction/reflection could also be used to compute site-specific seismic velocities; however, if that step is taken, one should perhaps just use the seismic refraction method itself for determining depth to bedrock. While the multichannel, active seismic method is

more accurate than the passive seismic, HVSR method in determining depth to bedrock under alluvium (Goforth and Hayward, 1992), the HVSR method is an alternative with many advantages (Chandler and Lively, 2016). The main advantages include simplicity (easier to train personnel), efficiency (requires less time), versatility (works better in urban settings), and value (far less costly than seismic refraction or electrical resistivity). HVSR methods provide estimates of depth to bedrock under an overburden cover with errors of around 14-25%—making them a good option for low-cost, quick reconnaissance (Bignardi, 2017; Chandler and Lively, 2016).

A Tromino Zero 3G+ 3-component seismometer was used in this study, rented from Exploration Instruments, LLC (Austin, TX) at a cost of $40/day. The parameters chosen before recording include sampling frequency, window size, gain, and recording length. Sampling frequency was set to 128 Hz, the recommended rate for stratigraphic applications (Micromed, 2009). Window size (used for stacking or removing data) was set to 20 seconds and the Tromino was set to full gain (Micromed, 2009). With depths to bedrock of 100 ft (~30.5m) or less, peak frequencies always exceeded 1 Hz meaning that a 10-minute recording length was adequate (SESAME, 2004). A 12-minute recording length was used in noisier areas so that even with the removal of several 20-second windows there were still enough data to meet length guidelines. Data processing included triangular smoothing of each seismic trace, cleaning to remove 20-second windows influenced by transients (passing cars, pedestrian traffic, etc.), and locating “anthropic peaks” which are peaks in the H/V curve caused by manmade machinery such as pumps, electrical transmission lines, vibrating bridges etc. (Figure 2.2). These do not reflect stratigraphic layers and must be ignored.

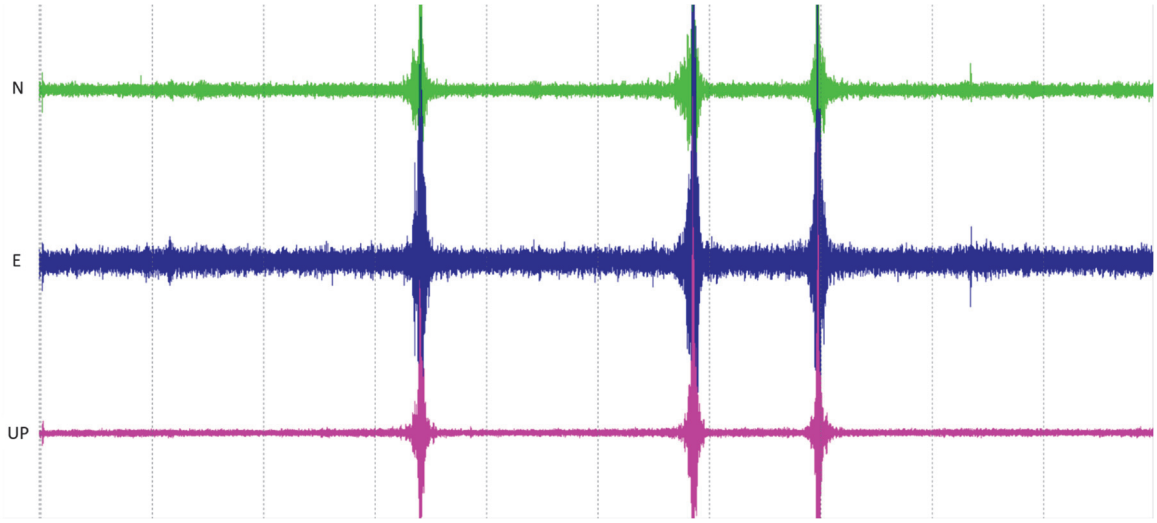

Figure 2.1. Raw seismic noise (microtremors) from calibration reading PV2 in Steinbeck Bend. The three sensors are north-south (green), east-west (blue) and up-down (pink) . The three jumps in seismic noise are the result of transients (passing cars in this case).

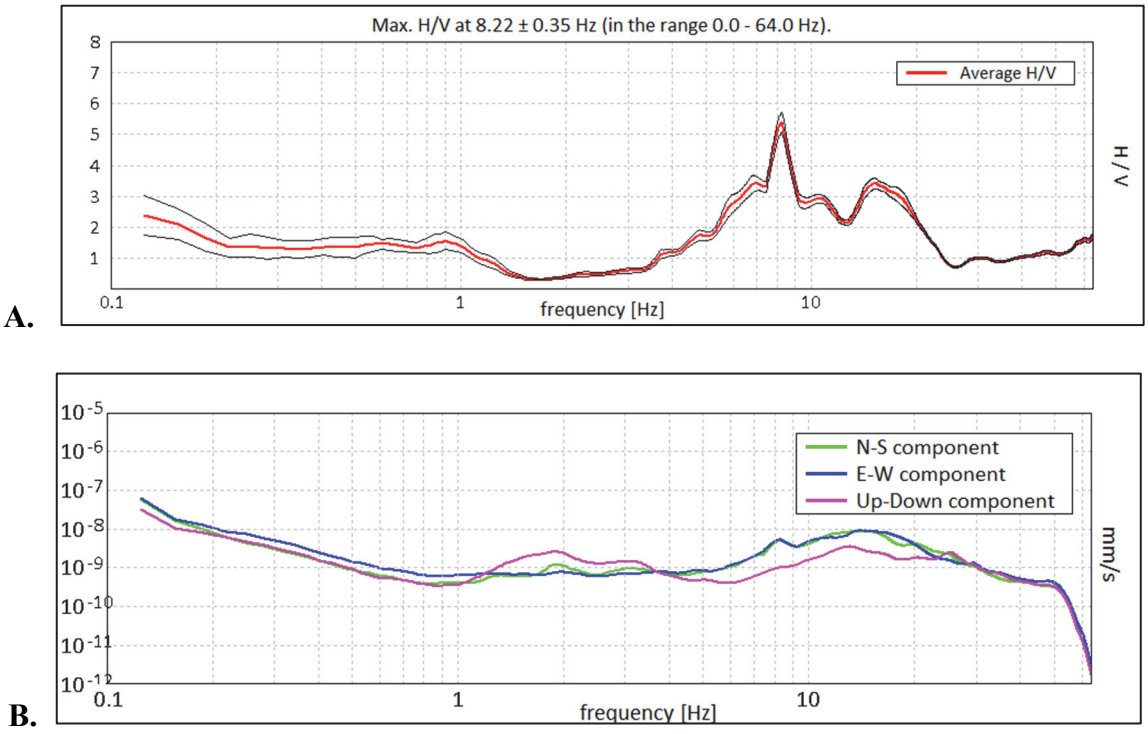

Figure 2.2. **A.** H/V curve for the Speight / 5th St. calibration station acquired on the Baylor Campus showing a narrow, high-amplitude anthropic peak not usable for making a depth to bedrock estimate. **B.** Individual, Fourier-transformed curves for each component (N-S, E-W, up-down) at the Speight / 5th St. station. The identical sharp rise in horizontal seismic noise in both directions also signifies an anthropic peak.

Using the Grilla software package (Micromed, 2018), seismic data were separated by frequency using a Fourier transform function. Then, the location on the curve at which the horizontal frequency divided by the vertical frequency is at its highest was identified. This is f_0, the resonance frequency of the site (Figure 2.3).

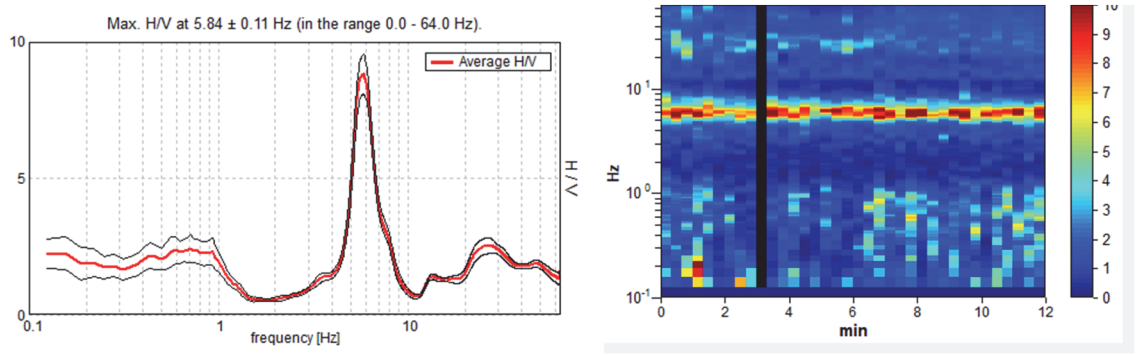

Figure 2.3. H/V curve (left) and H/V stability plot (right) for site MCCHR NE Corner. The peak H/V, 5.84 Hz, represents the site resonance frequency, f_0. The stability plot is used to see if maximum H/V is consistent throughout the measurement.

Data reports were generated for each passive seismic measurement using the Grilla software package (Micromed, 2018). Each trace was evaluated to test whether data "pass" SESAME criteria—a group of nine statistical criteria that determine if an H/V peak is "clear" and "reliable" (SESAME, 2004). In order to obtain the correct coefficients to be used in Equation 2, passive seismic data were collected at 93 locations throughout the study area where depth to bedrock was known. The known depths were mainly obtained from well reports stored by the Texas Water Development Board, but other sources included Jarvis (2019), Nordt and others (2015), Wong (2012), and boreholes drilled during this study. These calibration points were collected throughout the study area based on data availability and property access (locations shown in Figure 2.4).

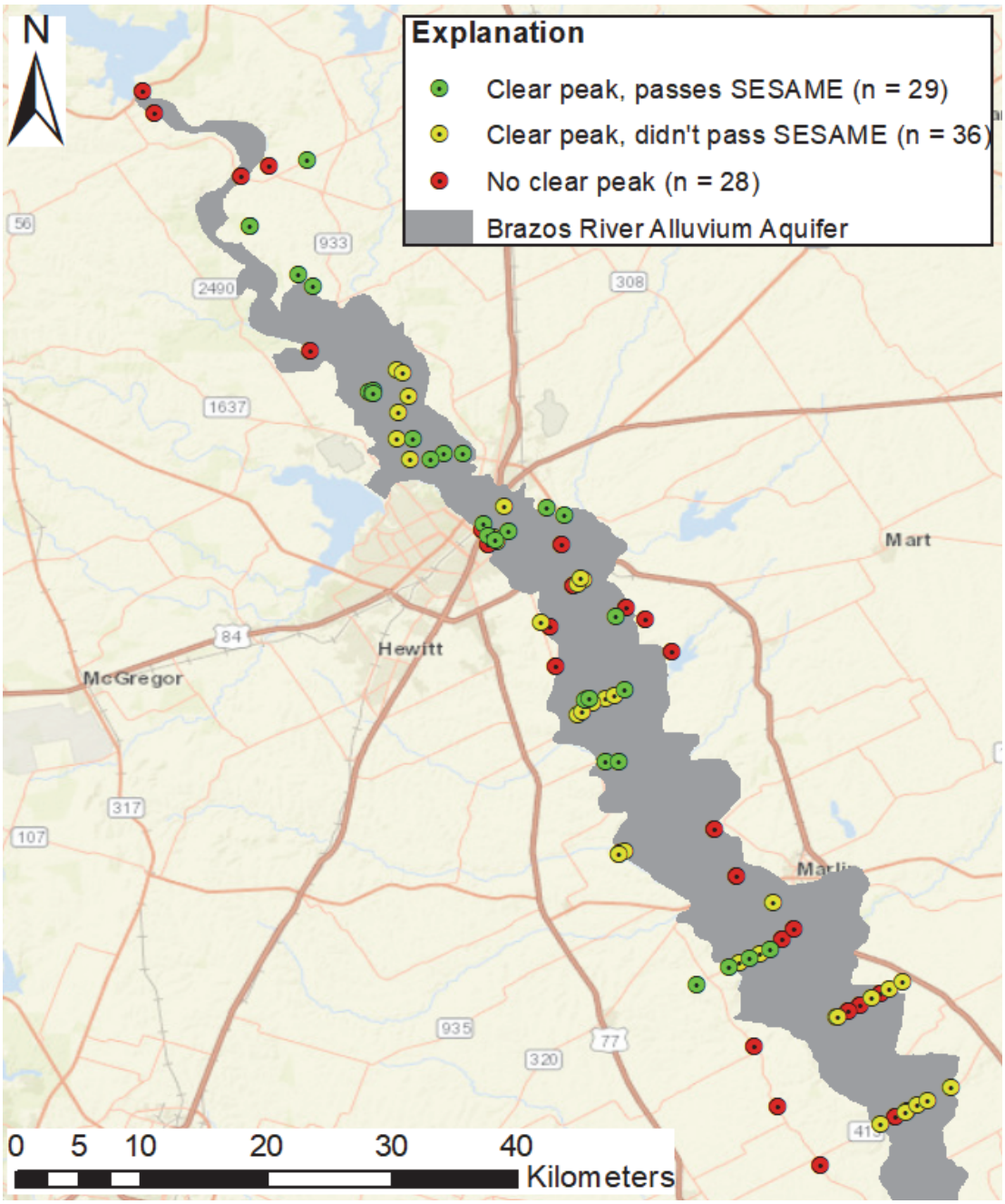

Figure 2.4. Map of the Northern Segment of the Brazos River Alluvium Aquifer (grey) showing Tromino calibration stations, separated by H/V peak quality.

Most calibration H/V curves had clear peaks marking a singular site resonance frequency (f_0) and could be used in making the calibration curve; however, close to a third had no peak or multiple peaks meaning that there was no reliable f_0 at that particular

site. Of the sites with clear peaks, not all had data quality sufficient to pass SESAME guidelines (SESAME, 2004). These non-pass "dropout" traces were still used for the calibration curve because the inclusion of clear peaks that did not pass SESAME strengthened the regression by adding more data. Furthermore, average and median error versus known depths to bedrock were lower using all clear peaks compared to a calibration curve derived solely from the H/V curves that passed SESAME. The study area-wide calibration curve is shown in Figure 2.5.

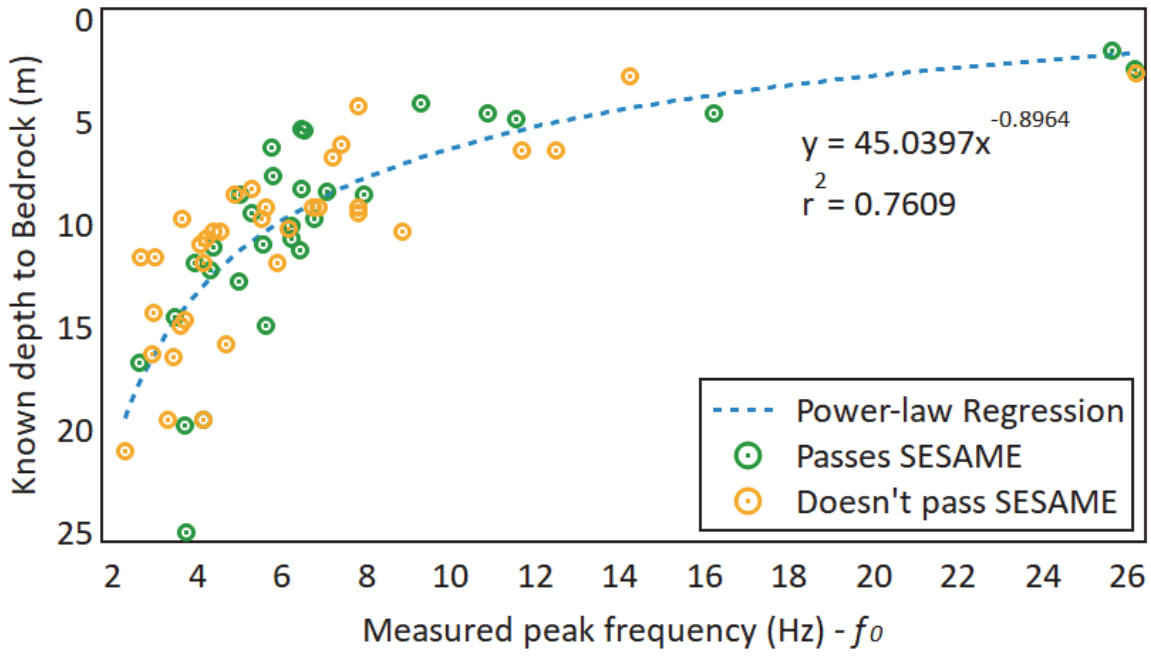

Figure 2.5. Brazos River Alluvium Aquifer power-law regression calibration curve derived from the calibration measurements with clear peaks in Figure 2.4. Both traces that passed and did not pass SESAME were included.

The r^2 value for the study area-wide BRAA curve, 0.761, is lower than ideal (most references had r^2 values > 0.8); however, this probably reflects some of the normal difficulty in attempting HVSR in an alluvial setting where the sediments vary in shear-wave seismic velocity, v_s, from location to location. A calibration curve produced solely

from traces that passed SESAME had a slightly higher r^2 value, 0.807. The BRAA curve was the primary tool used to convert gathered peak resonance frequencies, f_0, into depth to bedrock estimations.

Field Methods

The Tromino seismograph was placed whenever possible on natural ground with the spikes pressed into the ground to ensure necessary instrument–ground coupling (SESAME, 2004). This often required removing a small patch of grass with a shovel. The Tromino was checked to be roughly level, though leveling is less important than ensuring good coupling with the ground (Micromed, 2009). Weather conditions were noted with attention to wind speed. If wind was judged to be higher than about 10 mph (~4.5 m/s), a small hole was dug to place the Tromino in order to protect from direct wind which can negatively affect measurements (Mucciarelli and others, 2005).

Figure 2.6. Picture of the Tromino seismograph placed in a shallow hole to protect from wind at the Buster Chatam Rd field site.

The SESAME data collection form was completed for each site location noting wind speed, transients (cars, pedestrians), distance from structures, and other features that may have affected passive seismic measurements such as power or water lines (SESAME, 2004). With the Tromino protected from direct wind and all signals well above >1 Hz (depths to bedrock less than about 100 m), wind should not affect the HVSR solution, but only increases the amplitude of each component (Mucciarelli and others, 2005).

Gravity Method

Theoretical Overview

Changes in subsurface density can be detected by measuring small variations in gravitational acceleration. In an alluvial setting such as the Brazos River Alluvium Aquifer, the largest measured changes in gravity are expected to reflect changing depth to bedrock and to a lesser extent, changes in textural heterogeneities of aquifer material (differing amounts of clay, sand, gravel, and/or groundwater). These hypotheses are reliant on expected density contrasts between sediments and/or bedrock (displayed in Table 2.1). Gravity anomalies can be modeled using Bouguer slabs (infinite horizontal slabs with density and thickness). The following equation defines gravitational acceleration from a Bouguer slab, g_b, in m/s^2 (Hinze and others, 2013):

$$g_b = 2\pi G \Delta \rho z \quad (3)$$

where G is the gravitational constant, 6.674 E-11 m^3/kg s^2, $\Delta\rho$ is the density contrast in kg/m^3 of the slab, and z is the thickness of the Bouguer slab in m.

Table 2.1. Textbook densities used for initial estimations of density contrasts (Hinze and others, 2013 and Carmichael, 1989).

Sediment/Rock Type	Density (kg/m^3)	Average Density (kg/m^3)
Clay (unsaturated)	1100-1600	1350
Sand (unsaturated)	1400-1650	1525
Gravel (unsaturated)	1500-2030	1765
Limestone	2000-2700	2350
Shale	2060-2760	2410

Since local bedrock densities may be slightly different than textbook averages, twelve dry bulk density measurements were made with bedrock samples collected from core samples or outcrops of formations in or just outside the study area (locations shown in Figure 2.7). Most outcrop locations were located from A.O. Beall's study of the Lower Taylor Marl (Beall, 1964). Samples were baked at 105ºC for over 24 hours to remove moisture, weighed in 20-50 g increments, and submerged in a graduated cylinder. Another source of bulk density data was data shared by local engineering firm Langerman Foster Engineering, LLC. Typical dry bulk densities for local clay, sand, and Lower Taylor Marl (Ozan Fm) are 90-110 lbs/ft^3 (1440-1760 kg/m^3), 115-120 lbs/ft^3 (1840-1920 kg/m^3), and 125-135 lbs/ft^3 (2000-2160 kg/m^3) respectively (Langerman Foster LLC, 2020). Average bedrock dry bulk densities were 2060 kg/m^3 from measurements (recorded in Appendix A) and 2102 kg/m^3 from Langerman Foster data (Langerman Foster LLC, 2020). A bedrock density around 2060 to 2102 kg/m^3 is on the low end of textbook ranges for shale and limestone in Table 2.1. Hence, the density contrast between a sand and gravel layer and a bedrock layer is likely to be in the 200-600 kg/m^3 range.

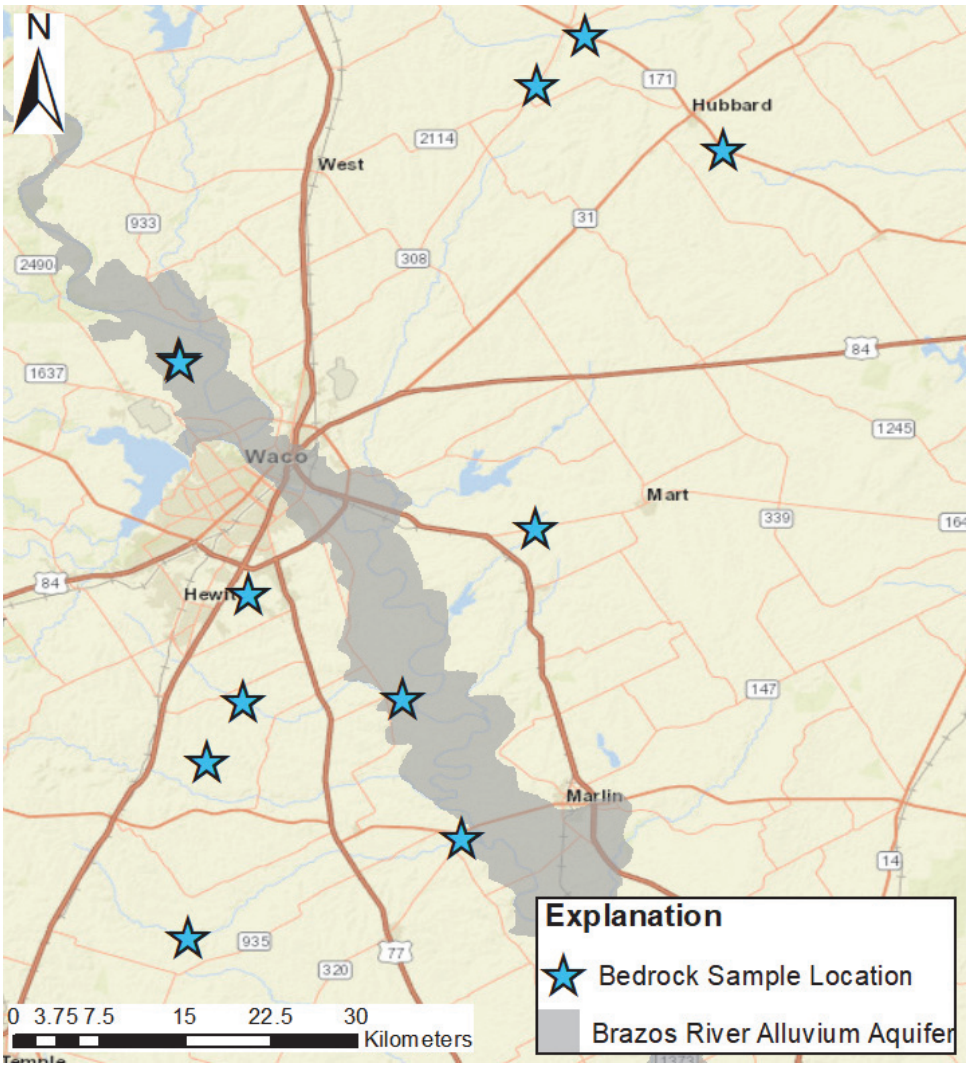

Figure 2.7. Map displaying the locations where bedrock samples were obtained to measure bulk density. All bulk density measurements are recorded in Appendix 1.

Corrections

Raw gravity data need be corrected for several outside influences in order to be useful. The five main corrections, in the order they were applied in this study are the earth-tide correction, instrument drift correction, free air correction, Bouguer correction, and regional correction.

First, the earth-tide correction corrects for the exertion of gravity depending on the current position of the sun and moon. These positions can change gravity readings by

over 0.15 mGals (1 x 10^5mGal = 1 m/s^2) over the course of a day (Hinze and others, 2013). The earth-tide correction used is the ETGTAB tidal model developed by Wenzel (1994) and is built-in to the CG-6 Autograv's software. Data were collected for several days continuously in office to ensure the built-in earth-tide correction was working properly.

Second, the instrument drift correction corrects for the slow stretching of the gravimeter's own spring which affects measured gravity linearly over time, typically resulting in higher gravity readings over time or a positive drift. Repeat measurements were made at one or more base stations in order to calculate a linear drift rate to remove from all gravity measurements. Drift rates averaged about 0.171 mGal/day.

Third, the free air correction corrects for decreasing pull of gravity with increasing elevation above sea level. Gravitational acceleration decreases by 0.3086 mGal for every meter increase in elevation above sea level (Hinze and others, 2013). For the surveys in this project the anticipated gravity anomalies were sufficiently small (tens to hundreds of μGals), that surveying with a real-time kinematic (RTK) GPS with a precision < 5 centimeters, was necessary to avoid large errors in corrected gravity due to errors in elevation measurements.

Fourth, the Bouguer correction accounts for near-surface gravity influences—removing effects from soil between measurements taken at the lowest elevation of the survey (the datum) and all other, higher elevations. This correction also relies on having precise elevation measurements at each station from the RTK GPS. The Bouguer correction is calculated by assuming a density for surficial material, calculating gravity using Equation 3, and subtracting the surficial slab from measured gravity. Densities used

for this correction varied by site but ranged from 1370 kg/m^3 to 1520 kg/m^3 depending on the average reported bulk density of the soil at each site by the Natural Resource Conservation Service (found on the Web Soil Survey) (NRCS, 2019). Using these values as first approximations, near-surface soil densities were adjusted slightly higher and lower to see if another density could further minimize gravity variation from station to station. This is known as Nettleton's Method (Hinze and others, 2013). Specifically, the densities used for the Bouguer correction were 1510 kg/m^3 for Hirsch, 1600 kg/m^3 for MCC, 1440 kg/m^3 for Moon River, 1550 kg/m^3 for Buster Chatam, and 1380 kg/m^3 for Arcosa Falls.

Fifth, the regional gravity correction corrects for broad trends in gravity due to deep structures such as buried fold belts, subducting slabs, or deep facies changes. There are several methods to correct for regional trends. Initially, gravity data from a USGS database that includes 76,000 measurements throughout the state of Texas were downloaded and interpolated in order to glean the regional trend at each survey location (Bankey, 2006). However, when these trends were applied to measured gravity, regional trends were reduced, but not wholly eliminated. Instead, gravity along each transect continued to trend upward in one direction. Another method to find regional trends in gravity is to calculate linear regressions from otherwise corrected gravity data and remove the trend. The two regional methods are displayed in Figure 2.8 for the Hirsch Dairy site. The main drawback of the linear regression method is that it could potentially mask lithologically sourced changes in gravity along a transect and accidentally correct for them; however, it was deemed superior to the former interpolated method because the magnitudes in Bouguer gravity anomalies produced by the interpolated method are too

large to be explained by changes in alluvium thickness or bedrock elevation changes, especially when compared to data from boreholes.

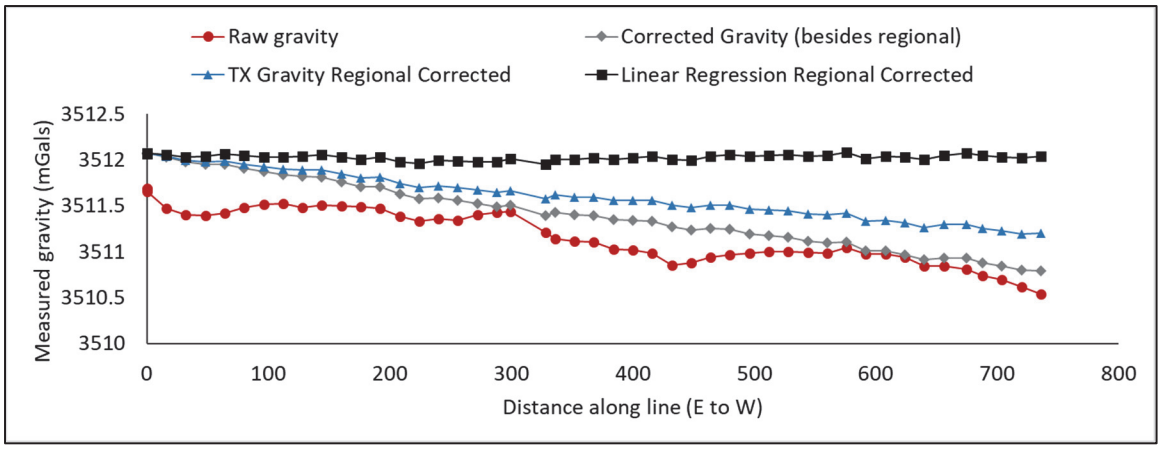

Figure 2.8. Comparison of a regional correction derived from the Texas Gravity Station Database (Bankey, 2006) and a regional correction derived from the linear regression.

While each of the five corrections is important, depending on the survey some corrections produce higher magnitude corrections than others. The larger the elevation variation, the higher the magnitude of free air and Bouguer corrections. The longer the transect was, the higher the magnitude of the regional correction. The step-by-step progression from raw gravity to corrected gravity at the Buster Chatam transect is displayed in Figure 2.9.

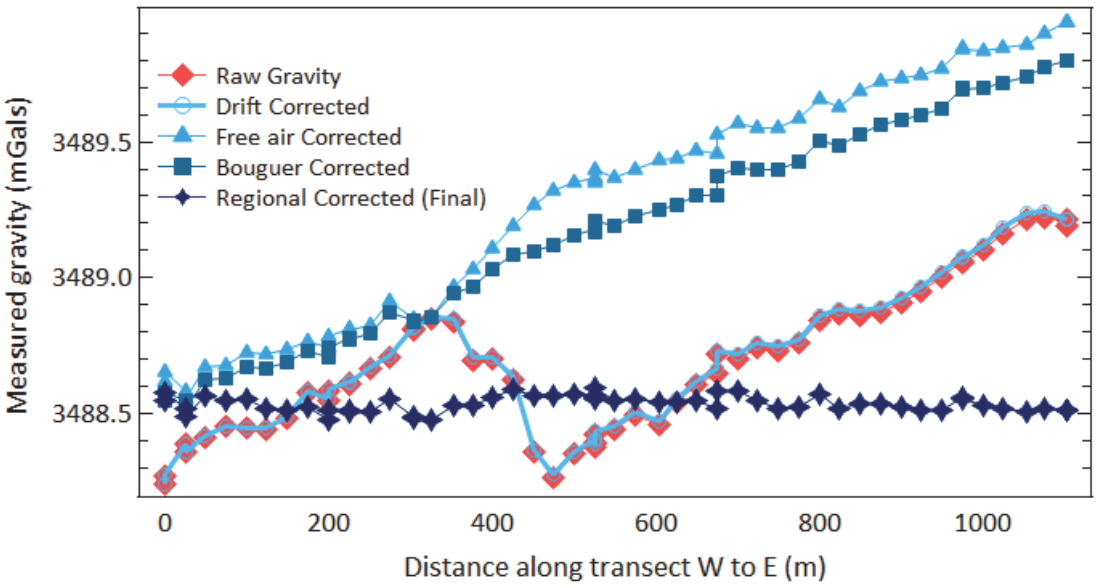

Figure 2.9. Successive progression from raw gravity (red diamonds) to corrected gravity (dark blue stars) at the Buster Chatam survey site. The highest magnitude corrections were the free air and regional corrections.

Field Methods

Gravity data were collected and recorded using a Scintrex CG-6 Autograv gravimeter (owned by the Baylor University Department of Geosciences). This highly advanced instrument has a resolution of 0.1 μGal or one-billionth of a m/s^2 with reasonable precision down to several μGals (Scintrex, 2019). To prepare each station, a small patch of ground was cleared of grass and shrubs. Then, the gravimeter was leveled to within 10 arcseconds of level using its accompanying tripod and a reading was made over 60-seconds. As the CG-6 makes a reading, its internal computer measures how off level it is each second and makes a level-correction, adding back gravity for not being perfectly perpendicular to the surface. An average value of measured gravitational acceleration with these corrections was calculated along with error statistics. The standard deviation (σ) of each reading was monitored in real time during each measurement on an accompanying tablet that controls the CG-6 over a Bluetooth

connection. A measurement was repeated if σ exceeded about 0.04 mGals (40 μGals). There was some subjectivity due to both weather conditions and soil type—both windy conditions and soft, spongy soils inevitably lead to higher standard deviations in measured gravity as the gravimeter more-easily shifts out of level. The exact location of each gravity measurement was surveyed using a Leica GS18 T GNSS RTK (real-time kinematic) Rover GPS system (owned by the Baylor University Department of Geosciences) which records latitude, longitude, state plane coordinates, and elevation to a precision of several centimeters along with the "coordinate quality" of each measurement based on the connection between the GPS and satellites. The coordinate quality statistic represents a "two third (66.6%) probability that the computed position deviates from the true position by less than the coordinate quality value" (Leica SmartNet, 2016). At the Arcosa Falls field site, for example, coordinate quality averaged 0.017 m or 1.7 cm in the Z direction (height).

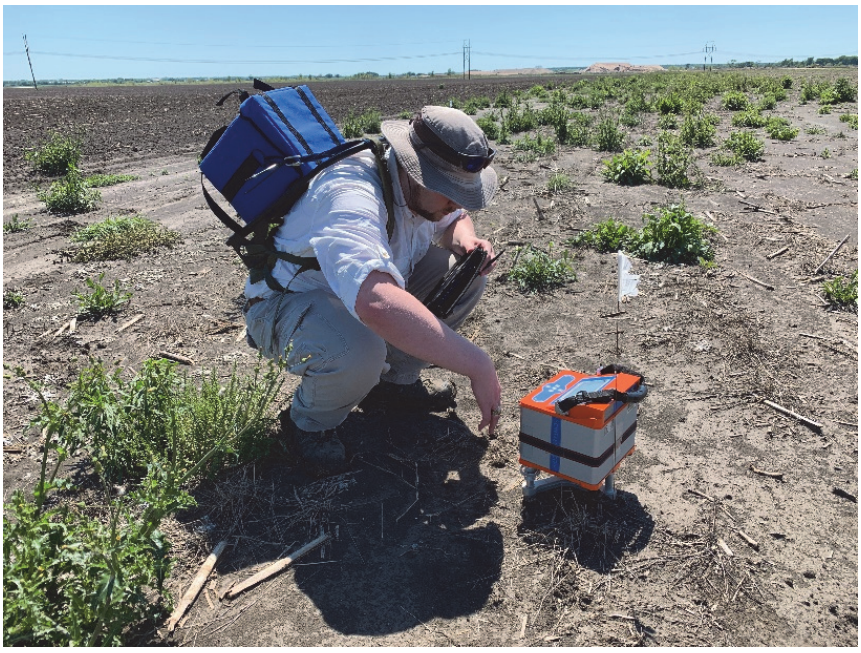

Figure 2.10. Picture of Christopher Mitchell leveling the CG-6 Autograv before making a gravity measurement. In his left hand is the tablet that communicates with the CG-6.

Gravity surveys were all linear transects in order to cover the most ground while spending the least amount of time. Spacing between gravity stations (locations where gravity measurements were taken) varied based on the anticipated depth to bedrock found from nearby boreholes or water wells. Since it is recommended to space gravity stations roughly the depth to the expected anomaly (Hinze and others, 2013), spacing was kept at twice the expected depth to bedrock or less as several previous studies used a spacing of twice the depth to bedrock (Carmichael and Henry, 1977; Ibrahim and Hinze, 1972). Repeat measurements were made at a minimum of one base station in order to calculate and correct for linear instrument drift. If possible, additional measurements were made past either end of the survey transect in order to better calculate and correct for regional gravity trends.

Modeling Gravity Data

Bouguer gravity anomalies were modeled using typically two Bouguer slabs (Equation 3) representing three distinct layers – clay, sand & gravel, and bedrock. Sand and gravel were consolidated and combined into a single slab for simplicity since the two have similar anticipated densities (Table 2.1). Four different density contrasts were used to calculate bedrock slab thicknesses and the sand & gravel slab thicknesses. These exact density contrasts varied slightly by site but were typically 200-600 kg/m^3 for the bedrock slab and 50-350 kg/m^3 for sand & gravel slab. Then, ten different proportions of gravity anomaly derived from bedrock or sand & gravel slab changes were used. The modeled result was 160 unique scenarios of bedrock thickness and sand & gravel thickness, all of which added up to measured Bouguer gravity anomalies. The thickness of each slab increased depending on the magnitude of measured gravity and the density contrasts

used. Since gravity measurements are relative, Bouguer gravity anomalies only reflect how bedrock depth or sand and gravel thickness *changed* along a transect (i.e. no absolute depth to bedrock or sand and gravel thickness estimates can be made from gravity data alone). 'Best fit' modeled scenarios were those that had changes in bedrock thickness similar to changes in bedrock elevation estimates from passive seismic or borehole data (if available)—allowing relative changes in bedrock slab thicknesses and sand and gravel thicknesses to be converted into absolute sand and gravel thickness estimates and absolute depth to bedrock estimates.

Several important assumptions were made when modeling gravity data. First, each model result (scenario) assumed that a uniform proportion of gravity anomaly was derived from each Bouguer slab (e.g. 70% from changes in bedrock, 30% from changes in sand & gravel) across the entire transect. In reality, the proportion of gravity anomaly sourced from each slab could be different at every gravity station. In other words, one modeled scenario could be correct along one part of a transect, but others may be correct in different parts of the transect. Second, the model's density contrasts are reliant on the assumption that there is always some clay, sand, and gravel present in some proportion. If sand & gravel were completely absent, for example, the modeled density contrast between bedrock and overlying alluvium would likely need to be increased. Third, the model only allows for positive changes in bedrock slab thickness and sand & gravel relative to the station where the gravity anomaly is 0. Generally, the station with the lowest gravity anomaly should be at the location with deepest bedrock; however, this assumption may not always be accurate. For instance, a low gravity anomaly value could be explained by an increase in less dense clay content with no change in bedrock height.

Geoprobe Coring Method

Core samples and depth to bedrock information at survey locations without an existing core or well were obtained at six locations using a Geoprobe 6620DT direct-push hydraulically powered drill rig (owned by the Baylor University Department of Geosciences) shown in Figure 2.11. These boreholes confirmed hypothesized bedrock elevation and sand and gravel thickness from geophysical interpretations. Drilling returned 2-inch diameter sediment cores in four-foot increments. Cores were sealed upon recovery to hold sediments from escaping until they were logged back in the lab according to sediment description guidelines from *Groundwater and Wells* (Driscoll, 1986). Depth to the water table and depth to the bedrock contact were recorded in the field.

A. 

B. 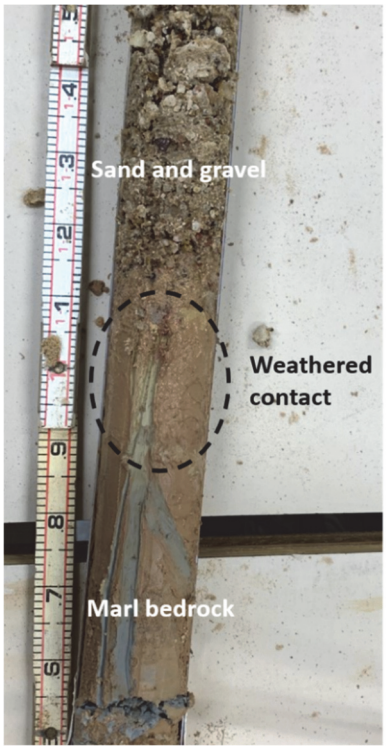

Figure 2.11. **A.** Picture of Wayne Hamilton with the Geoprobe 6620DT drill rig. **B.** Picture of a core sample showing the alluvium – Grayson Marl bedrock contact from core MCCHR 4 (ruler is in decimal feet). Note the large gravel present directly above the weathered contact.

The two methods, passive seismic and microgravity, worked together to reveal depth to bedrock and changing alluvial composition along each transect. Bouguer gravity data were more reliant on passive seismic data than vice versa, as the depth to bedrock estimates from passive seismic allowed relative changes in Bouguer gravity to be tied to particular bedrock elevations. Still, without a core sample or a well with a detailed stratigraphic log along the transect, it was difficult to ascertain exactly how much sand and gravel is present. Bouguer gravity anomalies may indicate the *change* in sand and gravel thickness, but absolute amounts of sand and gravel cannot be estimated with confidence without a calibration core or well.

CHAPTER THREE

Results and Discussion

Microgravity and passive seismic surveys were performed at five different sites throughout the Northern Segment of the Brazos River Alluvium Aquifer (Figure 3.1). The five sites are discussed in chronological order of survey completion. Each site was slightly different in ranges of depth to bedrock and alluvial composition. Hirsch Dairy had roughly 15 m of alluvium overlying a flat bedrock surface. MCC Highlander Ranch had about 5 to 8 m of terrace alluvium overlying a mostly flat bedrock profile. Moon River Ranch had as little as a meter to over 19 m of alluvium overlying a highly variable bedrock surface. Buster Chatam Road had roughly 11 m of alluvium overlying a bedrock profile that was interpreted to change in elevation by several meters along the transect. Finally, the Arcosa property, Falls County (Arcosa Falls) had about 8-11 m of alluvium overlying a mostly flat bedrock surface.

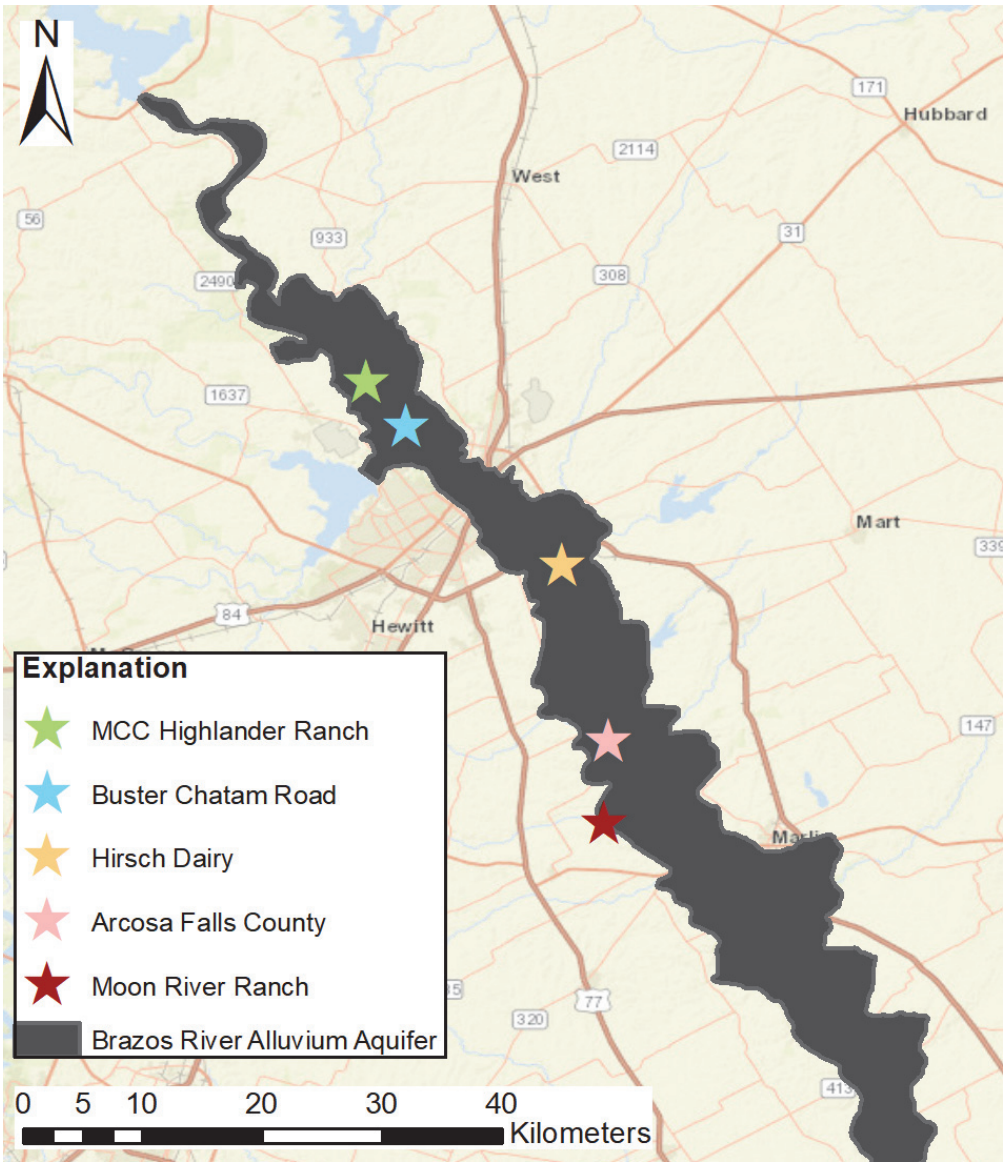

Figure 3.1. Location map of the five gravity and passive seismic surveys performed in this study.

Hirsch Dairy

Measured H/V site resonance frequencies ranged from 2.9 to 5.2 Hz and Bouguer gravity anomalies ranged by 127 µGals at the Hirsch Dairy site. Previously drilled boreholes by Jarvis (2019) reveal that there is 14 to 16.5 m of alluvium overlying shale bedrock (Ozan Fm). Alluvium thickness is greater where surface elevation is higher, suggesting that the bedrock surface is likely flat at this site.

The gravity and passive seismic survey at Hirsch Dairy, McLennan County, TX was completed June 26, 2019. The survey was planned based on the location of several pre-existing piezometers with accompanying sediment cores logged by Jarvis (2019). Gravity stations were spaced 16 meters, with passive seismic (Tromino) stations spaced 80m (one per every five gravity stations). A total of 50 gravity measurements were made at 47 stations; 14 passive seismic measurements were taken—ten along the transect and one adjacent to each piezometer. Passive seismic data were collected for 12 minutes at each station. Water level measurements were taken on the same day as the survey at the two piezometers along the transect, Upper and Middle Hirsch. The locations of gravity stations, passive seismic stations, and existing piezometers are shown in Figure 3.2.

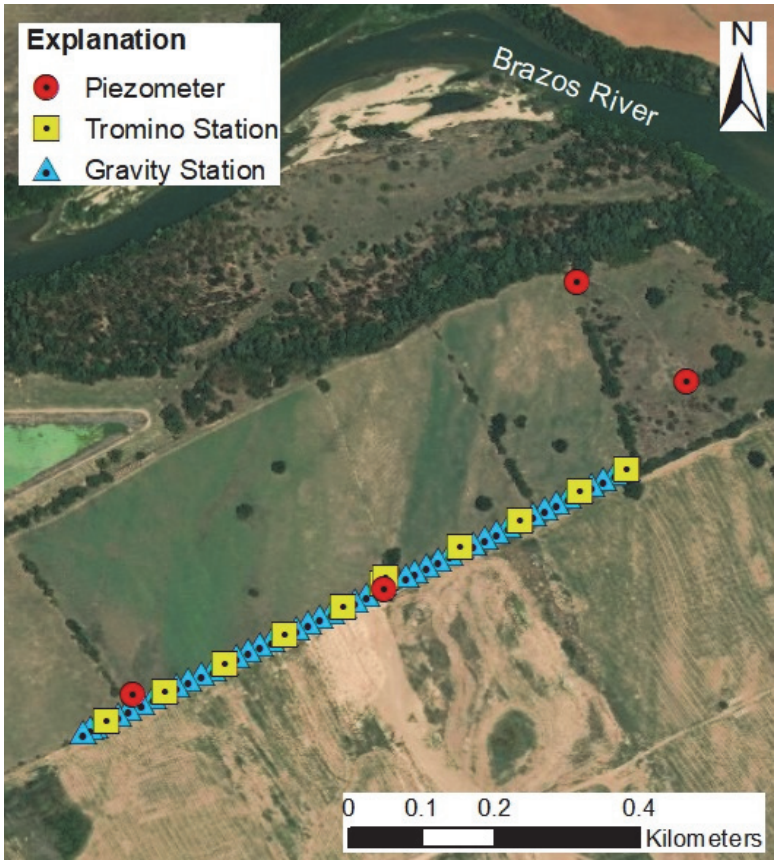

Figure 3.2. Aerial photograph of Hirsch Dairy. The locations of gravity stations, passive seismic (Tromino) stations, and piezometers are displayed.

By design, the survey passed directly over Upper Hirsch and Middle Hirsch piezometers, the far west and central piezometers displayed in Figure 3.2. The accompanying cores from the two piezometers differ slightly in depth to bedrock, alluvial sediment distribution, and saturated thickness. The biggest difference is a 2.6 m difference in the thickness of the sand and gravel layer. Depth to bedrock changes by only 0.6 m between the two piezometers; however, when surface elevation is stripped away the bedrock elevation appears to be roughly flat (Table 3.1, Figure 3.3).

Table 3.1. Comparison of the Upper Hirsch and Middle Hirsch cores logged by Jarvis, 2019 and surveyed during this study.

Site	Elevation (m)	DTB (m)	Bedrock elevation (m)	Sand & Gravel thickness (m)	Clay thickness (m)
Upper Hirsch	114.59	14.0	100.6	11.7	2.3
Middle Hirsch	115.03	14.6	100.4	9.1	5.5

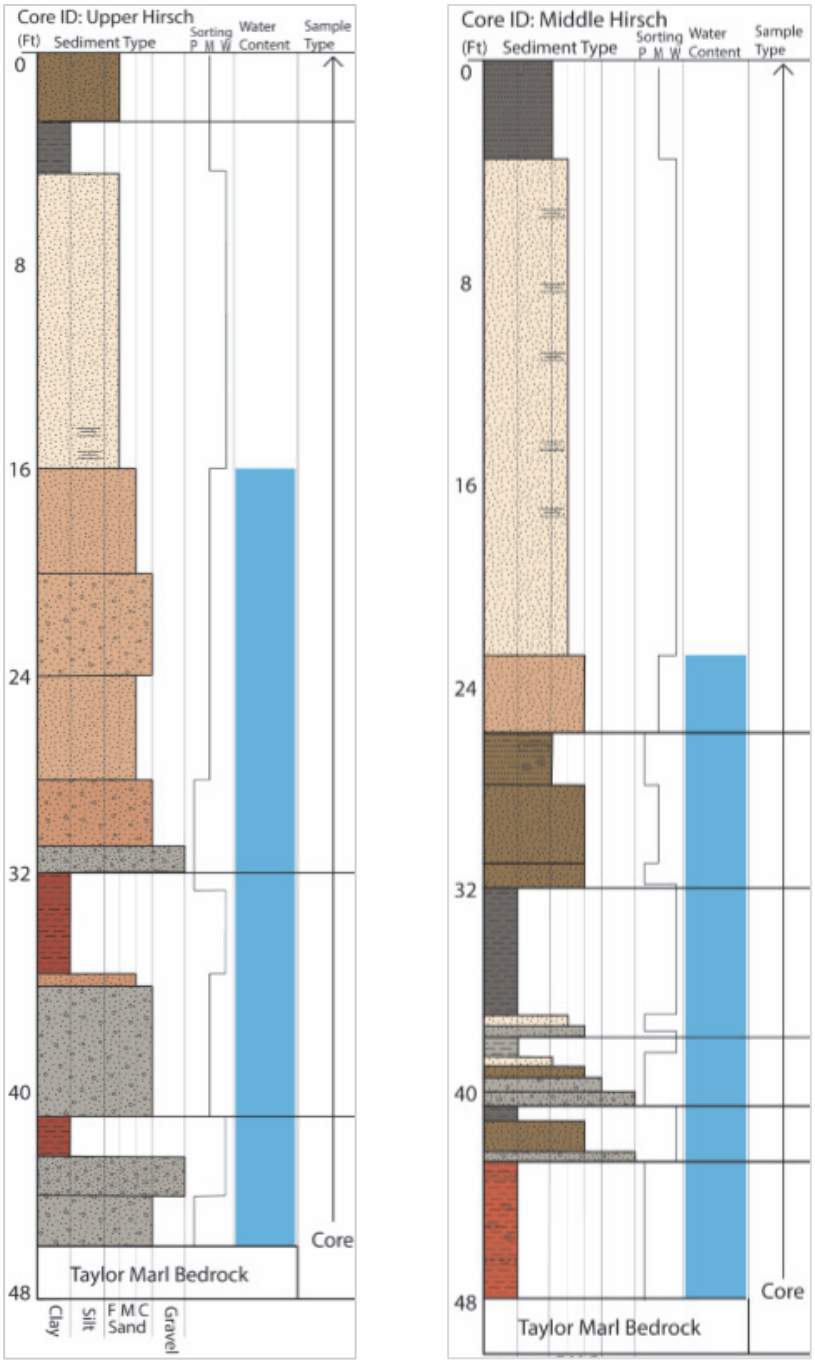

Figure 3.3. Stratigraphic logs of Upper Hirsch and Middle Hirsch from Jarvis, 2019. Upper Hirsch contains more sand and a higher saturated thickness compared to Middle Hirsch.

Once corrected for earth-tidal influences, instrument drift, surface elevation (Free air correction), near-surface soil (Bouguer correction), and regional trends in gravity, the range of corrected gravity was 127 μGals (1 $m/s^2 = 1x10^8$ μGal) at Hirsch. The lowest

gravity measurement was 21 stations (328 m) from the east end of the survey, coincidentally adjacent to the Middle Hirsch piezometer. For ease of observation and modeling, this measured gravity value was subtracted from all measurements, so that all measurements could be observed as positive anomalies. Site resonance frequencies (f_0) derived from passive seismic data ranged from 2.94 to 5.22 Hz with estimated depths to bedrock ranging from 17.2 to 10.2 m using the aquifer-wide BRAA calibration curve (Figure 2.5). HVSR curves at Hirsch had mixed clarity—seven HVSR curves showed one distinct peak frequency (Figure 3.4A), while the other seven had broad or multiple peaks (Figure 3.4B). Depths to bedrock were still estimated from the poor quality HVSR curves; however, these estimations had standard deviations sometimes an order of magnitude higher than the clear peak, good quality H/V curves.

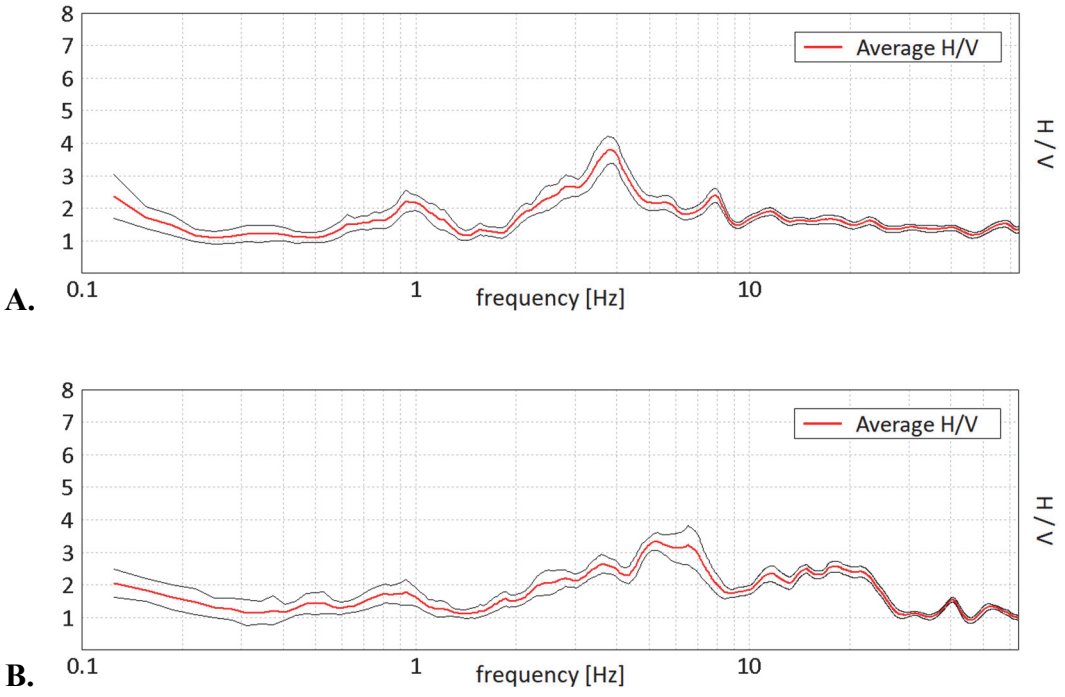

Figure 3.4. **A.** H/V curve for station Hirsch 10 showing one distinct peak frequency at 3.8 Hz with a standard deviation of 0.09 Hz. **B.** H/V curve for station Hirsch 35 showing a broad peak from 5 to 7 Hz. The maximum H/V, 5.22 Hz, has a large standard deviation (1.37 Hz).

Bouguer gravity anomalies seem to reflect changing depth to bedrock (DTB) (Figure 3.5A). The y-axes of Figure 3.5A are scaled so that each meter of bedrock depth (right axis) aligns with about 25 μGals of gravity anomaly (left axis). This represents the gravity from a 1-meter thick slab of bedrock with a density contrast of 600 kg/m^3 according to Equation 3. If the bedrock/alluvium interface is the source of each gravity anomaly, then bedrock and gravity anomaly should track in the same direction. If the assumed density contrast is correct, the magnitudes of gravity anomaly in μGals and bedrock depth in meters should also align. The core at Middle Hirsch validates the passive seismic DTB estimate, while the cores at Upper Hirsch and Lower Hirsch shows that DTB is overestimated by 2.5 meters and underestimated by 2 meters respectively. Also, the Bouguer gravity anomalies do show a slight, though not overpowering resemblance to variations in surface elevation (shown in Figure 3.5B), indicating that a slightly higher density for the Bouguer correction may need to be used to flatten anomalies by subtracting the gravity from near surface influences.

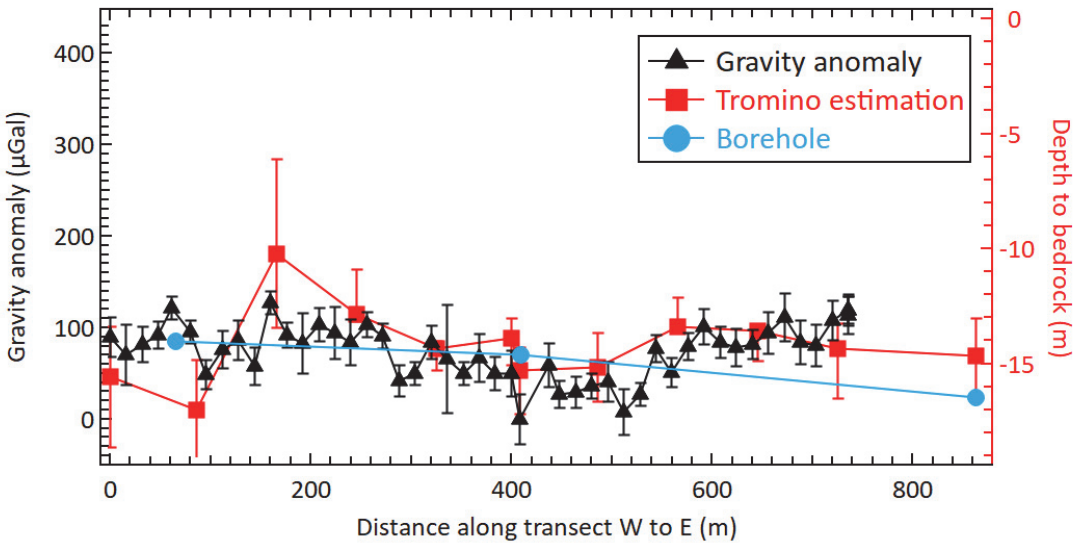

A.

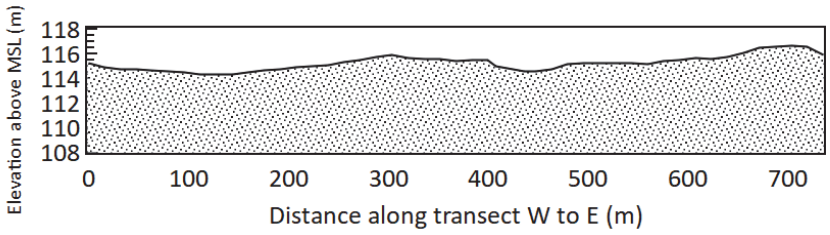

B.

Figure 3.5. **A.** Graph displaying Bouguer gravity anomalies (black triangles, left axis), depth to bedrock estimates from passive seismic (red squares, right axis), and known depth to bedrock from boreholes (blue circles, right axis). **B.** Elevation profile obtained from the RTK GPS measurements made along the Hirsch Transect. Elevation ranged by 2.34 m.

As shown in Figure 3.5A, over most of the transect gravity appears to track with depth to bedrock (if Tromino depth estimates are to be trusted), while at either end of the survey the two series separate significantly. This suggests that there are other influences on gravity besides simply a changing depth to bedrock. The other candidates are changes in alluvial sediment distribution (amounts of clay, sand, or gravel), saturated thickness, or density variations in the bedrock itself due to faulting or facies changes. First, differences in the amounts of clay, sand, and gravel seem likely as the alluvium is known to be heterogeneous (Cronin and Wilson, 1967). Furthermore, comparing the two cores shows a difference of 2.6 m in the amount of sand and gravel present (Table 3.1). Second,

looking back at the core descriptions in Figure 3.3 it appears that saturated thickness is about 6 ft (~1.5 m) different between Upper and Middle Hirsch; however, on the day of the gravity survey (6/26/19), water levels were measured with an E-line to be only 2.75 ft (~0.8 m) different—13.15 ft BGL at Upper Hirsch and 15.9 ft BGL at Middle Hirsch. Accounting for differing ground and bedrock elevations, saturated thickness was only 1.75 ft (~0.5 m) different at the two piezometers. A saturated thickness change of only 0.5 m over the 350 m distance between the two piezometers means that it is unlikely that much of the measured gravity anomaly is coming from a change in saturated thickness. Third, while it is entirely possible that the bedrock does not have exactly uniform density, there is no way (short of drilling boreholes through bedrock) to anticipate or verify those possible changes in density that would cause gravity anomalies.

Bouguer gravity anomalies at Hirsch were modeled by solving for two Bouguer slab thicknesses summed to equate to the anomaly. Many of the 160 modeled scenarios produced are unlikely to reflect what is actually at Hirsch. The modeled result was clearly wrong if the sum of the bedrock slab and sand and gravel slab thicknesses exceeded ~16 m as drilled depths to bedrock were only 14-16 m at three locations at Hirsch. There were also many scenarios in which the bedrock slab varies wildly from 0 to over 8 meters in thickness (meaning that depth to bedrock varies from about 15 m to under 7 m below the surface). While these scenarios are mathematically possible, since the bedrock is essentially the same elevation at each of the 3 boreholes, they are unlikely. In fact, only a few out of the 160 solutions come close (within 2 m) to producing results that align with the known changes in bedrock and sand and gravel from the Upper Hirsch and Middle Hirsch boreholes. The modeled scenario which best fits information from the two

boreholes is shown in Figure 3.6. Changes in passive seismic DTB estimations along the transect roughly correlate with changes in bedrock height in this scenario except for the far western Tromino stations.

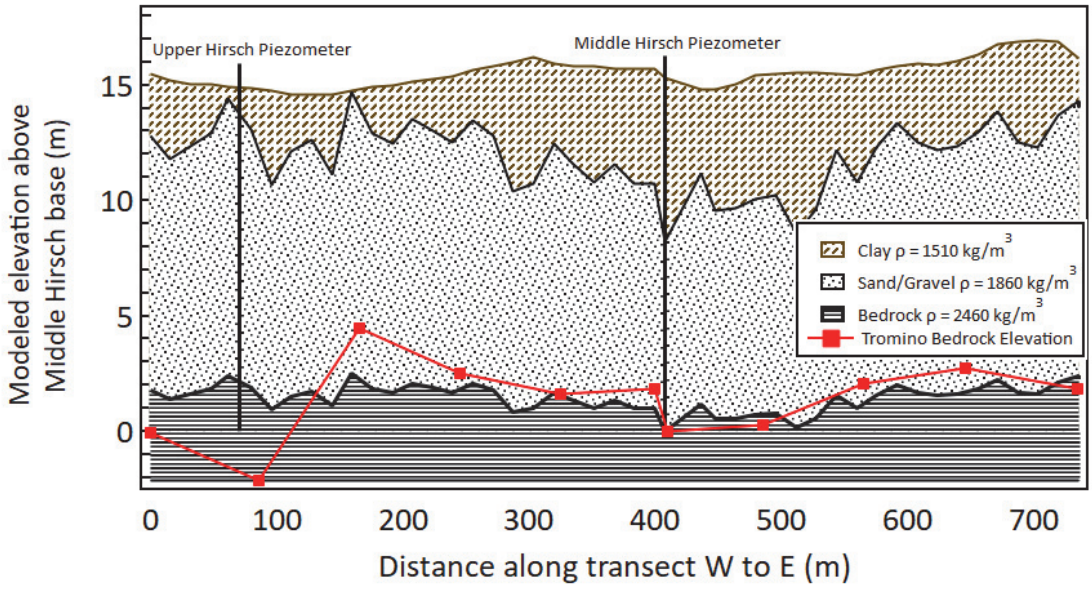

Figure 3.6. Best fit modeled scenario for the Hirsch Dairy transect. Results are calibrated to the changes in bedrock and sand & gravel thickness at Upper Hirsch and Middle Hirsch piezometers. This best fit result assumed 50% of measured gravity was from the bedrock slab and 50% was from the sand and gravel slab. The calibrated results for bedrock and sand & gravel thicknesses are within 2 m compared to cores from Jarvis, 2019.

The modeled result displayed in Figure 3.6 comes close to matching the known depth to bedrock and the sand and gravel thickness at the two piezometers; however, the 95 μGal difference in Bouguer gravity between the two piezometers could not quite be explained by just a 0.6 m change in the bedrock slab and a 2.6 m change in the sand and gravel slab (using reasonable density contrasts). The cause(s) for this are probably either that one of the gravity corrections was slightly off, such as the Bouguer correction or regional correction. Alternatively, the gravity anomaly may be real and partially caused by deeper variations in bedrock density.

MCC Highlander Ranch

Measured H/V site resonance frequencies ranged from 5.6 to 6.5 Hz at MCC Highlander Ranch (MCC HR), suggesting the alluvium is thinner than at the Hirsch Dairy site. Bouguer gravity anomalies ranged by 165 μGals along the NW – SE transect and 105 μGals along the NE – SW transect. Four confirmation boreholes drilled to bedrock at MCC HR reveal that there is 5.3 to 7.6 m of mostly sandy alluvium over a marl bedrock interpreted to be the Grayson Marl formation. Like at the Hirsch Dairy site, alluvium thickness correlates with elevation, suggesting that the bedrock surface may be relatively flat.

The gravity and passive seismic survey at MCC Highlander Ranch (MCC HR), McLennan County, TX, was planned based on land access to an open field in a young terrace/ Brazos River Alluvium setting. The survey was completed on June 25 and June 28, 2019. Gravity stations were spaced 10 meters, with passive seismic (Tromino) stations spaced 50 m (one per every five gravity stations). A total of 101 gravity measurements were made at 95 stations. Twenty-one passive seismic measurements were taken—11 along the NW-SE transect and 10 along the NE-SW transect. Passive seismic data were collected for 12 minutes at each station. One water level measurement was taken at the piezometer located on the northwest edge of the field with a depth to water of 3.17 m below ground surface. Two nearby wells were located during site reconnaissance in the Texas Water Development Board database. These had well depths of 19 ft (~6 m) (east well) and 24 ft (~7 m) (south well) respectively with the south well's completion report noting that bedrock was located at a depth of 24 ft. After collecting and processing the gravity and seismic data, four borehole cores were drilled to confirm estimated depth

to bedrock and to gain insight into type and distribution of alluvial sediments. Stratigraphic logs from each of the four cores are located in Appendix 2. The locations of gravity stations, passive seismic stations, existing piezometers/ wells, and boreholes are shown in Figure 3.7.

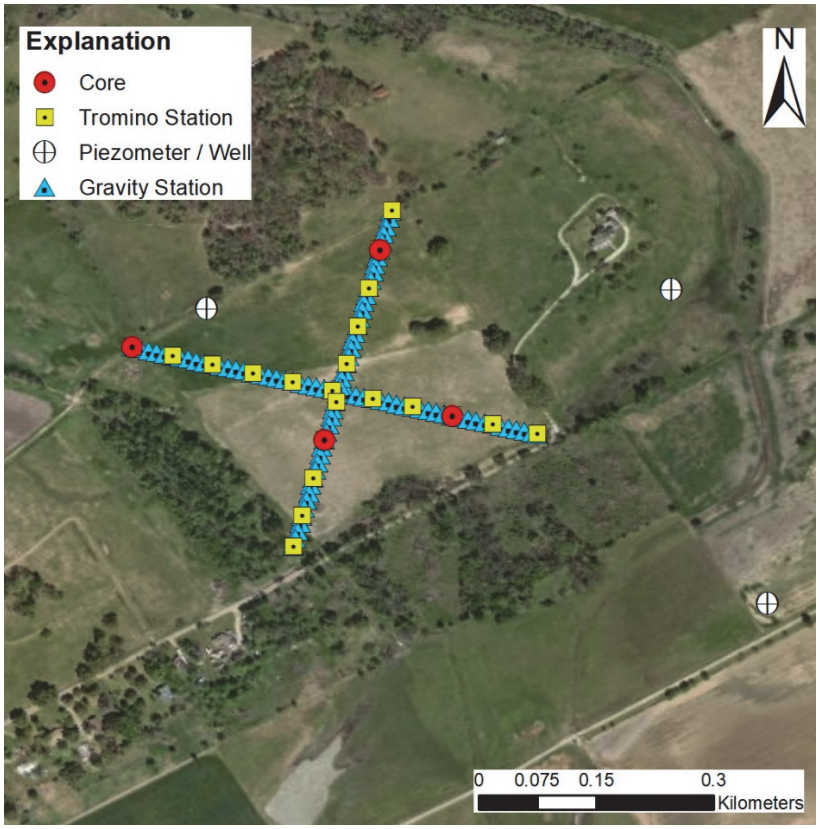

Figure 3.7. Aerial photograph of the MCC Highlander Ranch site. Gravity stations, passive seismic (Tromino) stations, and nearby wells are shown.

Once all the gravity corrections were applied, the range of measured gravity was 165 μGals (1 $m/s^2 = 1x10^8$ μGal) along the NW – SE transect and 105 μGals along the NE – SW transect. For ease of observation and modeling, the lowest measured gravity value on each transect was subtracted from all measurements so that data could be observed as positive anomalies. Measured site resonance frequencies from passive seismic data had a narrow range at MCC HR from 5.63 Hz to 6.53 Hz with estimated

depths to bedrock ranging from 9.6 m to 8.4 m using the BRAA calibration curve (Figure 2.5). HVSR curves at MCC HR showed excellent clarity—seventeen of the curves showed one distinct peak frequency (Figure 3.8A), while four had instrument-to-ground coupling issues and less trustworthy peaks with high standard deviations (Figure 3.8B). Compared to other surveys the H/V peaks at MCC HR some of the clearest and most reliable.

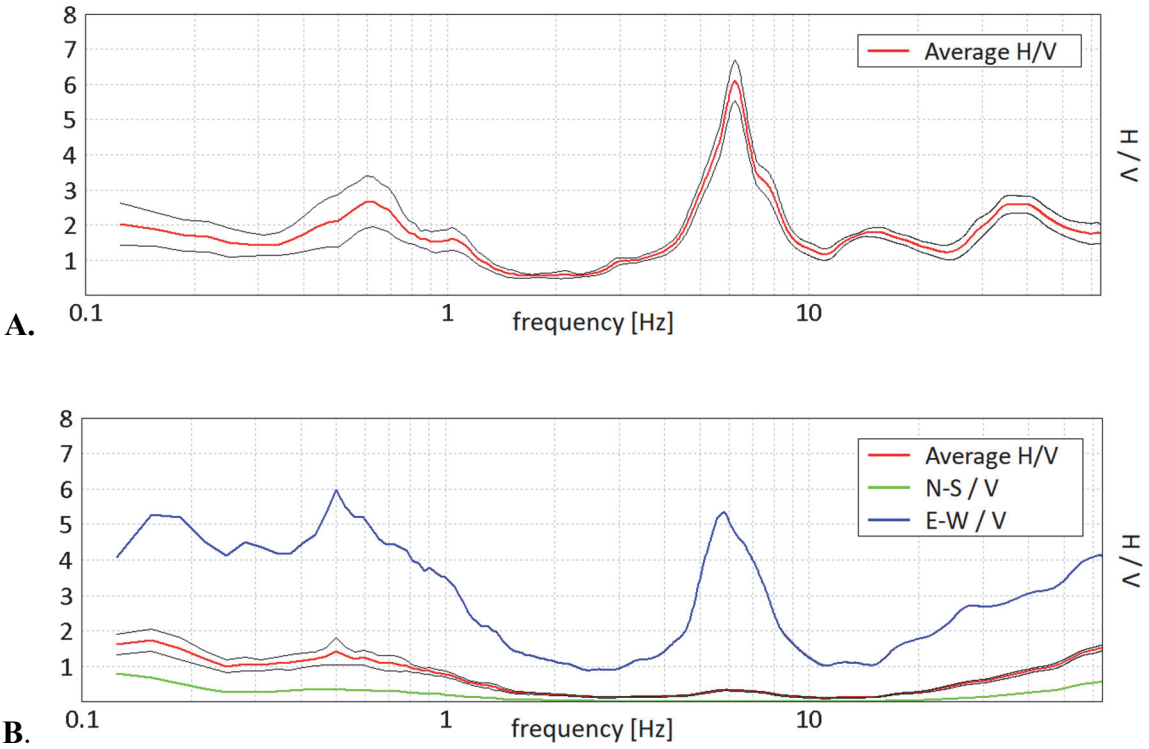

Figure 3.8. **A**. H/V curve from Tromino station MCC HR 69. The curve shows one distinct peak frequency and is high amplitude—making it a reliable H/V peak. **B.** H/V curve from Tromino station MCC HR 16. The north-south sensor did not have solid contact with the ground resulting in a flat N-S / V curve (green). The E-W sensor did have contact and shows a reasonable peak frequency.

Despite HVSR curves at MCC HR being some the best of the study, when using the BRAA calibration curve, depth to bedrock was systematically overestimated by roughly 2 to 4 m. Rearranging Equation 1 to solve for v_s reveals that the power-law

regression BRAA calibration curve used a v_s of 215-218 m/s for the DTB estimations made at MCC HR. This seems like a reasonable v_s; however, a miniature calibration curve built from only the four boreholes at MCC HR would theoretically assume a v_s of roughly 150 m/s—indicating that it may be preferable to develop a separate calibration curve for the MCC HR site to more accurately estimate bedrock depth. This custom calibration curve is shown in Figure 3.9 with the regression between the four boreholes forecasted one period positive and negative.

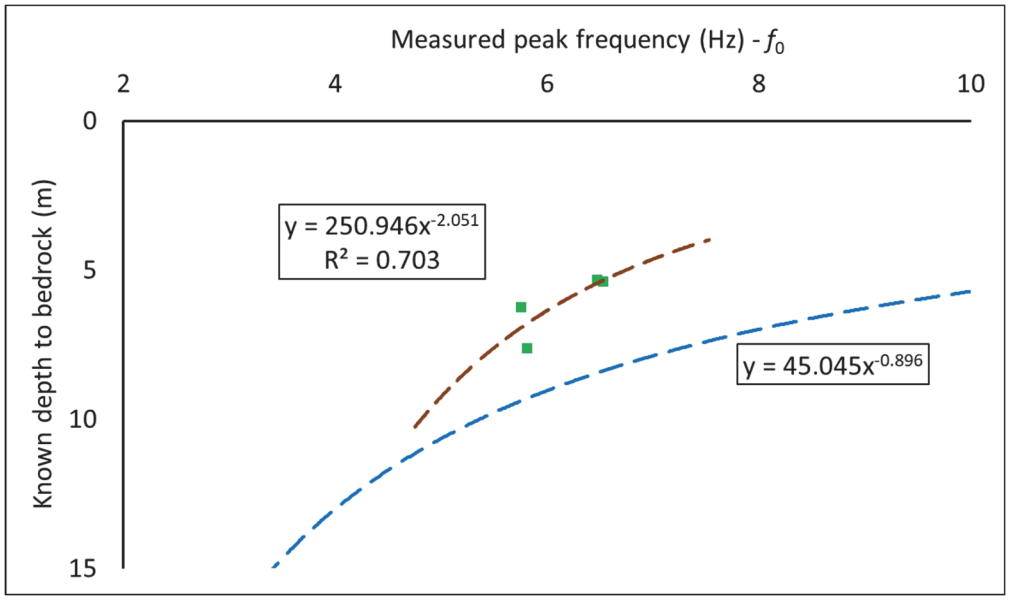

Figure 3.9. Comparison between a calibration curve made from known depth to bedrock from four cores at MCC HR, shown as green squares, and the aquifer wide, BRAA calibration curve (Figure 2.5).

Another possibility is that there is a facies change with an impedance contrast (difference in v_s) larger than the alluvium/bedrock boundary located a few meters beneath the bedrock surface that alternatively is causing the H/V peaks. The Grayson Marl bedrock at MCC HR is soft and it was somewhat surprising that such clear peaks were produced from the alluvium/bedrock contrast. The former low v_s explanation is more probable and adding just a single borehole to calibrate to at MCC HR improves passive

seismic DTB estimates significantly. Figure 3.10A displays the Bouguer gravity anomalies, estimated DTB, and borehole DTB along the northwest to southeast transect at MCC. The axes are scaled so that the two series should vary in the same direction and magnitude if changing depth to bedrock is the source of the Bouguer gravity anomaly (with a density contrast of 450 kg/m^3). Elevation is fairly constant along the transect until the southeast corner as shown in Figure 3.10B.

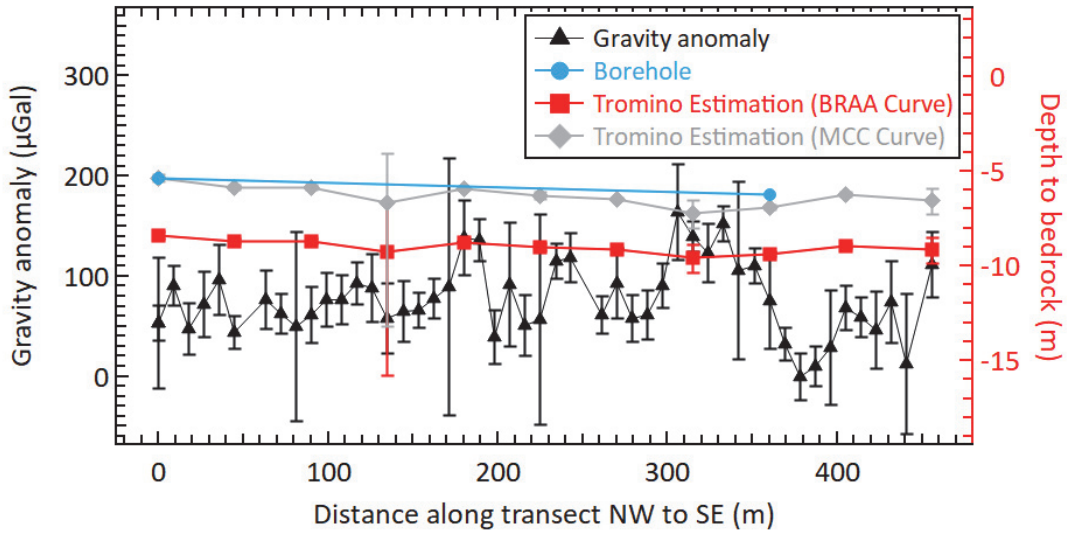

A.

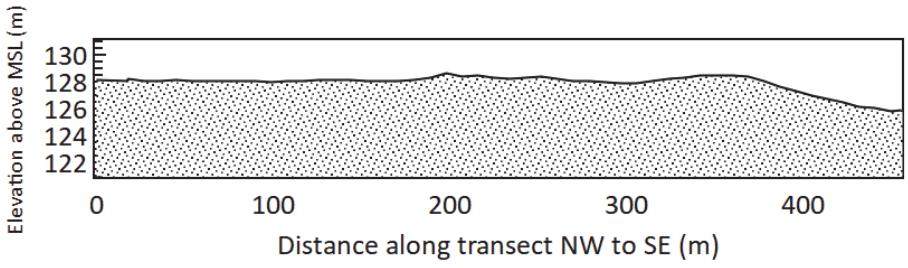

B.

Figure 3.10. **A.** Graph displaying Bouguer gravity anomalies (black triangles, left axis), depth to bedrock estimates from passive seismic with the BRAA curve and MCC Curve (red squares/grey diamonds, right axis), and known depth to bedrock from boreholes (blue circles, right axis) along the MCC HR NW–SE transect. **B.** Elevation profile for the MCC HR NW-SE transect. This transect was flat over the first 380 meters before dropping a few meters in the southeast corner of the field. Elevation ranged 2.84 m.

The Bouguer gravity anomaly along the NW to SE transect does not seem to be caused by changing depth to bedrock. The anomalies at each of the two boreholes along the NW to SE transect are the inverse of expected based on depth to bedrock from the two boreholes. As shown in Table 3.2, the anomaly at the southeast borehole (DTB = 6.2 m) is over 60 μGals higher than the anomaly at the northwest borehole (DTB = 5.4 m). Stripping elevation, bedrock elevation drops only 0.4 m between the NW core and the SE core; however, there is no ready explanation for the gravity anomaly high at the SE core.

Table 3.2. Summary of boreholes along the MCC HR NW-SE transect. Surprisingly, the Bouguer gravity anomaly was higher at the borehole with lower bedrock elevation. Both cores typify the fining upward sequence represented generally throughout the Brazos River Alluvium Aquifer. Detailed core logs are located in Appendix B.

Site	Bouguer gravity anomaly (μGals)	Elevation (m)	DTB (m)	Bedrock elevation (m)	Sand & gravel thickness (m)	Clay thickness (m)	Saturated thickness (m)
NW Core	53.2	128.14	5.4	122.7 m	3.6	1.8	3.0
SE Core	110.3	128.49	6.2	122.3 m	5.0	1.2	2.0

Bouguer gravity anomalies along Transect 1 were modeled using a simple two-layer model with sand above bedrock because of the dominance of sand (known from boreholes). Unfortunately, there is not a way to make the gravity data fit perfectly with the sand & gravel thickness and depth to bedrock data from boreholes. Increasing the density used for the Bouguer correction helps decrease the high anomaly at the SE core; however, the anomaly is too high for this to solve the problem. It is possible that the regional correction used is under-correcting for increasing gravity from the northwest to southeast, causing the SE core to show too high of an anomaly. The modeled results, shown in Figure 3.11, indicate a bedrock surface that changes up to six meters over the

course of the transect. The magnitude of that change is almost certainly an overestimation, especially since boreholes support a flat bedrock surface. The density contrast used in this scenario was 500 kg/m^3—if increased, the bedrock surface would have less drastic variations. The sharp decrease in gravity around 380 m along the transect, may indicate a dip in bedrock elevation; however, it could alternatively be caused by the section being clay dominated in that location. Unfortunately, a passive seismic measurement was not made at that location. Adjusted for elevation, passive seismic bedrock height estimation mirrors the ground surface closely.

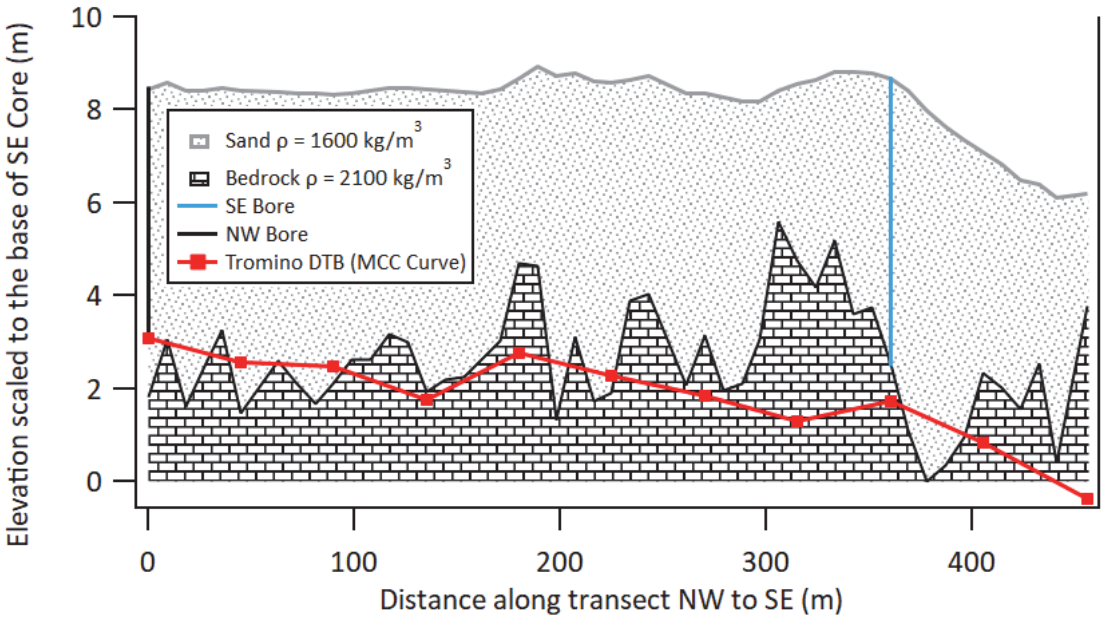

Figure 3.11. Best fit modeled scenario for MCC HR NW-SE transect. This scenario is the result using densities of 1520 kg/m^3 for sand and 2020 kg/m^3 for bedrock.

Similar to the NW to SE transect, the Bouguer gravity anomalies along the NE to SW transect (transect 2) may not be caused by a change in depth to bedrock (Figure 3.12A). The measured gravity anomaly at each of the two boreholes along this transect are similar – just 17.2 µGals higher at the northeast core (DTB = 7.6 m) than the

southwest core (DTB = 5.3). While depth to bedrock changes 2.3 meters, elevation changes by the same amount meaning that the bedrock elevation is the same at each borehole. If the Bouguer correction removed the effect of near surface sand properly, the anomaly caused by bedrock at each of these locations should be equivalent. The 17.2 µGals could then be explained by a small rise in the amount of sand and gravel at the northeast core (or is just measurement noise). The elevation profile of transect 2 is shown in Figure 3.12B. Comparing the elevation profile to the Bouguer gravity anomalies, it appears that the Bouguer correction adequately removed the influence of changing elevation along the transect.

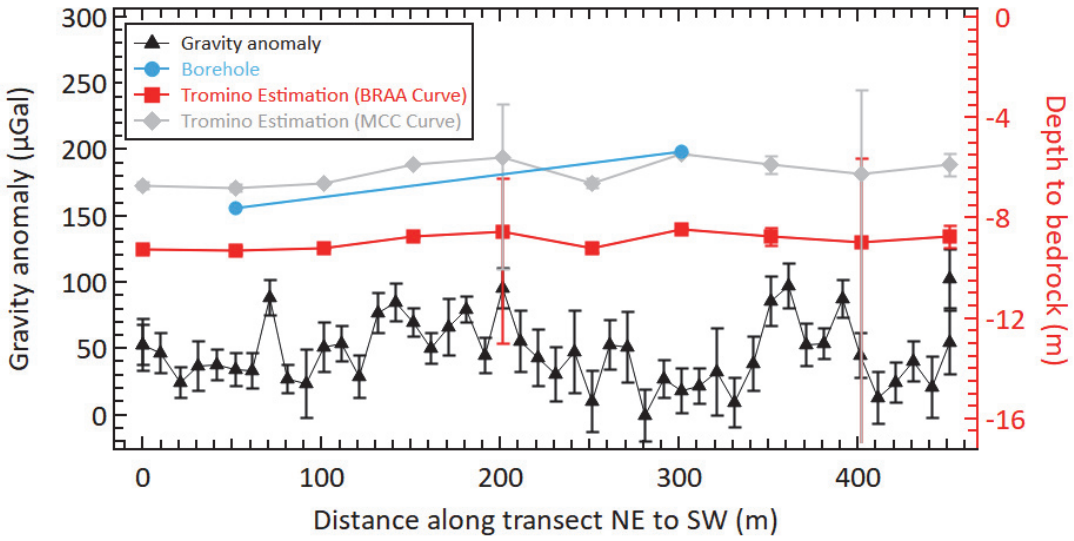

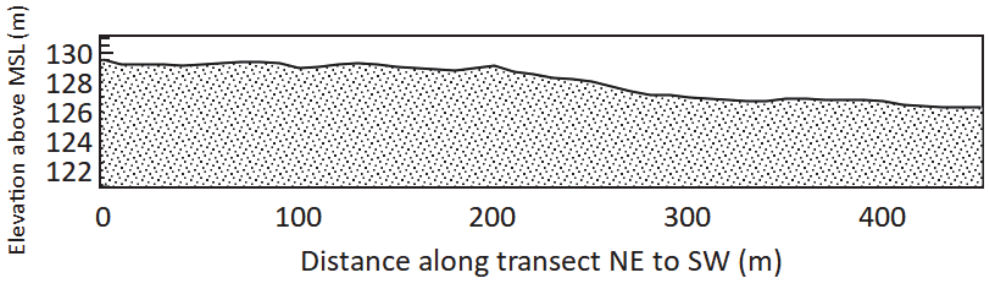

Figure 3.12. **A.** Graph displaying Bouguer gravity anomalies (black triangles, left axis), depth to bedrock estimates from passive seismic (red squares/grey diamonds, right axis), and known depth to bedrock from

boreholes (blue circles, right axis) along the MCC HR NE–SW transect. **B.** Elevation profile for the MCC HR NE-SW transect. The northeastern half of the transect is flat, with elevation dropping off by a few meters to the southwest. Elevation ranged 3.25 m.

Changes in saturated thickness could also explain some of the gravity anomaly difference between the two boreholes; however, there is no guarantee that the saturated thickness on the day the cores were drilled is the same as when the gravity survey was completed as the two were separated by several months. The two boreholes are compared in Table 3.3.

Table 3.3. Summary of boreholes along the MCC HR NE-SW transect The Bouguer gravity anomaly was slightly higher at the borehole with a greater depth to bedrock (though bedrock elevation was equivalent). Both cores typify the fining upward sequence represented generally throughout the Brazos River Alluvium Aquifer.

Site	Bouguer gravity anomaly (μGals)	Elevation (m)	DTB (m)	Bedrock elevation (m)	Sand and gravel thickness (m)	Clay thickness (m)	Saturated thickness (m)
NE Core	34.4	129.27	7.6	121.7	6.6	1.0	3.4
SW Core	18.1	127.00	5.3	121.7	5.3	0	4.1

Because of the dominance of sand (known from core), the simple, two-layer, sand/bedrock model was used, which assumed that changing bedrock produced the entire anomaly (shown in Figure 3.13). The core indicate that this is not quite true, but this modeled result is within a meter of borehole confirmed stratigraphy. Again, the highly variable bedrock surface is likely overestimated—perhaps due to a higher true density contrast, or perhaps because some of the anomaly is caused instead by changes in clay, sand, or gravel abundance. Adjusted for elevation, bedrock estimations from passive seismic display a bedrock that closely parallels the ground surface.

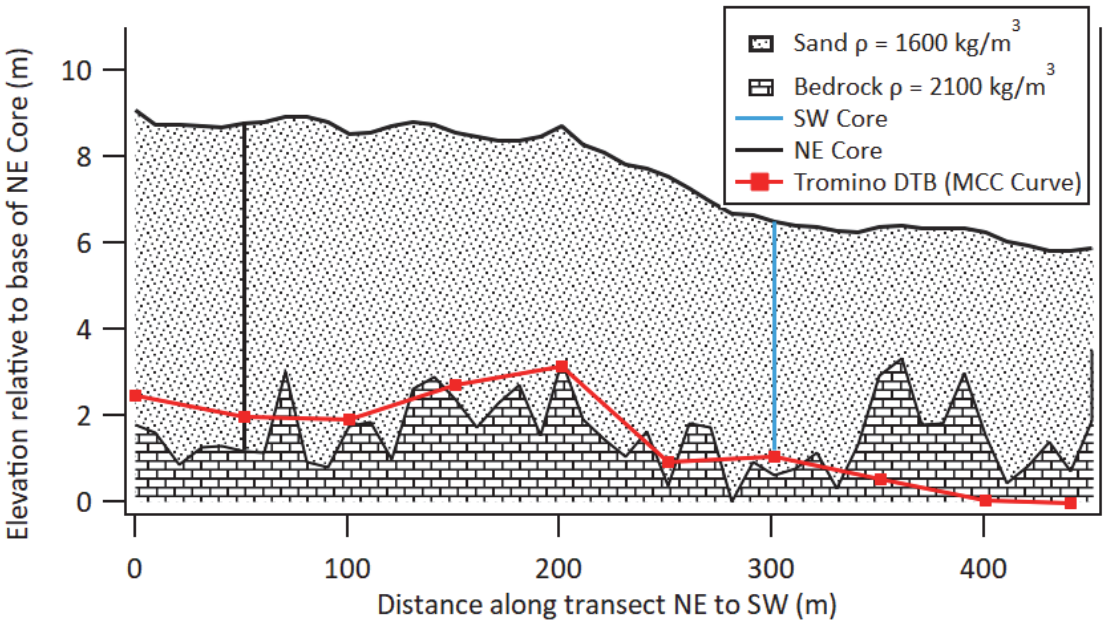

Figure 3.13. Best fit modeled scenario for MCC HR NE-SW transect. This scenario is the result from using densities of 1520 kg/m^3 for sand and 2020 kg/m^3 for bedrock.

Another way of looking at the Bouguer gravity anomalies at MCC HR is to contour them. First, the anomalies have to be recalculated, where the lowest gravity measurement over the whole survey becomes the datum and is subtracted from all of the others. Since surveys were undertaken on different days, absolute gravity may not necessarily be equivalent due to instrument drift over the few days between. To correct for this, the difference between gravity measurements at the point where the two transects cross is subtracted from all of Transect 1 (NW – SE). The resulting Bouguer gravity anomaly contour map is shown in Figure 3.14. Contours were linearly interpolated using the contour tool in Igor Pro 8 graphing software (WaveMetrics, 2019).

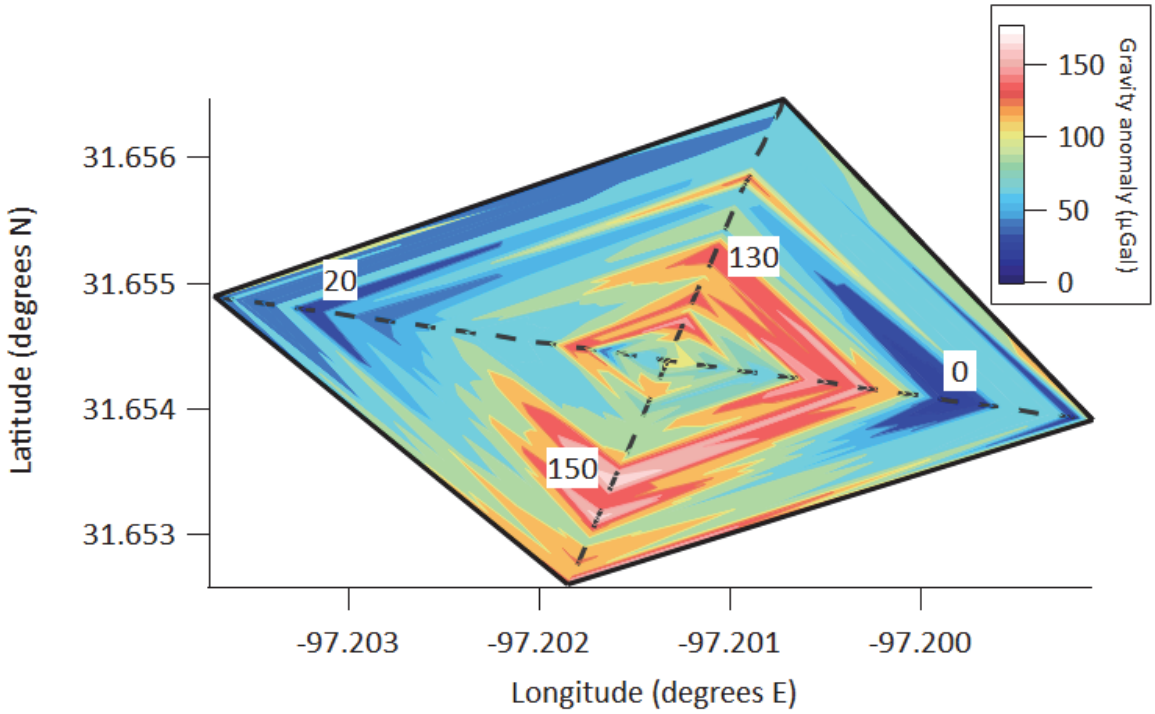

Figure 3.14. Bouguer gravity anomaly contour map for the MCC HR site. The lowest gravity measurements overall were located in the SE corner along transect 1 while the highest were in the southwest and middle of the field.

The large gravity low from transect 1 (NW-SE) stands out as a small ~ 2m channel potentially scoured in the bedrock or a feature of faulting. Gravity highs represent either thicker gravel, or higher bedrock surfaces. Interestingly, both the highest gravity (southwest) and lowest gravity (southeast) occur where surface elevation is several meters lower than the rest of the field. Finally, it is possible though unlikely, that some portion of increased gravity anomalies could be caused by increased saturated thickness. Each meter of saturated thickness with 30% porosity would create a +12.6 µGal signal.

Moon River Ranch

Measured H/V site resonance frequencies ranged from 2.5 to 26.2 Hz and Bouguer gravity anomalies ranged by 518 μGals at the Moon River Ranch site. Both measures suggest that alluvium thickness varies significantly over the length of the transect. Previously drilled boreholes by Jarvis (2019) indicate that 2.4 to 19.4 m of alluvium overlie the Wolfe City formation bedrock. Unlike the Hirsch Dairy or MCC Highlander Ranch sites, the bedrock surface elevation at Moon River Ranch changed significantly (by at least 19.5 m) while elevation only changed modestly (less than 5 m).

The gravity and passive seismic survey at Moon River Ranch was completed along CR 417, Falls County, TX on August 6, 2019. It was planned based on the location of several cores completed by Jarvis (2019) that infer a relatively steep sloping bedrock surface. This site is on the western edge of what the state defines as the Brazos River Alluvium Aquifer. The survey transect passed directly over the three core locations and crosses Cow Bayou, a medium sized creek. Gravity stations were spaced 7, 12, and 20 meters—incrementally increasing based on the known depths to bedrock at the boreholes. Passive seismic (Tromino) stations were spaced by 70 m. A total of 53 gravity measurements were made at 50 stations. Fourteen passive seismic measurements were taken, with ten along the gravity transect and four more farther to the east along CR 417A. Passive seismic data were collected for 10 minutes at each station. The locations of gravity stations, passive seismic stations along the gravity transect, and core locations are shown in Figure 3.15.

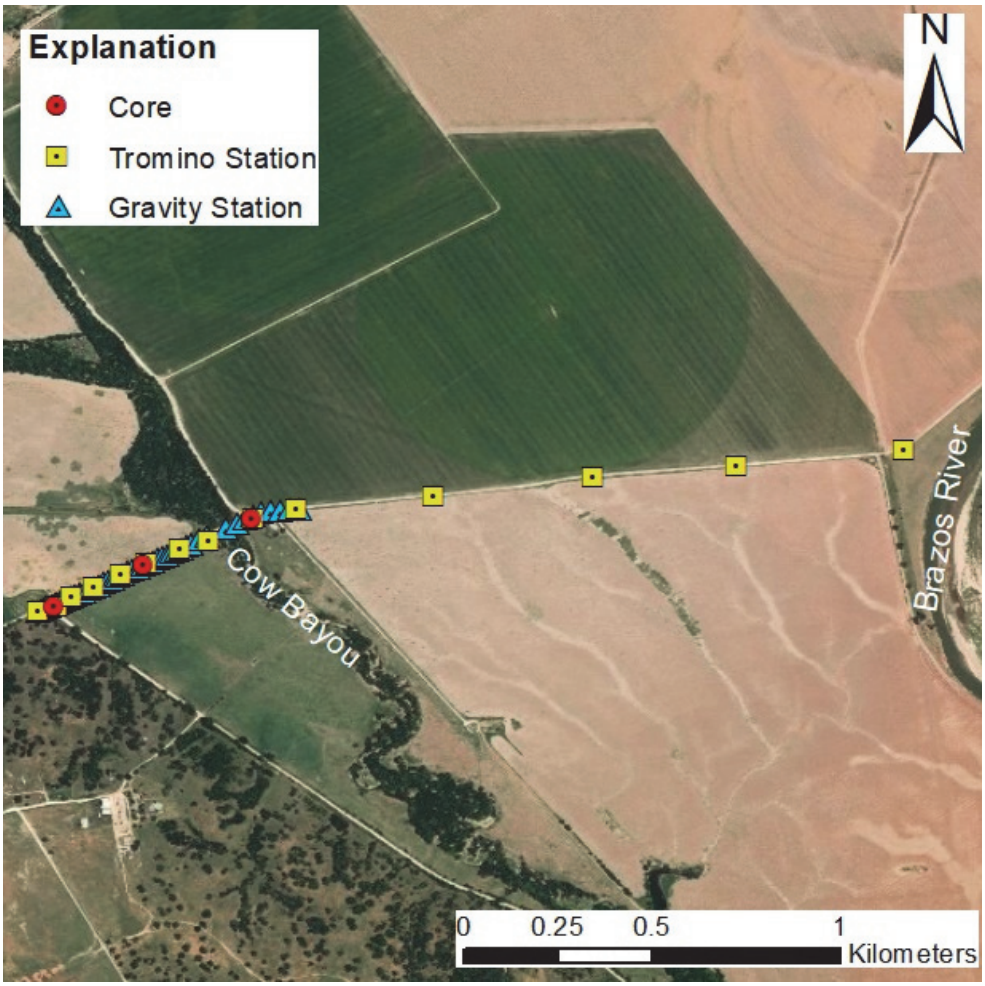

Figure 3.15. Aerial photograph of the Moon River Ranch site showing the location of gravity stations, passive seismic (Tromino) stations, and cores previously completed by Jarvis, 2019. The survey transect is divided by Cow Bayou, a medium sized creek that has downcut a roughly 8 m through the alluvium.

The three cores drilled by Jarvis (2019) at Moon River Ranch (cross-section shown in Figure 3.16) show a sloping bedrock profile from just a few meters depth on the western edge of the transect to over 19 meters at the eastern boring. The cores also suggest that alluvium west of Cow Bayou is more clay-dominated while the alluvium to the east has a thick section of sand and gravel (Table 3.4). One question of interest was whether the bedrock drops abruptly or gently to the east.

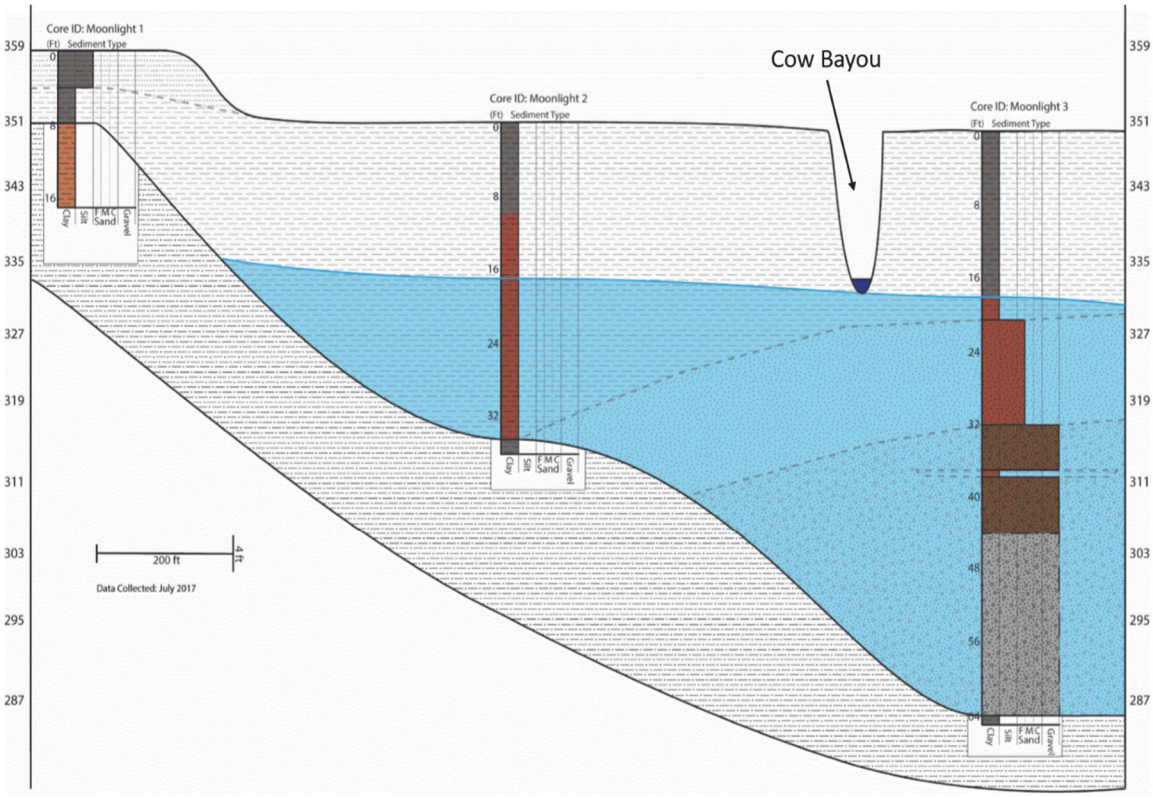

Figure 3.16. Stratigraphic cross-section of the BRAA at Moon River Ranch from Jarvis (2019) showing the bedrock surface and alluvial stratigraphy.

Table 3.4. Comparison of the three cores (west, middle, east) along the Moon River transect. The alluvium composition appears to be completely different on either side of Cow Bayou.

Site	Bouguer gravity anomaly (µGals)	Elevation (m)	DTB (m)	Bedrock elevation (m)	Sand & gravel thickness (m)	Clay thickness (m)
W Core	213.4	109.28	2.4	106.9	0	2.4
Mid Core	29.1	106.85	10.5	96.4	0	10.5
E Core	50.4	106.93	19.5	87.4	13.4	6.1

Because bedrock was so close to the surface in the far western portion of the transect, the Bouguer correction, with a density used of 1480 kg/m^3, did not remove all of the effects of the dense, near-surface bedrock. This was problematic for the regional correction, as the not fully corrected gravity values from the far west of the transect had an outsize influence on the calculated regional trend of gravity. To combat this problem,

a regression was run through the eastern 35 stations. This also helped reduce bias in the regional correction caused by having more measurements on the western end of the transect than the east.

After all gravity corrections were applied, the range of corrected Bouguer gravity anomalies was 518 μGals (1 $m/s^2 = 1x10^8$ μGal) along the Moon River Ranch transect (excluding the measurement on the bridge over Cow Bayou). The lowest gravity measurement, 28 stations (333 m) from the W of the survey, was subtracted from all gravity measurements so that all measurements could be observed as positive anomalies. Measured site resonance frequencies from passive seismic data ranged from 2.5 to 26.16 Hz with estimated depths to bedrock ranging from 19.8 m to 2.4 m using the BRAA calibration curve. Only three HVSR curves along the Moon River Ranch transect showed one distinct peak frequency (Figure 3.17A), while the other seven had broad peaks, multiple peaks, or no peak frequency at all (Figure 3.17B). The exact cause of poor passive seismic data quality at Moon River is not certain, but Tromino DTB estimations were less used in modeling gravity data along the transect because of this. A possibility is a poor impedance contrast between alluvium and bedrock caused by a gradational, weathered contact, similar to the problem Chandler and Lively (2014) faced in Minnesota measuring H/V peaks over soft saprolith.

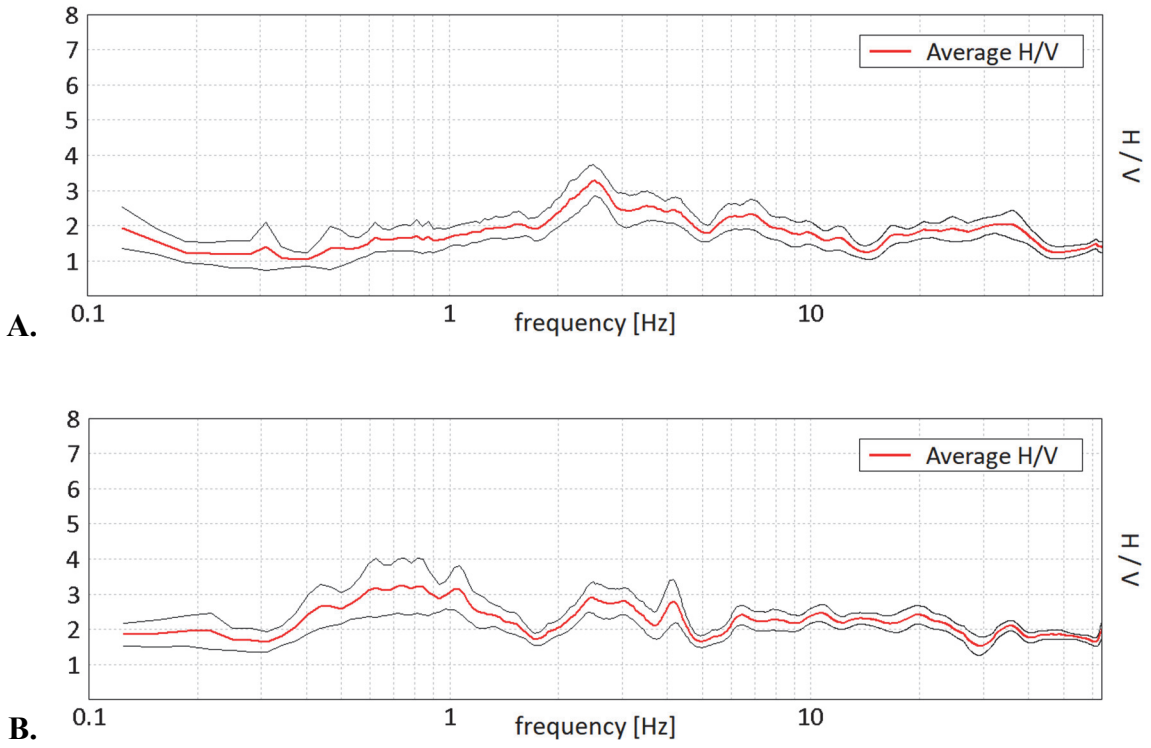

Figure 3.17. **A.** H/V Curve for Tromino station Moon River 7. The curve shows one clear peak frequency, though with low amplitude at 2.5 Hz. **B.** H/V curve for Tromino station Moon River 8. The curve has no clear peak frequency. High amplitude H/V results <1 Hz are primarily due to wind noise.

Elevation measurements along the transect, shown in Figure 3.18B, reveal that the surface elevation was mostly flat after a 4-5 m drop on the western edge. Bouguer gravity anomalies and estimated depth to bedrock values from the poor-quality passive seismic data are plotted in Figure 3.18A. The y-axes are scaled so that if the bedrock / alluvium interface is the source of each Bouguer gravity anomaly (with a density contrast of 450 kg/m^3), then bedrock and gravity anomaly should track in the same magnitude and direction along the transect. The two series track together on the western half of the transect, but not the eastern half. Depth to bedrock estimations from passive seismic succeeded at the west borehole, slightly underestimated the middle borehole, and grossly

underestimated the eastern borehole. The large gap between 450-500 m along the transect is due to the Cow Bayou bridge.

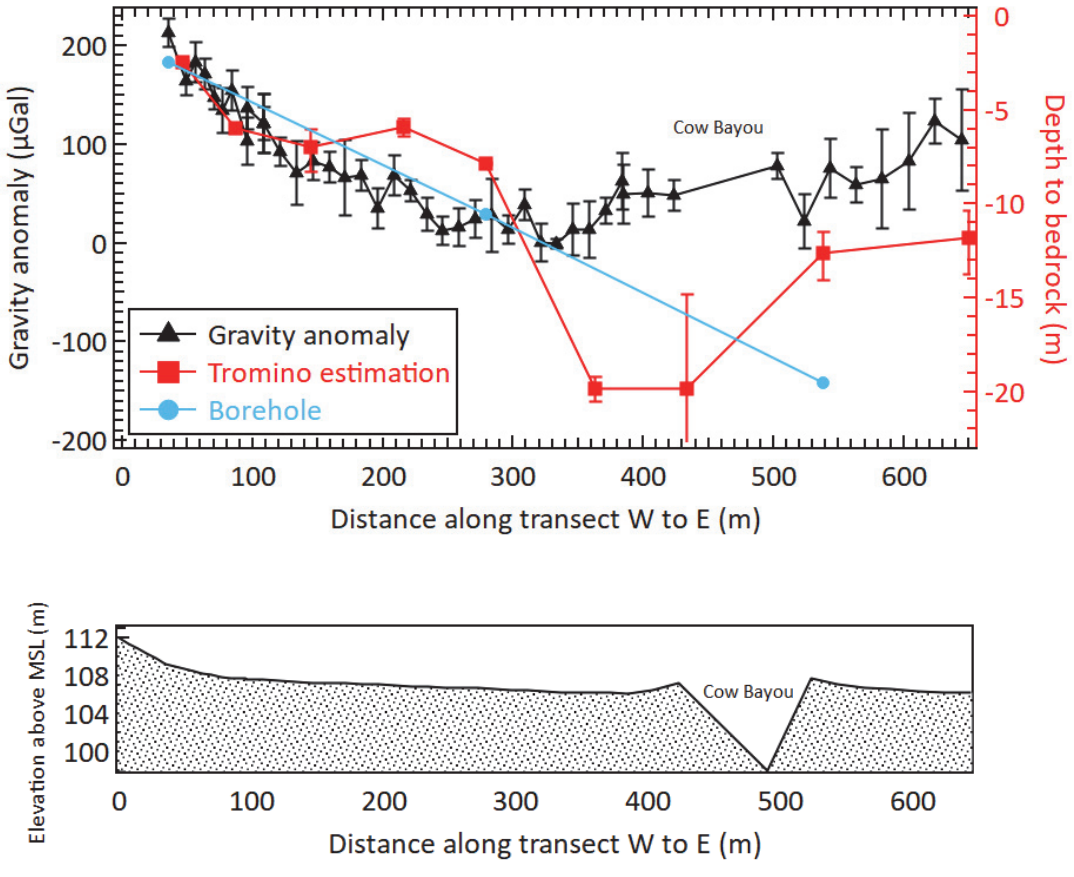

Figure 3.18. **A.** Graph displaying Bouguer gravity anomalies (black triangles, left axis), depth to bedrock estimates from passive seismic (red squares, right axis), and known depth to bedrock from boreholes (blue circles, right axis). As H/V peaks were poor quality at this site, DTB estimations are likely incorrect. **B.** Elevation profile for the Moon River Ranch transect. The land slopes down a hill on the western edge and drops a maximum of 8 meters at Cow Bayou.

While the gravity anomaly is higher at the west borehole compared to the middle borehole, this trend does not continue to the east borehole (Table 3.4). This is surprising considering the bedrock is 9 meters deeper at the east borehole than the middle borehole. Comparing the west and middle borehole first, gravity decreases by about 184 µGals and DTB increases by 8.1 m. Assuming that gravity change is only caused by changing

bedrock, the bedrock has a density of about 540 kg/m^3 higher than the overlying clay (1440 kg/m^3)—indicating that bedrock density may be roughly 1980 kg/m^3. Next, from the middle borehole to the eastern borehole gravity increases by roughly 20 μGals. This increase in gravity is counterintuitive since bedrock is 9 meters deeper at the eastern borehole. It appears that the wet sand & gravel found in the east borehole is nearly as dense as the bedrock, and much denser than overlying clay. Clay of 1440 kg/m^3, wet sand & gravel of 1840 kg/m^{3}and bedrock of 1980 kg/m^3 could fit this scenario. It is further possible that the regional correction used was not high enough magnitude to reduce the far eastern measurements appropriately. Based on the indication from boreholes, a simple, two-layer model was developed for the western half of the transect (clay vs. bedrock), while a three-layer model was made for the eastern half of the transect (clay, sand & gravel, bedrock) (Figure 3.19). The six stations on the far western part of the transect were removed from modeled results since they produced gravity anomalies too high to be modeled with reasonable Bouguer slab densities.

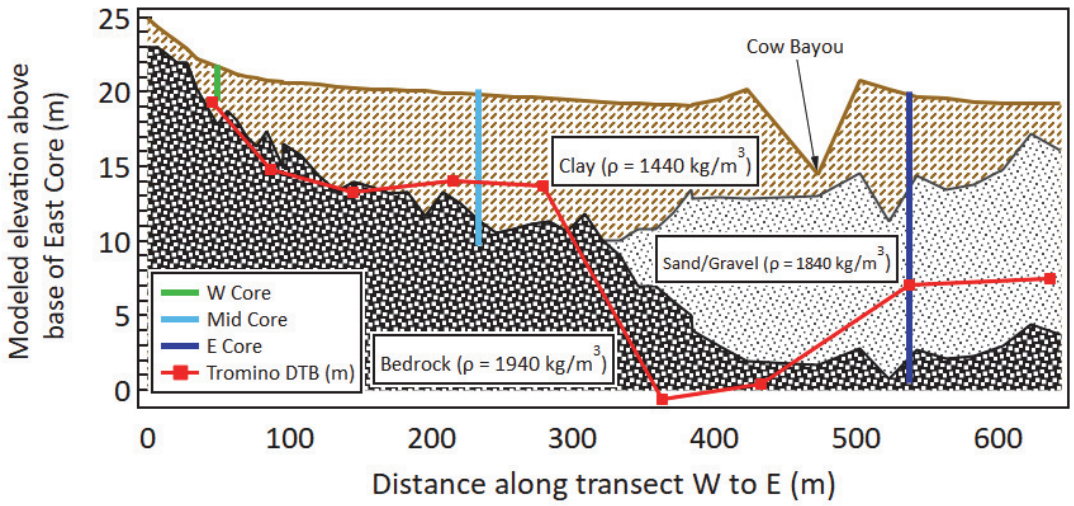

Figure 3.19. Best fit modeled scenario for the Moon River Ranch transect. This scenario is the result of a two-layer model for the west half of the survey combined with the three-layer model for the east half.

Regrettably, it is still difficult to determine the profile of the 9 m decrease in bedrock elevation between the middle borehole and eastern borehole as it is partially masked by the 100 m gap in gravity and passive seismic stations due to the Cow Bayou bridge. The passive seismic DTB estimates suggest that bedrock drops suddenly around 300-370 m along the transect; however, it is difficult to know exactly where and if this is a sharp or gradual drop in bedrock elevation (both scenarios can fit measured gravity anomalies). While this modeled result is plausible and fits the gravity data relatively well, without boreholes it would have been difficult to anticipate the large drop in bedrock elevation to the east as gravity anomalies were slightly higher in the east than in the west (usually indicating shallower bedrock) and passive seismic depth estimates also indicated shallower bedrock. The middle and eastern boreholes were essential for coming to this modeled result.

Finally, the four passive seismic measurements made to the east of the combined gravity and passive seismic transect at Moon River Ranch (shown in Figure 3.15) suggest that 10.8 to 13.2 m of alluvium exists in this location (using the aquifer-wide calibration curve). However, these estimates are likely underestimates of true depths to bedrock as the DTB estimate made for the east core underestimated true DTB by 6 meters. Hence depths to bedrock of approximately 17 to 19 m are more likely to the east of the combined gravity and passive seismic transect.

Buster Chatam Road

Measured H/V site resonance frequencies ranged from 4.0 to 11.7 Hz and Bouguer gravity anomalies ranged by 112 μGals at the Buster Chatam Road site. The vast majority of site resonance frequencies were around 4 to 6 Hz suggesting that alluvium

thickness is thinner than at Hirsch Dairy but thicker than at MCC Highlander Ranch. Existing water wells near the survey transect suggest that approximately 11 to 14 m of alluvium overlie shale bedrock in this area. Passive seismic data, Bouguer gravity anomalies, and elevation measurements suggest that the bedrock surface roughly mirrors changing elevation along the Buster Chatam transect.

The gravity and passive seismic survey along Buster Chatam Road, was completed on October 25, 2019 (passive seismic) and February 21, 2020 (gravity). The survey was planned to explore a bend on the eastern side of the Brazos River northwest of Steinbeck Bend, McLennan County, TX. Gravity stations were spaced 25 meters, with passive seismic (Tromino) stations spaced roughly 50 m (every other gravity station). A total of 61 gravity measurements were made at 48 stations; 37 passive seismic measurements were taken—22 along the gravity transect and 16 at other locations in this bend of the Brazos. Passive seismic data were collected for 12 minutes at each station. Several nearby wells were identified using the TWDB Water Well Database with depths of 37–45 ft (~11–14 m) to bedrock. The closest well, just 80 m southeast of the transect reported a depth to bedrock of 37 ft (~11 m) in the well report and serves as the only calibration station along the transect. The locations of gravity stations, passive seismic stations, and nearby wells are shown in Figure 3.20.

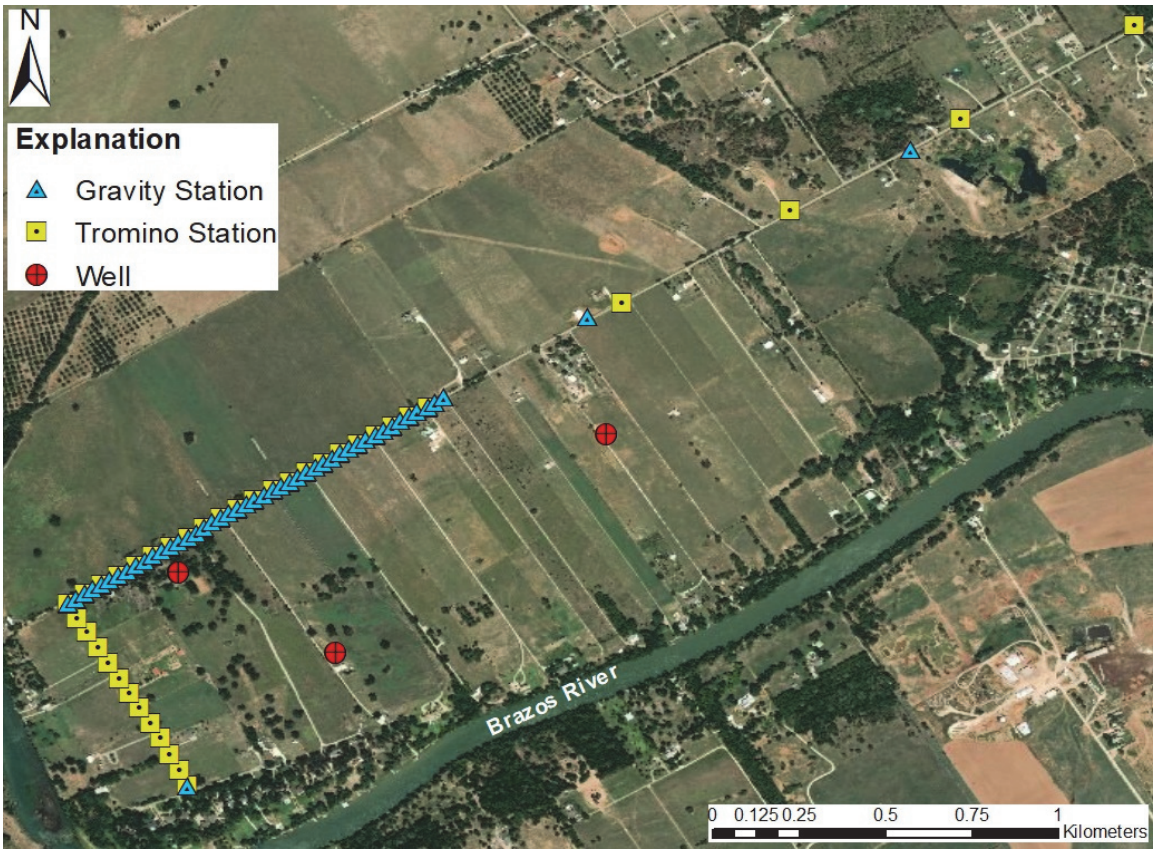

Figure 3.20. Aerial photograph of the Buster Chatam Rd survey showing the location of gravity stations, passive seismic (Tromino) stations, and nearby wells. The main, combined gravity and passive seismic transect was about 1100 m long.

The range of corrected Bouguer gravity at Buster Chatam was 112 μGals (1 m/s^2 = $1x10^8$ μGal). The lowest gravity measurement was subtracted from all measurements, so that all measurements could be observed as positive anomalies. Measured site resonance frequencies from passive seismic data ranged from 3.97 to 11.72 Hz with estimated depths to bedrock ranging from 13.1 to 4.9 m using the BRAA calibration curve. HVSR curves at Buster Chatam typically had good clarity with 32 of 37 having one distinct peak frequency (Figure 3.21A). A few Tromino stations had H/V curves with broad or multiple peaks (Figure 3.21B). The stratigraphic log from the well located about 80 m from Buster Chatam 7 (shown in Table 3.5) indicates that 4.3 m of sand and gravel

are located on top of the bedrock at the base of the alluvial section. The well report also noted the water level being 4.6 m below ground surface as of May 2009. No water level measurements were obtained or cores drilled during the Buster Chatam survey.

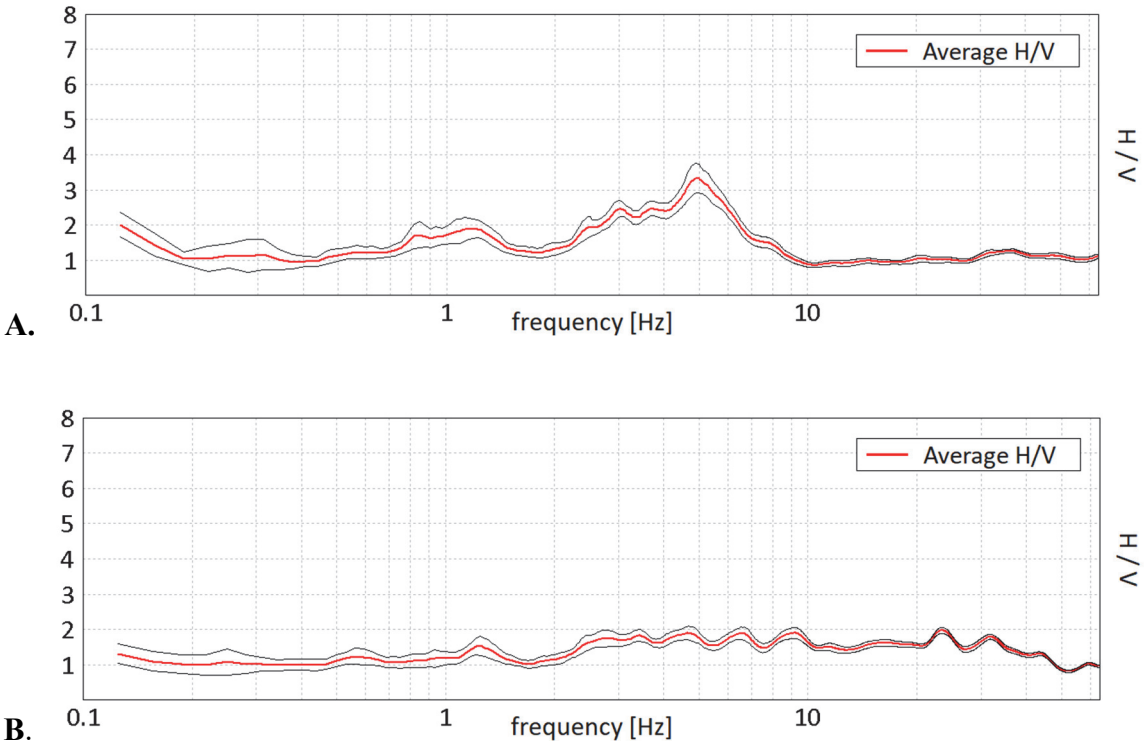

Figure 3.21. **A.** H/V curve for Tromino station Buster Chatam 2 showing one distinct peak frequency at 4.94 Hz. **B.** H/V curve for Tromino station Buster Chatam 19. This curve has no identifiable peak frequency and cannot be used to estimate bedrock depth.

Table 3.5. Lithologic log for State of Texas well No. 182138. These data were acquired from the well report filed with TWDB.

Top (m)	Bottom (m)	Description
0	7.0	Sandy Clay
7.0	11.3	Sand and Gravel
11.3	18.3	Shale

The elevation along the transect was stair-like with two flat benches separated by a ~4 m hill (Figure 3.22B). Bouguer gravity anomalies, estimated depth to bedrock values

from passive seismic data, and the depth to bedrock at the nearest well to the Buster Chatam transect are plotted in Figure 3.22A. The y-axes are scaled so that if the bedrock/alluvium interface is the source of each gravity anomaly (with an assumed 450 kg/m^3 density contrast), then bedrock and gravity anomaly should track in the same magnitude and direction along the transect. The depth to bedrock estimates from the Tromino align closely with the one known depth to bedrock from the nearby well (80 m from the transect).

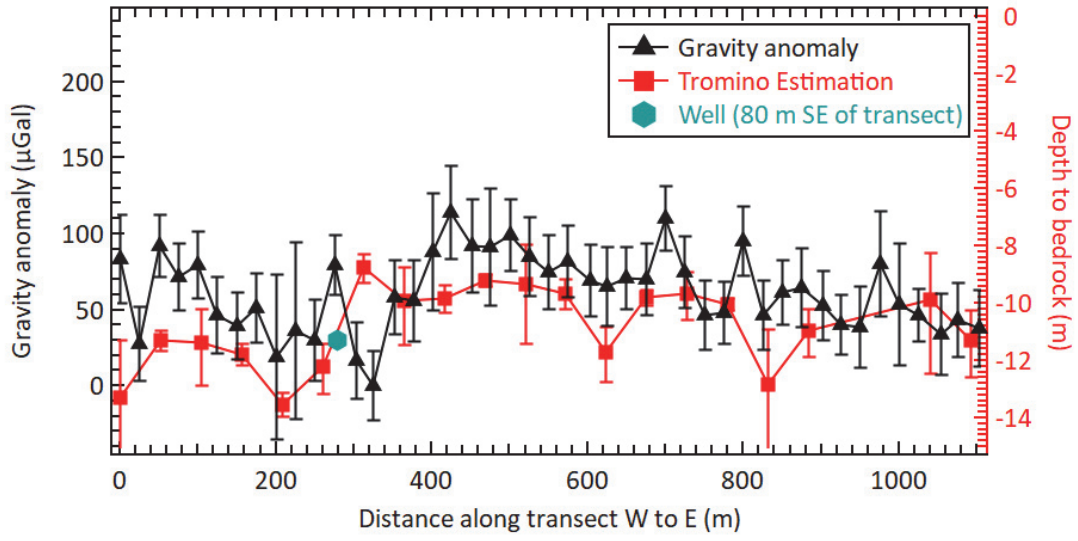

A.

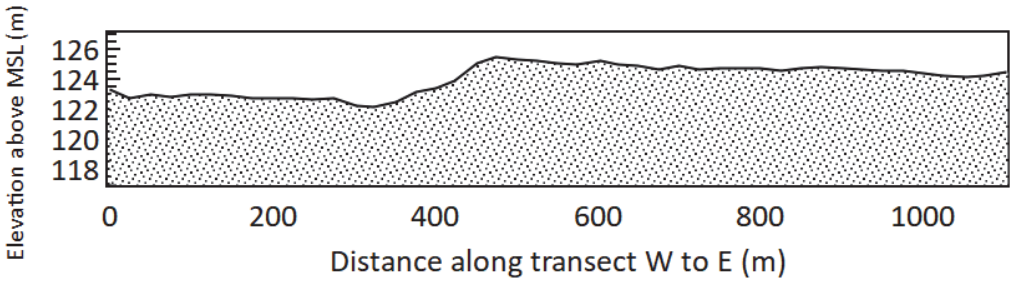

B.

Figure 3.22. **A.** Graph displaying Bouguer gravity anomalies (black triangles, left axis), depth to bedrock estimates from passive seismic (red squares, right axis), and depth to bedrock from the one nearby well (aqua hexagon, right axis). **B.** Elevation profile along Buster Chatam Rd. Elevation ranged by 3.4 m.

The gravity anomalies at Buster Chatam (left axis) appear to follow the depth to bedrock estimated from passive seismic data (right axis); however, at a few locations the two series diverge, indicating that other sources may contribute to the gravity anomaly. Gravity data were modeled with a 3-layer, two Bouguer slab model. The scenario that roughly aligned best with passive seismic depth to bedrock estimates is displayed in Figure 3.23. Passive seismic DTB estimates, adjusted for elevation in Figure 3.23, display an exaggerated resemblance to topography.

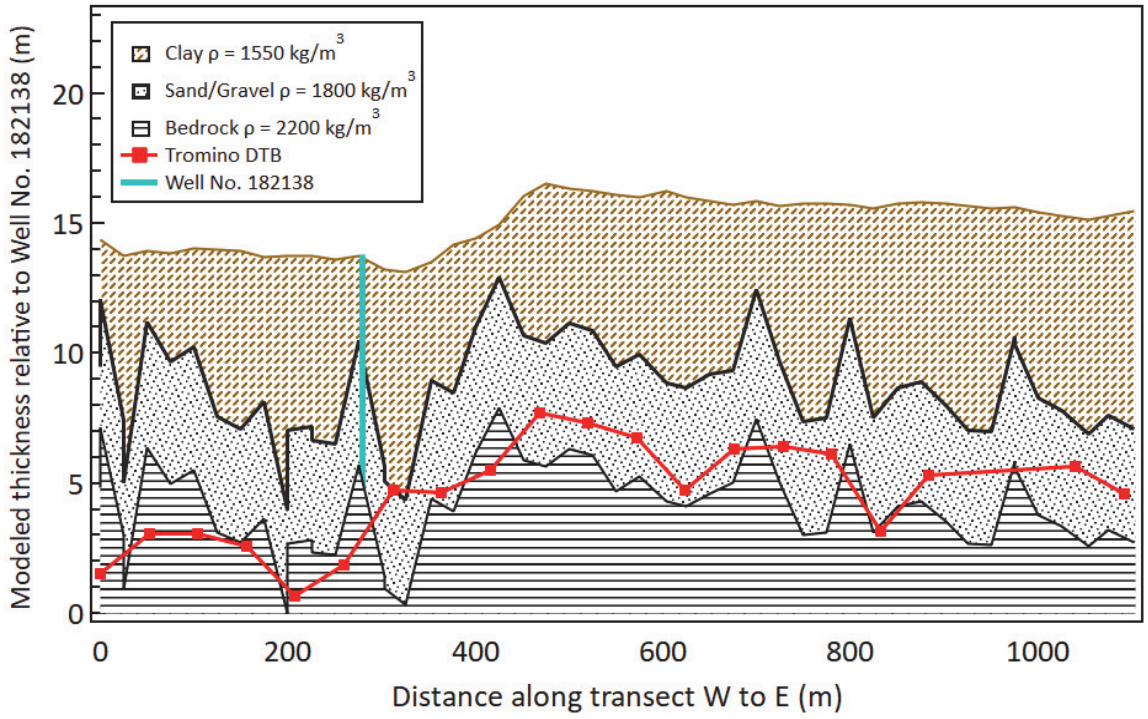

Figure 3.23. Best fit modeled result for the Buster Chatam Rd transect. This best fit result assumed 90% of measured gravity was from the bedrock slab and 10% was from the sand and gravel slab. Depth to bedrock estimations from passive seismic data are also plotted for comparison.

Assuming the modeled result in Figure 3.23 is roughly correct, the most interesting feature is located around 320 m along the transect where gravity anomaly is lowest, yet bedrock surface from passive seismic has a local maximum. A couple of

plausible explanations exist for this result. First, it is possible that there is a small scoured channel in the bedrock that causes the dip in gravity. In this case, the passive seismic high could be explained by the possibility that the highest impedance contrast is between clay and gravel instead of alluvium bedrock. It is also possible that the reverse scenario is true – where bedrock does rise a few meters according to passive seismic and the alluvial section is full of clay which causes the dip in gravity.

The four passive seismic measurements to the east of the combined gravity and passive seismic transect (Figure 3.20) suggest that alluvium thickness thins to the east to between 4.9 m to 7.8 m. Finally, the bedrock profile for the River Bend Rd transect, perpendicular to the combined gravity and passive seismic transect, is displayed in Figure 3.24. This transect was only surveyed with passive seismic and DTB estimates range from about 9.5 to 13 m. The low point at 100 m from the S end is the most interesting feature, with an estimated depth to bedrock over 13 meters.

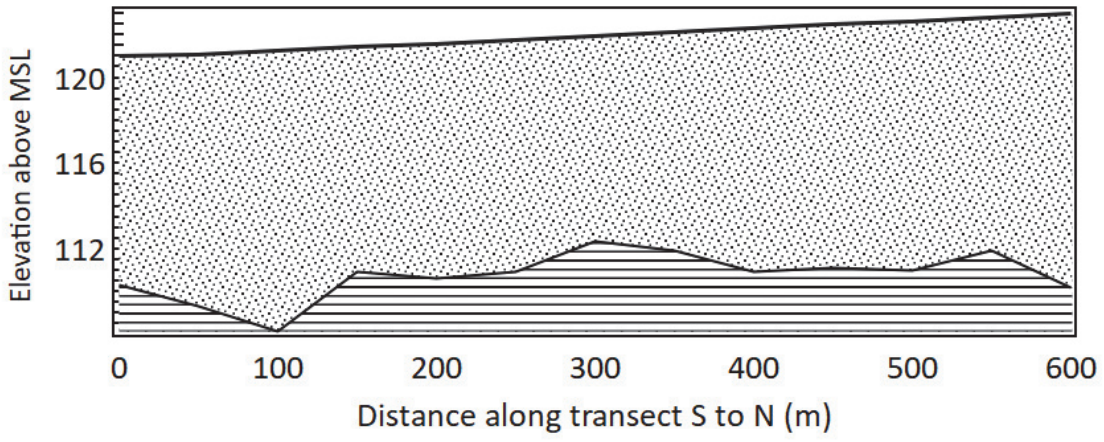

Figure 3.24. Bedrock elevation profile for the River Bend Road transect (perpendicular to Buster Chatam Rd) derived from the passive seismic DTB estimates. The surface elevation is an interpolation between surveyed points on either end of the transect.

Arcosa Property, Falls County, Texas

Measured H/V site resonance frequencies ranged from 4.3 to 7.2 Hz at the Arcosa Falls site suggesting that alluvium thickness was similar to alluvium thickness at the Buster Chatam site. Bouguer gravity anomalies ranged by 118 μGals (1 $m/s^2 = 1x10^8$ μGal) along the northwest transect and 107 μGals along the southeast transect. Confirmation boreholes indicate that 8.3 to 11.1 m of alluvium overlie a shale bedrock (Ozan Fm). Alluvium thickness is greater at the higher elevation borehole, but not as much as the change in elevation indicating that bedrock elevation may vary slightly at the Arcosa Falls site.

The gravity and passive seismic survey at the Arcosa property was planned after gaining land access to a property owned by Arcosa, Inc in Falls County, TX. The survey was completed on February 21 and 22, 2020. This site is squarely inside the Brazos River Alluvium Aquifer boundaries and is adjacent to the Brazos River and Bull Hide Creek. No previous boreholes had been drilled at this site, so transects were planned with the intention to cover the most ground and ideally find a buried channel. Gravity stations were spaced 20 m with passive seismic (Tromino) stations spaced 80 m with a few spaced 100 m apart. A total of 84 gravity measurements were made at 77 stations. Twenty-one passive seismic measurements were taken—eight along the NW transect and thirteen along the SE transect. Passive seismic data were collected for 10 or 12 minutes at each station. Two boreholes were drilled to obtain core samples and confirm passive seismic depth to bedrock estimations. The locations of gravity stations, passive seismic stations, and core locations are shown in Figure 3.25.

Figure 3.25. Aerial photograph of the Arcosa Falls survey site displaying gravity stations, passive seismic (Tromino) stations, and core locations.

Once all the gravity corrections were applied, the range of corrected Bouguer gravity was 118 μGals (1 $m/s^2 = 1x10^8$ μGal) along the northwest transect and 129 μGals along the southeast transect. For ease of observation and modeling, all measurements were converted to positive anomalies. Measured site resonance frequencies from passive seismic data ranged from 4.28 Hz to 7.19 Hz with estimated depths to bedrock ranging from 12.2 m to 7.7 m using the BRAA calibration curve. HVSR curves at Arcosa Falls were generally clear. Sixteen of the curves showed one distinct peak frequency (Figure 3.26A), while only five had broad peaks, multiple peaks, or no identifiable peak (Figure

3.26B). Compared to other surveys the H/V peaks at Arcosa Falls were slightly better than average.

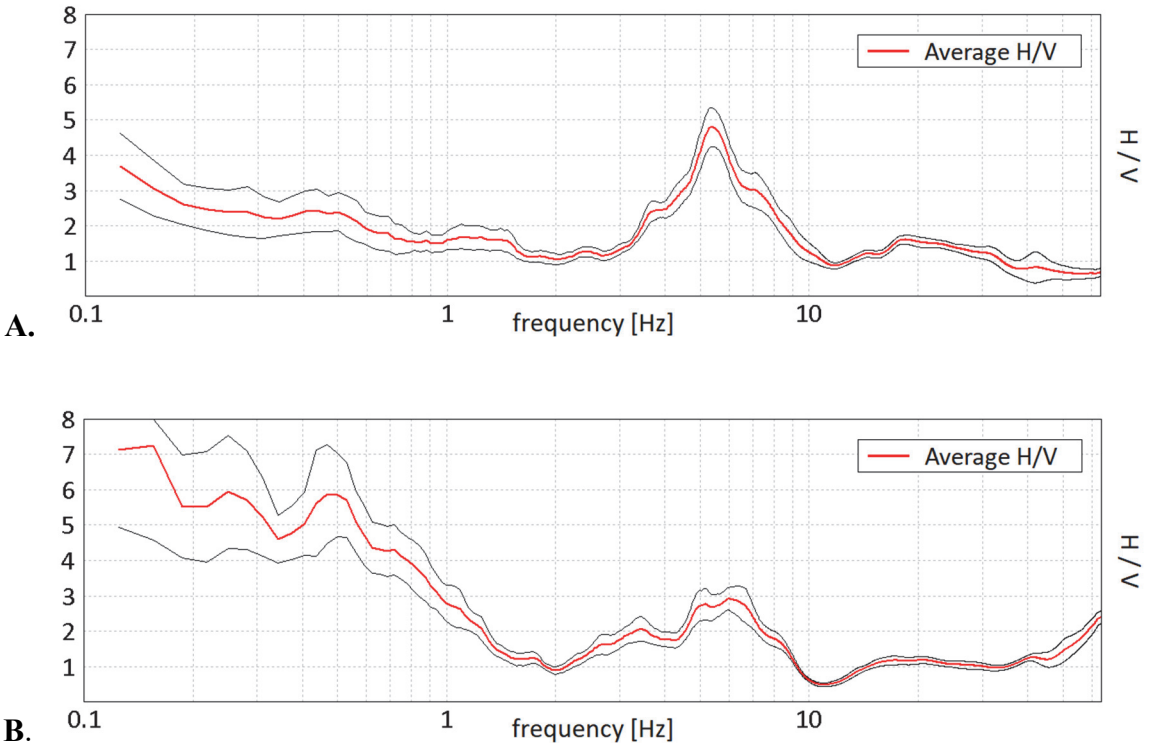

Figure 3.26. **A.** HVSR curve from Tromino station Arcosa Falls 3. The curve shows one distinct peak frequency and is high amplitude—making it a reliable H/V peak. **B.** HVSR curve from Tromino station Arcosa Falls 17. A broad peak exists from 5 to 6.5 Hz. The high amplitude H/V less than 1 Hz is caused by wind and/or noise from nearby trees.

The first core, AF 1, was completed at the far western edge of the northwest transect at one of the deepest DTB estimations from passive seismic (12.0 m). The core had an actual depth to bedrock of (11.1 m). Most of the alluvium was clay, but there was a substantial amount of sand and gravel near the base of the core. The second core, AF 2 was completed near the northwestern edge of the southeast transect at one of the shallowest DTB estimations from passive seismic (8.4 m). The core had an actual depth to bedrock of 8.3 m with most of the alluvium being sand and gravel. A summary of the

two cores is displayed in Table 3.6. Since passive seismic depth to bedrock estimates were within a meter of confirmed depths at these two boreholes, the Arcosa Falls site seems to be conducive to the HVSR method, and depth estimates are likely trustworthy along both transects.

Table 3.6. Summary of the two cores from boreholes drilled at the Arcosa Falls site. AF 2 had a shallower depth to bedrock, but had much more sand & gravel. Full core logs are located in Appendix B.

Site	Elevation (m)	DTB (m)	Bedrock elevation (m)	Sand & gravel thickness (m)	Clay thickness (m)	Saturated thickness (m)
AF 1	110.2	11.1	99.1	2.8	8.3	5.0
AF 2	108.4	8.3	100.1	5.2	3.1	2.93

The elevation profile for the NW transect shows a nearly flat surface (Figure 3.27B), with little need for a Bouguer correction. The Bouguer gravity anomalies along the NW transect trend somewhat in the same direction as passive seismic depth to bedrock estimations (shown in Figure 3.27A). The transect passes over an oil pipeline at around 320 m along the transect, though this does not obviously influence measured gravity. The passive seismic depth to bedrock estimation at the western borehole overestimated DTB by about 0.9 m.

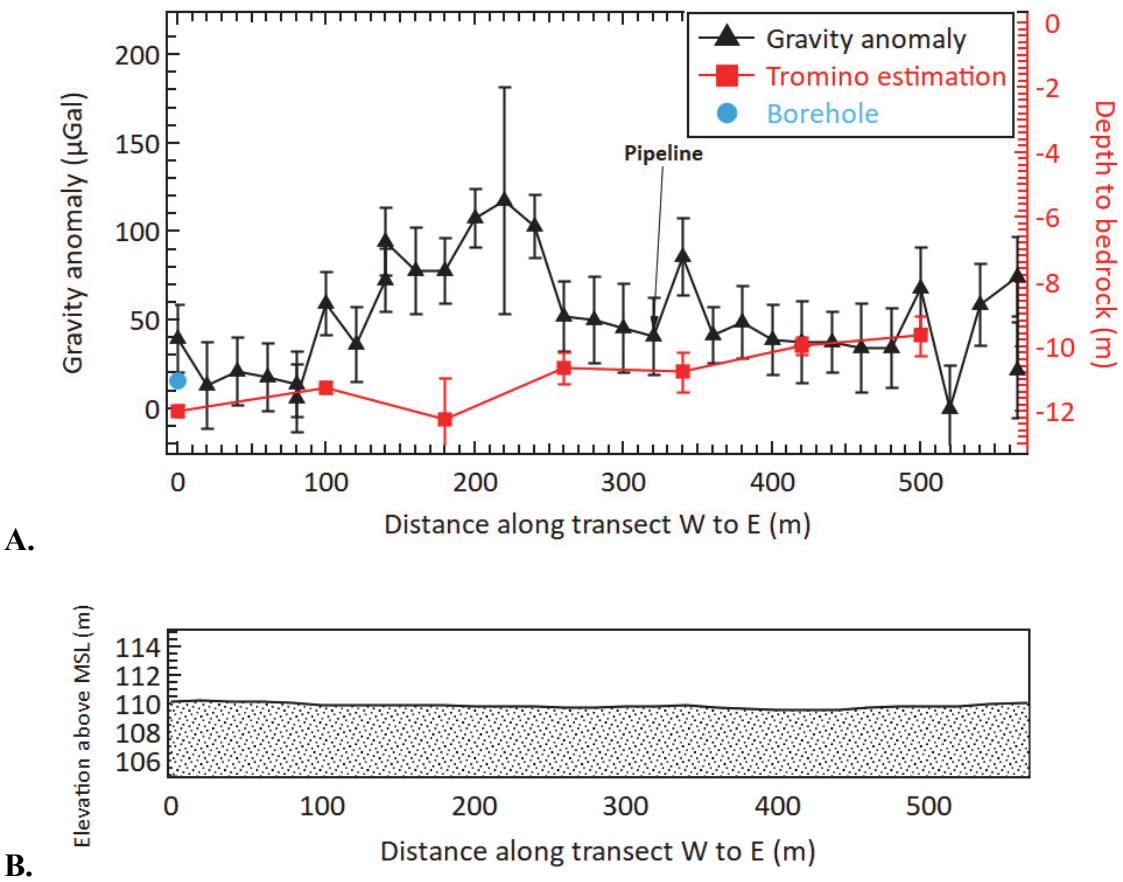

Figure 3.27. **A.** Graph displaying gravity anomalies (black triangles, left axis), depth to bedrock estimates from passive seismic (red squares, right axis), and known depth to bedrock from the one borehole (blue circle, right axis) along the Arcosa Falls NW transect. **B.** Elevation profile for the Arcosa Falls NW transect. Elevation ranged 0.7 m.

Bouguer gravity anomalies for the northwest transect were modeled based on an anomaly caused by a mixture of changing bedrock and changing thickness of sand and gravel (Figure 3.28). The modeled result shown was just one of many that could fit the data. The gravity high on the west-center of the transect is interpreted to be a mixture of a rise in bedrock and rise in sand & gravel; however, the passive seismic DTB estimation is not in agreement with this interpretation. This anomaly is likely to be either be a thick sand and gravel deposit or an anomaly from a deeper source. Since gravity anomalies

generally appear about the same width as their depth, this anomaly could be caused by some variation in bedrock ~150 m below ground.

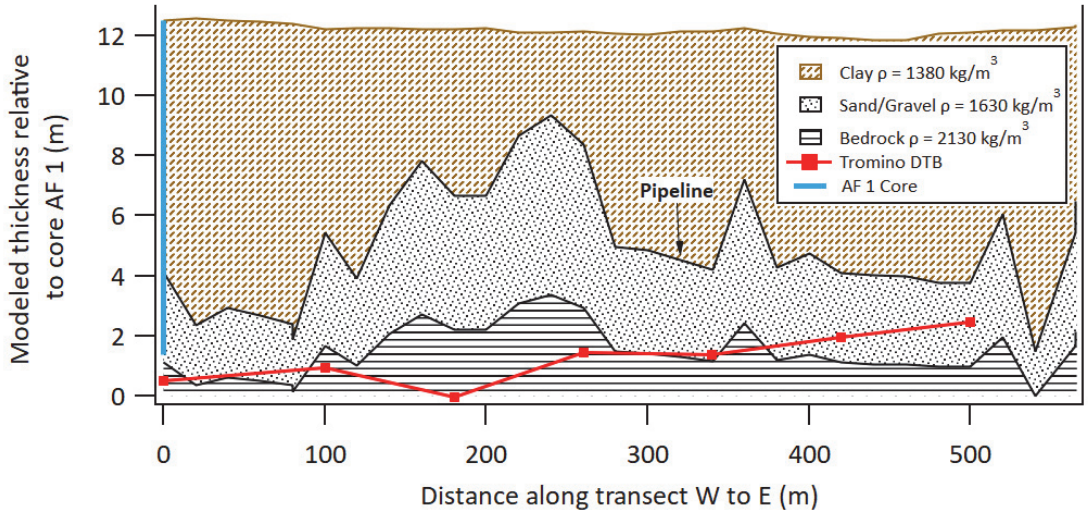

Figure 3.28. Best fit modeled scenario for the Arcosa Falls NW transect. This best fit result assumed 60% of measured gravity was from the bedrock slab and 40% was from the sand and gravel slab.

The elevation along the southeast transect at the Arcosa Falls property is also relatively flat (shown in Figure 3.29B). The gravity anomaly along the SE transect does not necessarily seem to correlate with depth to bedrock (Figure 3.29A); however, the two are similar in that passive seismic DTB estimations and Bouguer gravity anomalies are both flat. This suggests that most of the Bouguer gravity anomaly is made up of changes in alluvial composition. The depth to bedrock estimation at the borehole aligns well with the known depth from the core.

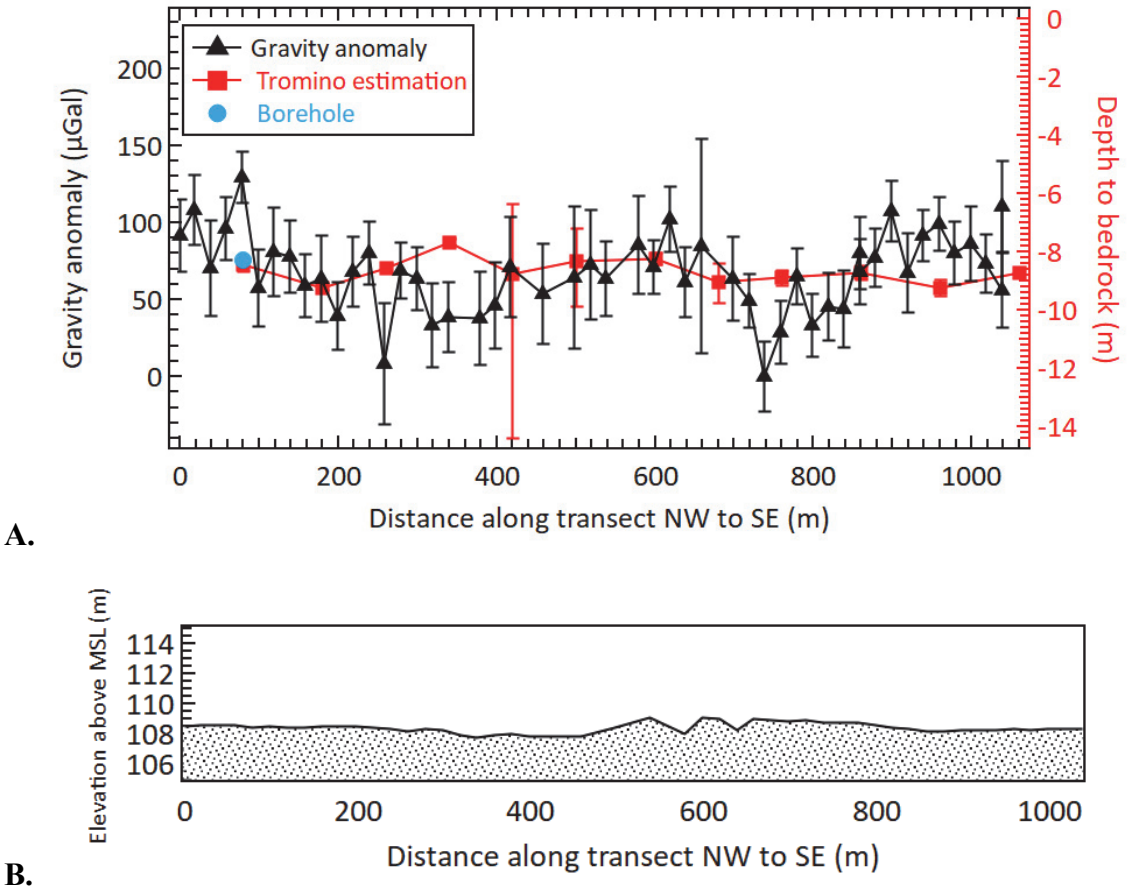

Figure 3.29. **A.** Graph displaying gravity anomalies (black triangles, left axis), depth to bedrock estimates from passive seismic (red squares, right axis), and known depth to bedrock from the one core along the Arcosa Falls SE transect. **B.** Elevation profile for the Arcosa Falls SE transect. There is a small variation around 600 m along the transect. Elevation ranged by 1.3m.

Passive seismic (Tromino) depth to bedrock estimations suggest that the alluvium – bedrock interface seems to be relatively flat, ranging by a meter or two over the SE transect. The largest change in Bouguer gravity anomaly, swinging by over 100 µGals around 700-900 m along the line, is likely caused by more than changing bedrock depth and may indicate an area of clay-dominated alluvium. Bouguer gravity anomalies from the southeast transect were modeled using slightly different densities than the northwest transect (Figure 3.30).

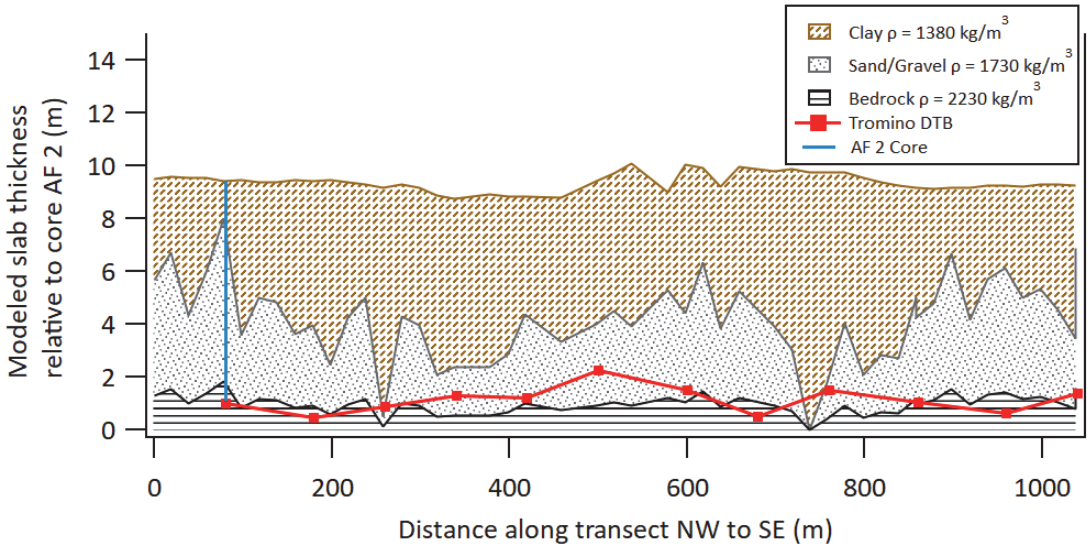

Figure 3.30. Best fit modeled scenario for the Arcosa Falls SE transect. This best fit result assumed 30% of measured gravity was from the bedrock slab and 70% was from the sand and gravel slab.

Though the best fit modeled result slightly overestimates the amount of sand and gravel at borehole AF 2, it was able to match closely with the passive seismic DTB estimations by attributing a greater proportion of Bouguer gravity anomaly to changing sand and gravel thickness than changes in bedrock elevation. From a geologic standpoint, it seems unlikely that there is no sand and gravel at two locations along this transect, so bedrock may have more variability while sand and gravel thickness may have less variability the modeled result in Figure 3.30 suggests.

General Discussion

It should be apparent that many of the modeled results (Hirsch, MCC, Moon River) rely heavily on stratigraphic data from boreholes. While it was important to verify the method in locations with existing boreholes, this borehole-calibrated modeling does paint the combined gravity and passive seismic method in a better light than if the method was standing on its own. For example, prior to drilling boreholes that allowed the

generation of a custom calibration curve at MCC HR, depth to bedrock was overestimated by an average of 2.7 m or 47% (some of the highest percent errors in the study), suggesting a much thicker saturated alluvial section than actually exists. Since gravity modeling solely relies on DTB estimates without the presence of boreholes, if the passive seismic estimations are off my several meters this could lead the modeled gravity solution to also overestimate / underestimate the amount of sand and gravel present. The introduction of just one borehole improves modeled results immensely. Hence, the ideal application of the gravity and passive seismic combination may be attempting to find a site for a well that is close to an existing well that can serve as a calibration point for geophysical measurements. Promisingly, depth to bedrock estimations made from passive seismic measurements at Hirsch Dairy, Buster Chatam, and Arcosa are generally within two meters of known depths from boreholes.

Gravity measurements are most useful when Bouguer gravity anomalies exceed approximately 100 μGals over a transect as anomalies greater than this are hard to explain solely from changes in alluvial composition. Wong (2012) found that the average thickness of the Brazos River Alluvium Aquifer in the Northern Segment is about 12 m. The expected difference in Bouguer gravity anomaly when transitioning from 12 meters of sand and gravel to 12 meters of clay would be about 150 μGals (assuming a density contrast of 300 kg/m^3). In other words, at a site with 12 m of alluvial thickness, a Bouguer gravity anomaly of 150 μGals or less could mathematically be explained by either bedrock elevation changes or alluvial composition changes. However, this drastic of a change in alluvial composition along a ~ 1 km transect is unlikely to occur, so if a Bouguer gravity anomaly exceeds about 100 μGals in magnitude, bedrock elevation has

likely changed. Since most anomalies in the study are less than 100 μGals it is hard to separate with confidence which anomalies are caused by slight bedrock changes or alluvial composition changes. Since passive seismic DTB estimations have approximately 20% error, these DTB estimations do not effectively narrow down the possible solutions unless large changes in bedrock height occur such as at the Moon River Ranch transect. Finally, while a 100 μGal Bouguer gravity anomaly is high enough magnitude in theory to conclude that bedrock elevation has changed, in practice, there may be some systematic error introduced by gravity corrections which may reduce the confidence of that conclusion.

Method Comparison

Comparing the two methods head-to-head, the passive seismic, HVSR method is easier to use in almost every aspect. Data are easier to collect, process, and interpret than with the gravity method. Each passive seismic reading itself is more time consuming in the field than a gravity reading, but measurements can be made by one person (a difficult task for gravity because stations must also be surveyed with an RTK GPS). The cost of the two instruments is about an order of magnitude different with a Tromino Zero 3G+ costing roughly $8000 while a Scintrex Autograv CG-6 costs roughly $100,000. However, the value that the addition of passive seismic data adds to gravity data especially when no boreholes are available should not be understated. Gravity data without any calibration borings or DTB estimates would be of marginal use to estimate DTB or alluvial composition. Despite the complementary nature of the two methods, they were incapable of delineating bedrock with <10% error and few concrete conclusions

about alluvial composition along a transect could be made in the absence of boreholes due to low magnitude gravity anomalies.

CHAPTER FOUR

Error Analysis

Passive Seismic (HVSR) Error

An obvious way to test passive seismic depth to bedrock estimates is to compare against known depths. Plotting the difference of all 65 calibration depth estimates from Figure 2.5 against known depths (Figure 4.1A), it is clear that most depth to bedrock estimates from the calibration curve fall within a meter or two of the actual depth to bedrock. Median error is 1.5 m while average error is 2.2 m. The outlier is a calibration point on a terrace with the deepest depth to bedrock in this study, 25 m. In terms of percent error, most measurements have an error < 20% (Figure 4.1B). Median error is 17% and average error is 21%. Average alluvial thickness and saturated thickness in the Northern Segment of the Brazos River Alluvium Aquifer are roughly 12 meters and 7 meters respectively (Wong, 2012). While an error of 20% may sound low, a 20% difference in saturated section is significant when attempting to assess the potential productivity of a water well. Furthermore, depth to bedrock estimates with 20% error do not help constrain possible modeled solutions of gravity data as much as hoped since bedrock elevation was typically relatively flat over a 1 km transect.

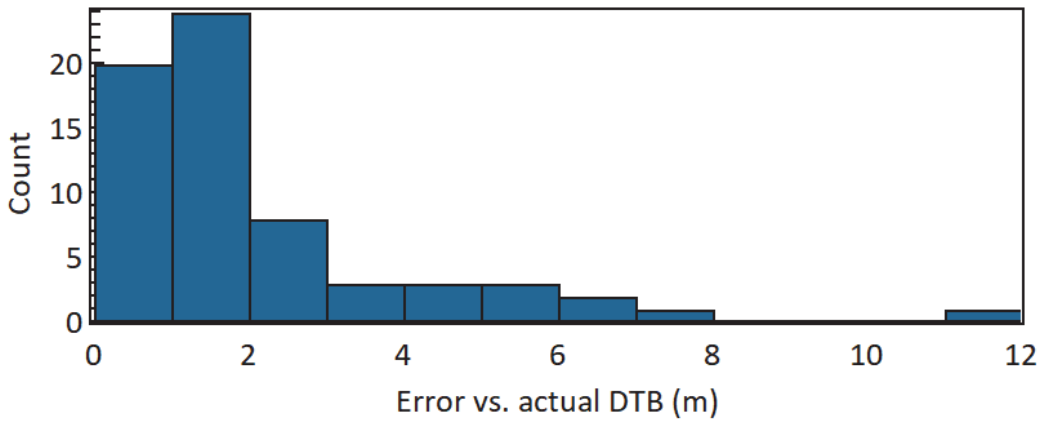

A.

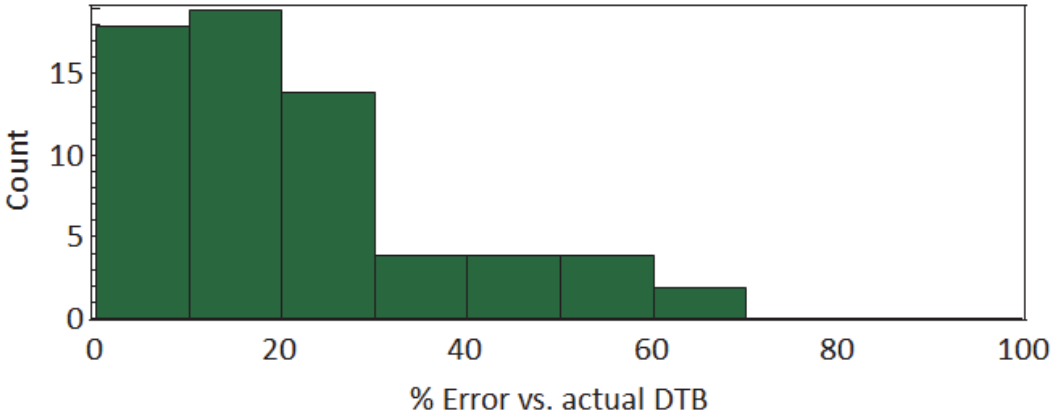

B.

Figure 4.1. **A.** Histogram of estimated depth to bedrock error when comparing calibration curve estimates to known depths to bedrock. Bin size is 1 m. **B.** Histogram of % error when comparing passive seismic depth to bedrock estimates to known depths to bedrock. Bin size is 10%.

The error statistics are somewhat biased as plotted DTB estimates imply that the HVSR curves were of good enough quality to have a clear H/V peak, which was not the case with almost a third of calibration measurements. Unclear H/V peaks are thought to be primarily caused by a site being inconducive to the HVSR method—i.e. the impedance contrast between alluvium and bedrock was not high enough (2:1) to generate a peak resonance frequency (Johnson and Lane, 2016). However, other causes of unclear peaks include interference from other anthropogenic frequency sources (electric lines,

water lines, etc.) or Tromino-ground coupling issues. It is also interesting that HVSR curves from sites in the younger, floodplain alluvium tended to be better quality than HVSR curves from sites on older, terrace alluvium—82% of HVSR curves in young alluvium but only 56% in terrace alluvium had clear H/V peaks. Cronin and Wilson (1967) noted that terrace alluvium can differ from floodplain alluvium in being more cemented. Terrace alluvium cementation and/or compaction may partially explain these differing results since the two could cause either a gradational contact or a low bedrock/alluvium impedance contrast, both of which are inconducive to the passive seismic, HVSR method.

Passive seismic depth to bedrock estimation errors are some combination of random and systematic error. The random error is derived from errors made during the measurement and is reflected in the standard deviation of f_0 in Hz. This error was small—typically less than 0.5 Hz, generally causing less than a meter of depth to bedrock estimation error. Systematic error is reflected in the process of using a calibration curve to estimate bedrock depth. Since the curve is built from measurements made all over the Brazos River Alluvium Aquifer (and terraces), the regression line represents the v_s profile from a sort of 'average' BRAA alluvium. Comparing the aquifer-wide, BRAA calibration curve (Figure 2.5) to various curves made using a single v_s (Figure 4.2), it is apparent that the 'average' alluvium has a v_s of about 195 – 250m/s (average = 217 m/s). The implication is that at locations where v_s is lower than average BRAA alluvium, depth to bedrock will be overestimated and vice versa. Since the deposits within the Brazos River Alluvium Aquifer are heterogeneous in nature, v_s naturally varies, causing systematic error.

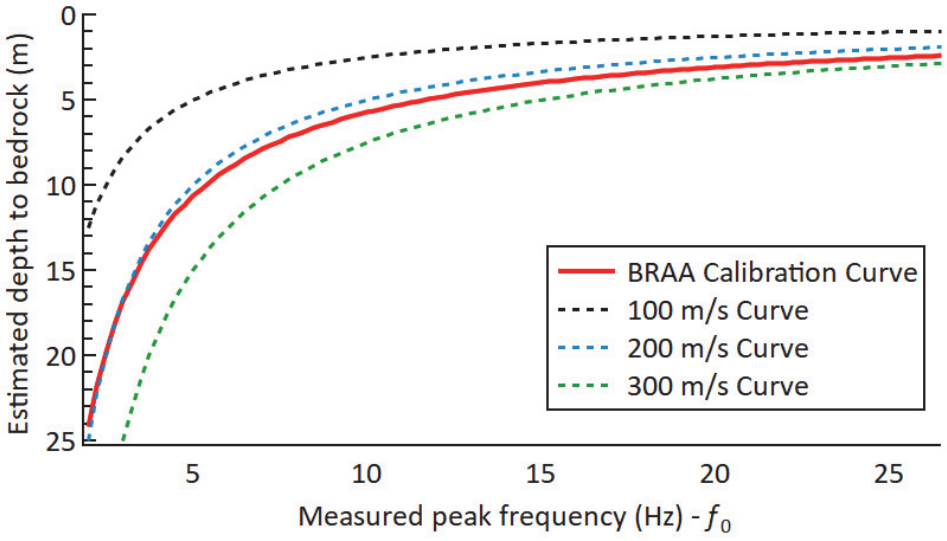

Figure 4.2. Comparison of BRAA calibration curve to curves that estimate depth to bedrock from Equation 1 using various v_s values.

Gravity Error

Gravity measurement standard deviations were computed by adding the standard deviation (recorded by the CG-6) for each measurement to the standard deviation of height error (converted from the Leica GPS z-direction coordinate quality) multiplied by the free air correction minus the Bouguer correction (Equation 4).

$$Total\ \sigma\ = \sigma_{CG6} + ((\ \sigma_{GPS} * 0.3086) - (2\pi \mathrm{G}\rho\sigma_{GPS} * 10^5) \quad (4)$$

Since the free air correction and Bouguer correction are applied with opposite signs, this helps reduce computed error to some degree. Standard deviations from all of the gravity measurements are shown in Figure 4.3. Gravity anomaly standard deviations from the 337 gravity measurements averaged 24.7 μGals with a median of 21.9 μGals.

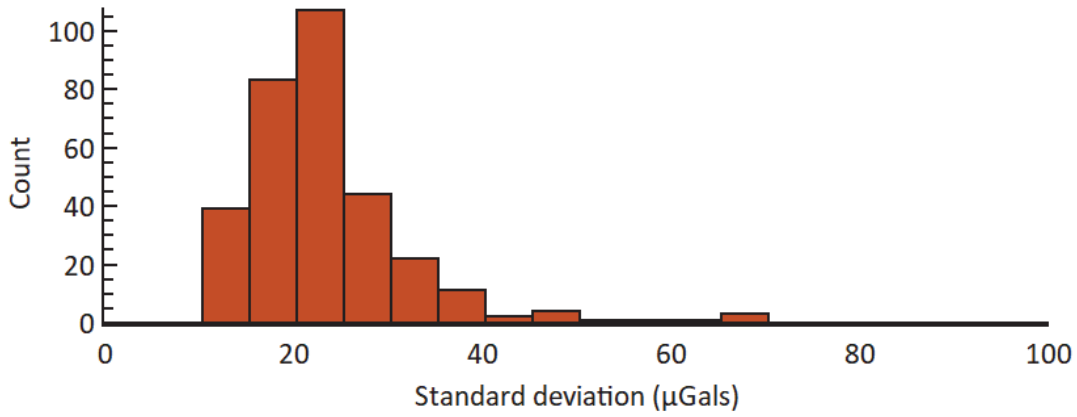

Figure 4.3. Histogram of total standard deviations for gravity measurements. Bin size is 5 µGals.

Gravity measurement standard deviations represent random error; however, systematic error also is introduced from several of the corrections applied during the process from raw to corrected gravity, especially from the Bouguer and regional gravity corrections. For instance, if a density off by 100 kg/m^3 is chosen for near-surface soil, corrected gravity anomalies will be off by 4.2 µGals for every meter of height above the datum. Higher elevation measurements are most sensitive to errors in the Bouguer correction. Also, an incorrect regional trend in gravity could increase or decrease gravity anomalies substantially and cause corrected gravity to increase in one direction. Gravity measurements on either end of a transect are most sensitive to errors in the regional correction.

CHAPTER FIVE

Summary and Conclusions

1. Bouguer gravity anomalies greater than roughly 30 μGals could be detected with confidence. The majority of standard deviations were < 25 μGals though systematic errors in Bouguer or regional corrections used could result in greater error.
2. Depth to bedrock could be estimated throughout the study area with passive seismic methods with an average error of 2.2 m or 21% and a median error of 1.5m or 17%.
3. The HVSR, passive seismic method is the preferred method over microgravity if limited to a single geophysical tool.
4. The interpreted bedrock elevation was mostly flat (Hirsch, Arcosa Falls), roughly paralleled surface elevation (MCC HR, Buster Chatam), or had large changes (Moon River).
5. The combined gravity and passive seismic method is most trustworthy in areas where at least one calibration boring is available. Multiple calibration borings with varying depths to bedrock are preferred as they allow the construction of a local, site-specific calibration curve
6. The method is better suited for areas with large variations in depth to bedrock (at least several meters), increasing the anticipated Bouguer gravity anomaly signal.

CHAPTER SIX

Recommendations

1. If possible, coring down into the bedrock 5-10 m would be ideal to verify a consistent lower bedrock layer for the model.
2. Caution must be exercised when using a calibration curve made over broad areas which may be different than a particular study area (e.g. MCC Highlander Ranch). If a calibration boring indicates a large divergence between estimated depth to bedrock and actual depth to bedrock, a local calibration curve or single v_s should be used instead.
3. If possible, it is recommended to make more gravity measurements surrounding a survey site of interest to better define regional gravity trends.
4. Passive seismic, HVSR methods are excellent for making individual, point source depth to bedrock estimates.
5. Overall, the method used in this study is recommended if one can tolerate ~20% error and is seeking a simpler, lower budget alternative compared to seismic refraction or electrical resistivity methods.

APPENDICES

APPENDIX A

Bulk Density Measurements

Table A.1. Bedrock dry bulk density measurements reported from collected Grayson Marl, Wolfe City, and Ozan Formation rock samples. Locations where bedrock samples were collected are shown in Figure 2.7.

Bedrock Sample Site	Formation	Latitude	Longitude	Mass 1 (g)	Vol 1 (mL)	Mass 2 (g)	Vol 2 (mL)	Average Density (kg/m^3)
MCC 1	Grayson Marl	31.6560	-97.2009	41.16	19.8	43.26	20.3	2110
MCC 2	Grayson Marl	31.6541	-97.2000	43.71	20.6	59.85	29.2	2090
FM 308	Ozan/Wolfe City	31.8712	-96.9193	33.93	16.5	43.27	20.7	2070
FM 171 Ash Creek	Ozan	31.9096	-96.8816	28.91	14.3	35.87	18.1	2000
FM 171 E of Hubbard	Wolfe City	31.8205	-96.7731	31.07	13.6	26.2	12.0	2230
Grieg Rd Flat creek	Ozan	31.4713	-97.1467	22.80	11.8	42.77	22.0	1940
TX 320 Deer Creek	Wolfe City	31.2795	-96.9783	26.00	12.1	30.23	13.5	2190
Iron Bridge Rd	Ozan	31.3868	-97.1506	39.68	19.7	43.06	20.2	2070
CR 459	Ozan	31.2015	-97.1937	36.12	19.5	51.54	24.2	1990
Woodlawn Rd	Ozan	31.3392	-97.1789	36.02	17.8	38.65	19.4	2010
FM 164	Ozan	31.5227	-96.9209	21.17	9.8	30.02	15.3	2060
Arcosa Falls Site	Ozan	31.3893	-97.0253	34.65	17.2	22.42	12	1940

APPENDIX B

Core Descriptions

Core descriptions from the six core samples collected during this study are recorded. Four core samples were collected at MCC Highlander Ranch and two core samples were collected at the Arcosa Falls site. Each core sample was described using the guide in Driscoll, 1986.

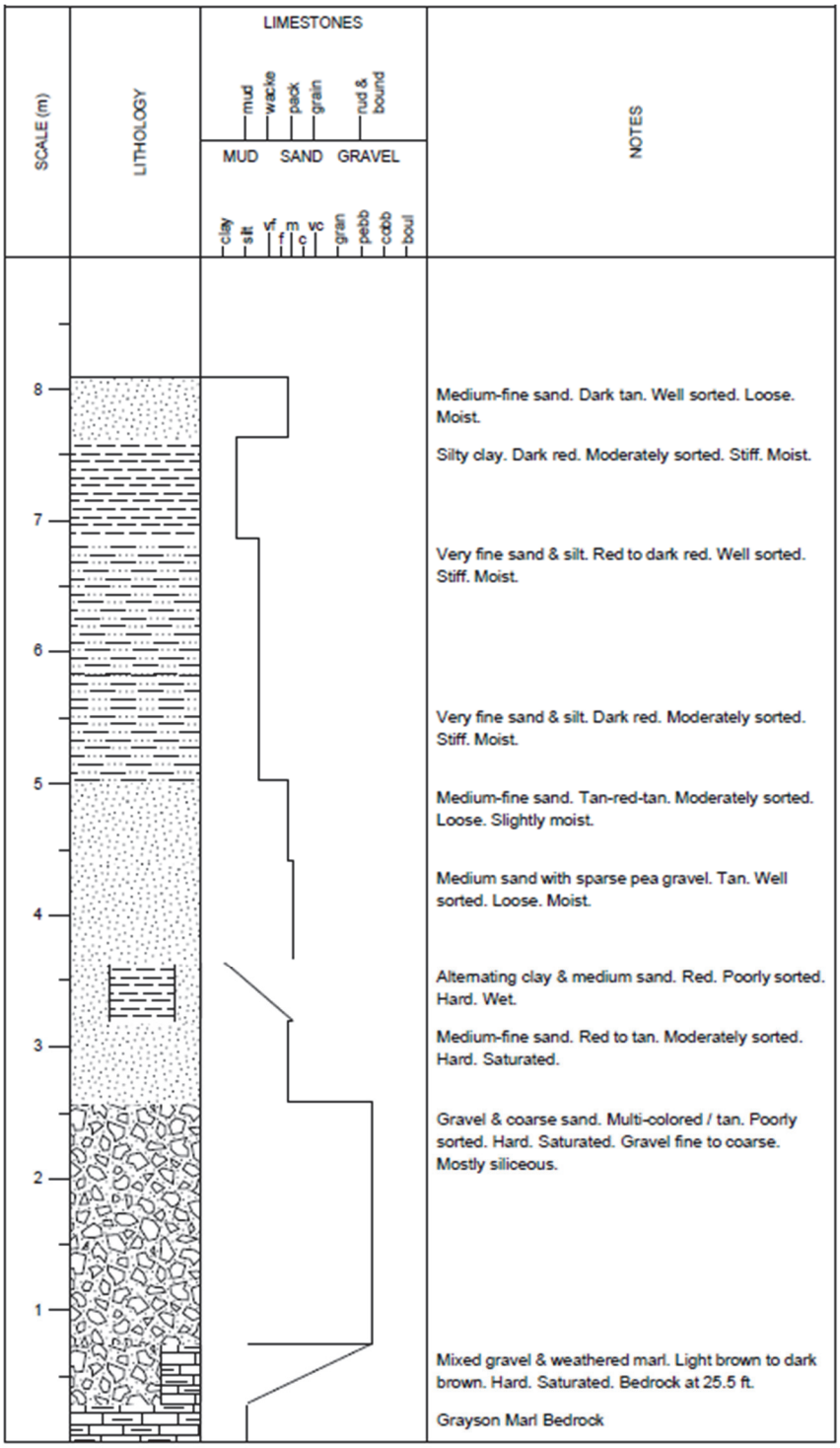

Figure B.1. Core description log for MCC 1.

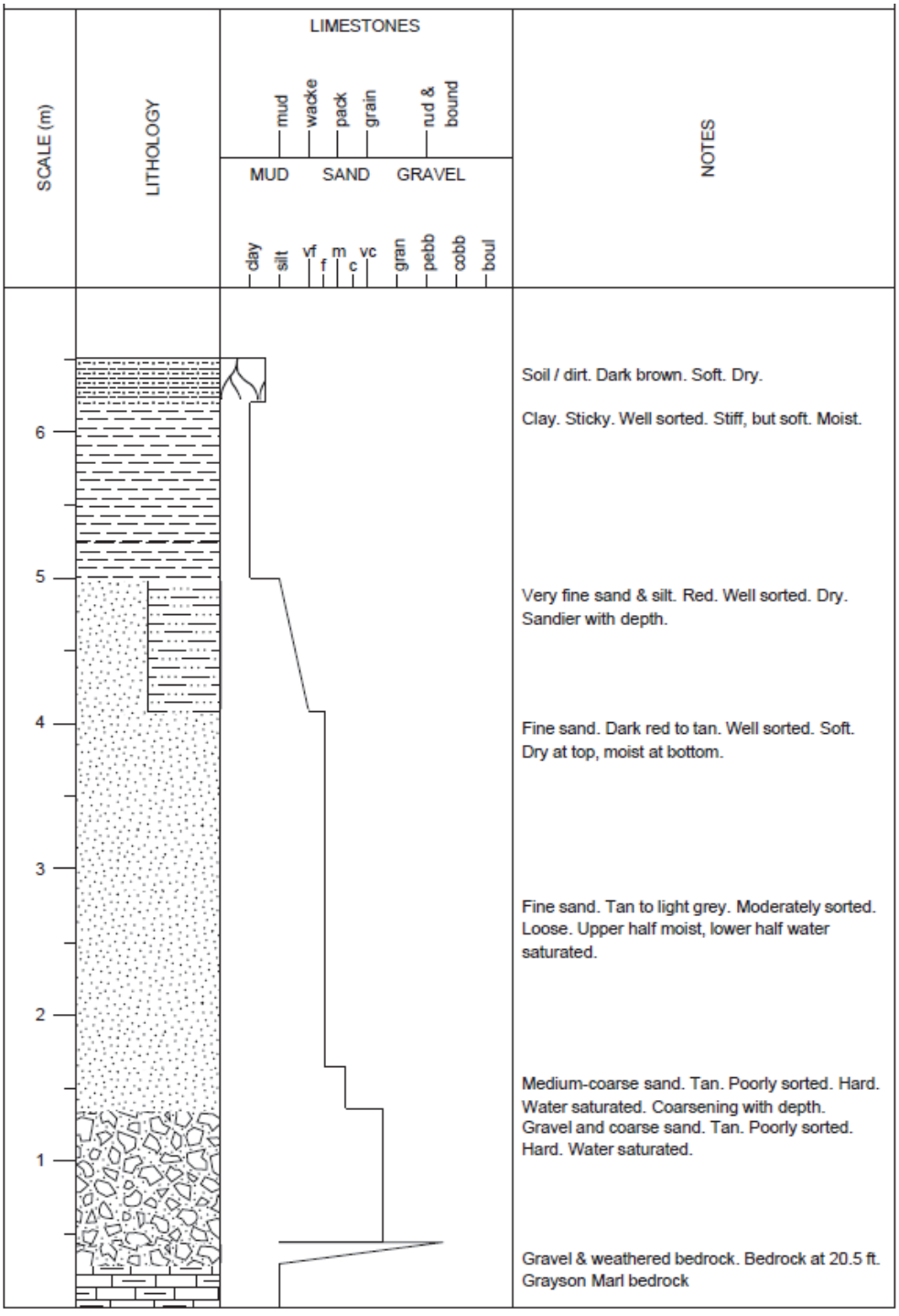

Figure B.2. Core description log for MCC 2.

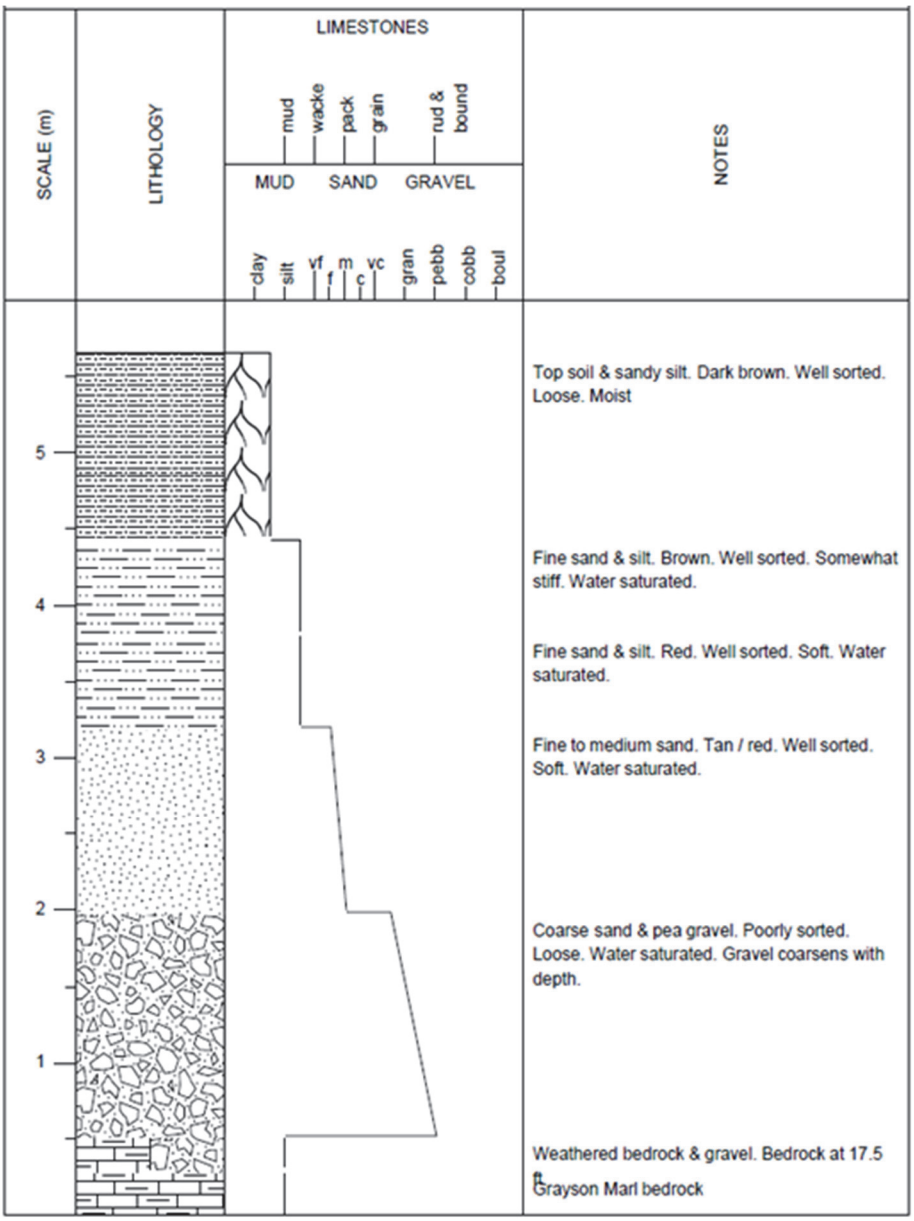

Figure B.3. Core description log for MCC 3.

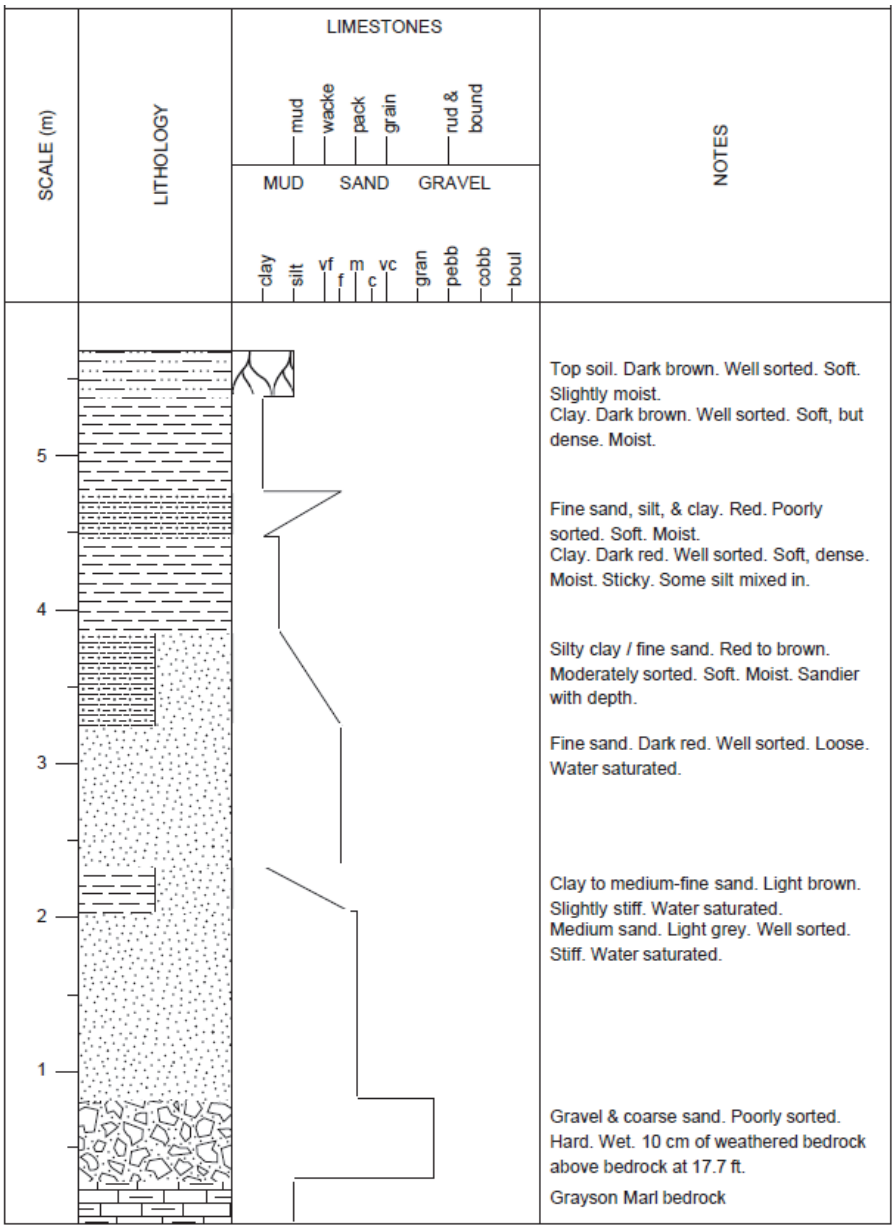

Figure B.4. Core description log for MCC 4.

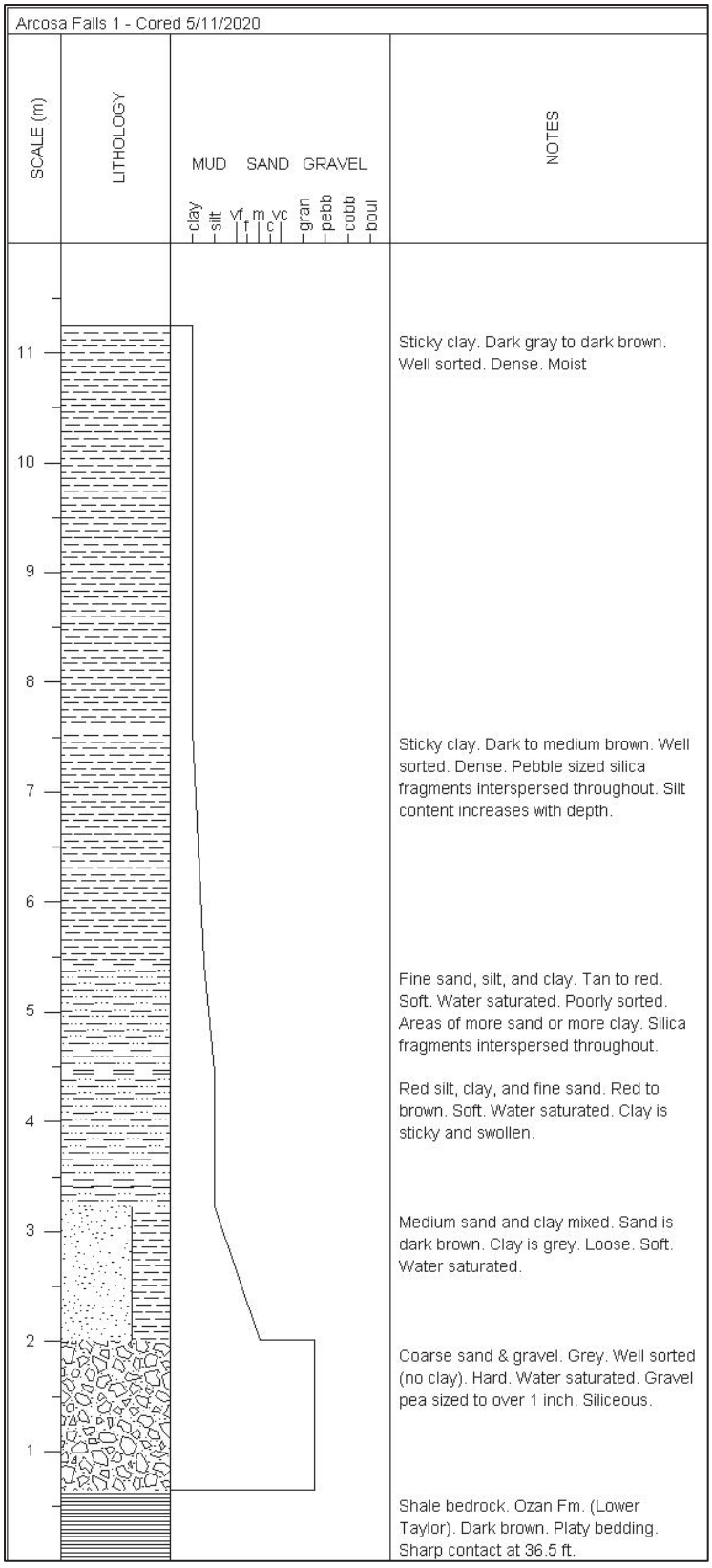

Figure B.5. Core description log for Arcosa Falls 1.

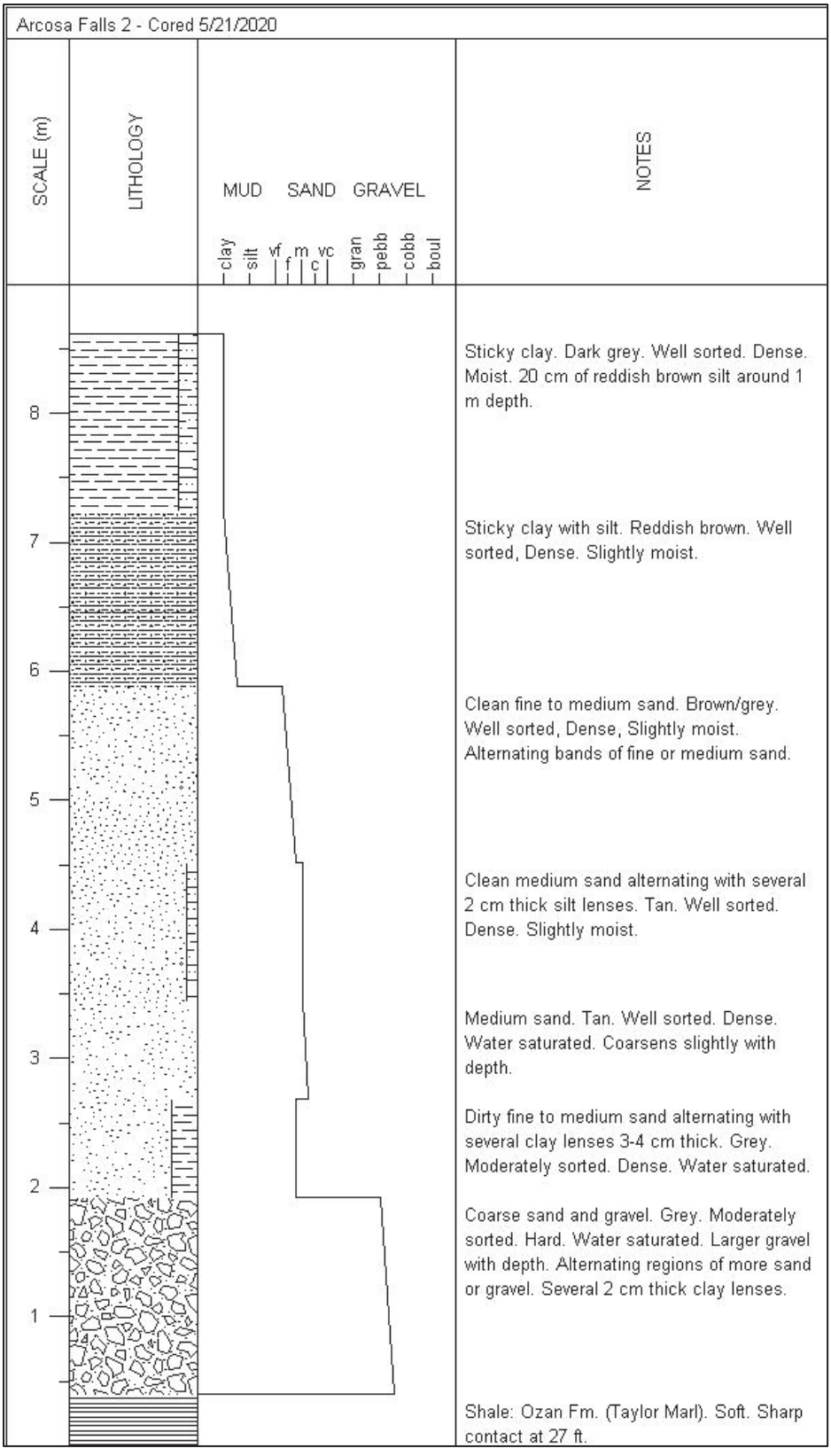

Figure B.6. Core description log for Arcosa Falls 2.

APPENDIX C

Table C.1. Passive Seismic (HVSR) Measurements

Site ID	County	Latitude	Longitude	Alluvium/Terrace	Peak Frequency (Hz)	Standard deviation (± Hz)	Passes SESAME?
FM 712 #3	Falls	31.24824	-96.93033	Alluvium	10.88	0.21	Yes
Dunlap Piez #1	McLennan	31.49412	-97.02645	Alluvium	7.09	0.22	Yes
Steiner Rd #6	McLennan	31.44051	-97.02013	Alluvium	6.78	0.75	Yes
MCC HR 4	McLennan	31.65490	-97.20370	Alluvium	6.53	0.15	Yes
MCC HR 3	McLennan	31.65383	-97.20149	Alluvium	6.47	0.03	Yes
Buster Chatam Rd	McLennan	31.62147	-97.17199	Alluvium	6.44	0.23	Yes
Asa 17-04	McLennan	31.43424	-97.04639	Alluvium	6.25	0.1	Yes
Asa 17-07	McLennan	31.43348	-97.04832	Alluvium	6.22	0.1	Yes
MCC HR 1	McLennan	31.65602	-97.20086	Alluvium	5.81	0.09	Yes
MCC HR 2	McLennan	31.65411	-97.20002	Alluvium	5.75	0.1	Yes
Asa 09-46	McLennan	31.43503	-97.04572	Alluvium	5.28	0.03	Yes
FM 712 #5	Falls	31.25477	-96.91517	Alluvium	5	0.04	Yes
Bellmead Buzz Billys	McLennan	31.55964	-97.12138	Alluvium	4.33	0.08	Yes
MLK & LaSalle	McLennan	31.55518	-97.10336	Alluvium	3.47	0.17	Yes
HCR 2200	Hill	31.77468	-97.28892	Terrace	25.63	1.16	Yes
1st St Garage	McLennan	31.55140	-97.11793	Terrace	16.22	0.15	Yes
PV2 Steinbeck WNA1	McLennan	31.61112	-97.14957	Terrace	11.56	0.22	Yes
Steinbeck Wesley Chapel Rd	McLennan	31.60609	-97.15939	Terrace	9.28	0.18	Yes
MJ2 Steinbeck Elk Rd near	McLennan	31.73102	-97.24373	Terrace	7.94	0.25	Yes
Wardlaw	McLennan	31.61031	-97.13656	Terrace	5.63	0.25	Yes
FM 712 #1	Falls	31.56680	-97.06309	Terrace	5.56	0.21	Yes
Clater Powell Rd	McLennan	31.24137	-96.94489	Terrace	5.03	0.08	Yes
BSB North Wing	McLennan	31.73990	-97.25371	Terrace	4.16	0.07	Yes
		31.54892	-97.11265	Terrace	3.94	0.14	Yes

Table C.1. Passive Seismic (HVSR) Measurements

Site ID	County	Latitude	Longitude	Alluvium/Terrace	Peak Frequency (Hz)	Standard deviation (± Hz)	Passes SESAME?
CR 1304	Hill	31.82160	-97.24777	Terrace	3.75	0.05	Yes
CR 406	Falls	31.22902	-96.96893	Terrace	3.72	0.14	Yes
Bellmead							
Colina&Crow	McLennan	31.57174	-97.07584	Terrace	2.63	0.16	Yes
Moon River 1	Falls	31.32269	-97.02469	Alluvium	26.16		Yes
FM 413 #4	Falls	31.13790	-96.81762	Alluvium	4.69	0.06	No, somewhat close
Horseshoe							
Bend Rd #3	McLennan	31.65177	-97.17524	Alluvium	2.66	3.4	No
FM 712 #4	Falls	31.25118	-96.92327	Alluvium	7.81	0.65	No
FM 413 #8	Falls	31.15469	-96.78638	Alluvium	5.53	1.67	No
FM 413 #3	Falls	31.13763	-96.81871	Alluvium	4.56	0.9	No
Moon River 3	Falls	31.32479	-97.02000	Alluvium	4.16	0.5	No
CR 202 #6	Falls	31.21919	-96.84281	Alluvium	3.62	0.36	No
FM 413 #5	Falls	31.14223	-96.81044	Alluvium	3.31	1.05	No
CR 202 #8	Falls	31.22570	-96.83075	Alluvium	2.97	2.18	No
CR 302	Falls	31.28752	-96.91403	Alluvium	2.29	0.22	No
FM 712 #2	Falls	31.24458	-96.93738	Terrace	14.22	1.2	No
CR 202 #9	Falls	31.23137	-96.82045	Terrace	8.85	1.5	No
S U Parks #1	McLennan	31.48978	-97.08012	Terrace	5.91	1.35	No
Steiner Rd #4	McLennan	31.43443	-97.03385	Alluvium	6.88	0.35	No, but very close
Steiner Rd #1	McLennan	31.42350	-97.05408	Alluvium	5.63	0.44	No, but very close
CR 202 #2	Falls	31.20587	-96.86800	Alluvium	4.38	0.22	No, but very close
Horseshoe							
Bend Rd #1	McLennan	31.67133	-97.18410	Alluvium	3.64	0.2	No, but very close
Lindsey Ln	McLennan	31.63998	-97.18276	Alluvium	12.5	2.19	No, but ok
Frances							
Rd/Steiner #3	McLennan	31.43114	-97.04301	Alluvium	7.81	1.18	No, but ok
Steiner Rd #2	McLennan	31.42510	-97.05032	Alluvium	7.81	4.73	No, but ok
FM 413 #6	Falls	31.14608	-96.80290	Alluvium	4.07	0.52	No, but ok
Hirsch Lower	McLennan	31.51968	-97.05005	Alluvium	3.44	2.47	No, but somewhat close
Steiner Rd #5	McLennan	31.43707	-97.02784	Alluvium	6.75	0.53	No, but close
Washington							
Ln	McLennan	31.62141	-97.18379	Alluvium	4.89	0.32	No, but close
Hirsch							
Middle	McLennan	31.51710	-97.05380	Alluvium	3.72	0.32	No, but close
Horseshoe							
Bend Rd #2	McLennan	31.66885	-97.17964	Alluvium	3	0.2	No, but close

Table C.1. Passive Seismic (HVSR) Measurements

Site ID	County	Latitude	Longitude	Alluvium/Terrace	Peak Frequency (Hz)	Standard deviation (± Hz)	Passes SESAME?
Hirsch Transducer	McLennan	31.52090	-97.05140	Alluvium	2.94	0.32	No, but close
CR 202 #3	Falls	31.20582	-96.86740	Alluvium	4.16	0.53	No kinda close
FM 413 #1	Falls	31.12826	-96.83681	Terrace	11.69	0.64	No but close
BSB Middle Wing	McLennan	31.54818	-97.11216	Terrace	4.22	0.3	No (very close)
Bogey Ln (WacMam MC-2)	McLennan	31.60697	-97.17442	Terrace	26.2	2.37	No (somewhat close)
Art Building NE Corner	McLennan	31.55022	-97.11428	Terrace	7.41	0.61	No (somewhat close)
Asa 17-01	McLennan	31.43376	-97.04764	Alluvium	6.16	1.4	No
Baylor BRIC	McLennan	31.57298	-97.10704	Terrace	7.21	0.92	No
BSB South Wing	McLennan	31.54742	-97.11215	Terrace	5.31	0.47	No
CR 183	Falls	31.30680	-96.93958	Alluvium	No Clear Peak	N/A	N/A
FM 712 #6	Falls	31.26204	-96.90709	Alluvium	No Clear Peak	N/A	N/A
FM 413 #2	Falls	31.13363	-96.82643	Terrace	No Clear Peak	N/A	N/A
HWY 6 Borehole	McLennan	31.54539	-97.06492	Alluvium	No Clear Peak	N/A	N/A
Speight & 5th St.	McLennan	31.54551	-97.11840	Terrace	No Clear Peak	N/A	N/A
Rosenfeld Rd	McLennan	31.48643	-97.07396	Terrace	No Clear Peak	N/A	N/A
FM 2027 #1	Falls	31.18511	-96.92725	Terrace	No Clear Peak	N/A	N/A
FM 2027 #2	Falls	31.14090	-96.91026	Terrace	No Clear Peak	N/A	N/A
FM 2027 #3	Falls	31.09923	-96.87997	Terrace	No Clear Peak	N/A	N/A
CR 202 #5	Falls	31.21459	-96.85142	Alluvium	No Clear Peak	N/A	N/A
CR 202 #7	Falls	31.22232	-96.83688	Alluvium	No Clear Peak	N/A	N/A
CR 202 #4	Falls	31.20999	-96.85988	Alluvium	No Clear Peak	N/A	N/A

Table C.1. Passive Seismic (HVSR) Measurements

Site ID	County	Latitude	Longitude	Alluvium/Terrace	Peak Frequency (Hz)	Standard deviation (± Hz)	Passes SESAME?
CR 103 USGS	Falls	31.34102	-96.95623	Alluvium	No Clear Peak	N/A	N/A
FM 712 #7	Falls	31.26898	-96.89862	Terrace	No Clear Peak	N/A	N/A
Goldman Ln	McLennan	31.68490	-97.24617	Terrace	No Clear Peak	N/A	N/A
Hirsch Upper	McLennan	31.51580	-97.05690	Alluvium	No Clear Peak	N/A	N/A
Lake Creek Power	McLennan	31.46802	-96.98590	Terrace	No Clear Peak	N/A	N/A
Moon River 2	Falls	31.32344	-97.02314	Alluvium	No Clear Peak	N/A	N/A
Dead River Ranch Trom	McLennan	31.49138	-97.00489	Terrace	No Clear Peak	N/A	N/A
Dunlap Windmill	McLennan	31.49989	-97.01863	Alluvium	No Clear Peak	N/A	N/A
S U Parks #2	McLennan	31.45820	-97.07017	Terrace	No Clear Peak	N/A	N/A
U Parks Borehole	McLennan	31.55591	-97.12251	Terrace	No Clear Peak	N/A	N/A
HCR 2200	Hill	31.77468	-97.28892	Terrace	No Clear Peak	N/A	N/A
CR 2114	Hill	31.81041	-97.29540	Terrace	No Clear Peak	N/A	N/A
CR 2202N	Hill	31.81783	-97.27549	Terrace	No Clear Peak	N/A	N/A
CR 3610A	Bosque	31.85524	-97.35797	Terrace	No Clear Peak	N/A	N/A
Riverside Park	Hill	31.87089	-97.36590	Terrace	No Clear Peak	N/A	N/A
Hirsch 1 (closest to river)	McLennan	31.51859	-97.05078	Alluvium	3.59	0.52	No, but close
Hirsch 5	McLennan	31.51831	-97.05137	Alluvium	3.81	0.37	No, but close
Hirsch 10	McLennan	31.51795	-97.05210	Alluvium	3.88	0.08	Yes
Hirsch 15	McLennan	31.51762	-97.05285	Alluvium	3.38	0.34	No, but close
Hirsch 21	McLennan	31.51717	-97.05381	Alluvium	3.34	0.41	No, somewhat close
Hirsch 25	McLennan	31.51689	-97.05430	Alluvium	3.59	0.25	No, but very close
Hirsch 30	McLennan	31.51653	-97.05503	Alluvium	4.06	0.11	Yes
Hirsch 35	McLennan	31.51618	-97.05577	Alluvium	5.22	1.37	No

Table C.1. Passive Seismic (HVSR) Measurements

Site ID	County	Latitude	Longitude	Alluvium/Terrace	Peak Frequency (Hz)	Standard deviation (± Hz)	Passes SESAME?
Hirsch 40 West end (near Hirsch 45)	McLennan	31.51584	-97.05651	Alluvium	2.97	1.08	No
MCC1 - NW Corner	McLennan	31.51547	-97.05723	Alluvium	3.28	0.6	No
MCC6	McLennan	97.20370	31.65490	Alluvium/young terrace	6.53	0.15	Yes
MCC11	McLennan	97.20324	31.65480	Alluvium/young terrace	6.25	0.08	Yes
MCC16	McLennan	97.20278	31.65470	Alluvium/young terrace	6.25	0.1	Yes
MCC21	McLennan	97.20232	31.65460	Alluvium/young terrace	5.85	2.62	Yes, but 1 comp
MCC26	McLennan	97.20186	31.65450	Alluvium/young terrace	6.22	0.04	YES
MCC31	McLennan	97.20140	31.65440	Alluvium/young terrace	6.03	0.14	YES
MCC36	McLennan	97.20094	31.65431	Alluvium/young terrace	5.94	0.06	YES
MCC41	McLennan	97.20048	31.65421	Alluvium/young terrace	5.63	0.48	No, but close
MCC46	McLennan	97.20002	31.65411	Alluvium/young terrace	5.75	0.1	YES
MCC51- SE Corner	McLennan	97.19956	31.65401	Alluvium/young terrace	6.06	0.08	YES
MCC53 - NE Corner	McLennan	97.19904	31.65390	Alluvium/young terrace	5.91	0.49	No, but 1 comp
MCC59	McLennan	97.20072	31.65647	Alluvium/young terrace	5.84	0.11	YES
MCC64	McLennan	97.20086	31.65602	Alluvium/young terrace	5.81	0.09	YES
MCC69	McLennan	97.20098	31.65558	Alluvium/young terrace	5.88	0.04	YES
MCC74	McLennan	97.20111	31.65514	Alluvium/young terrace	6.25	0.04	YES
MCC79	McLennan	97.20124	31.65471	Alluvium/young terrace	6.4	2.39	No, but 1 comp
MCC84	McLennan	97.20136	31.65427	Alluvium/young terrace	5.88	0.14	YES
		97.20149	31.65383		6.47	0.04	YES

Table C.1. Passive Seismic (HVSR) Measurements

Site ID	County	Latitude	Longitude	Alluvium/Terrace	Peak Frequency (Hz)	Standard deviation (± Hz)	Passes SESAME?
MCC89	McLennan	-97.20162	31.65339	Alluvium/young terrace	6.25	0.28	YES
MCC94	McLennan	-97.20175	31.65296	Alluvium/young terrace	6.06	4.15	No, but 1 comp
MCC98 - SW Corner	McLennan	-97.20185	31.65261	Alluvium/young terrace	6.25	0.37	No, very close
Moon River 1	Falls	31.32257	-97.02516	Alluvium	No Clear Peak	N/A	N/A
Moon River 2	Falls	31.32269	-97.02469	Alluvium	26.16	0.4	Yes
Moon River 3	Falls	31.32291	-97.02433	Alluvium	9.53	0.39	Yes
Moon River 4	Falls	31.32315	-97.02379	Alluvium	8	1.41	No
Moon River 5	Falls	31.32344	-97.02314	Alluvium	9.69	0.82	No, somewhat close
Moon River 6	Falls	31.32372	-97.02254	Alluvium	9.63	0.09	Yes
Moon River 7	Falls	31.32406	-97.02176	Alluvium	2.5	0.09	Yes
Moon River 8	Falls	31.32424	-97.02105	Alluvium	2.5	0.96	No
Moon River 9	Falls	31.32479	-97.02000	Alluvium	4.13	0.46	No
Moon River 10	Falls	31.32501	-97.01897	Alluvium	4.47	0.7	No, but looks ok
Moon River 11	Falls	31.32532	-97.01570	Alluvium	4.72	0.08	Yes
Moon River 12	Falls	31.32578	-97.01187	Alluvium	3.94	0.52	No, but close
Moon River 13	Falls	31.32603	-97.00848	Alluvium	4.88	14.04	No
Moon River 14	Falls	31.32641	-97.00446	Alluvium	4.69	0.15	Yes
River Bend 13	McLennan	31.61530	-97.17144	Alluvium	4.97	0.87	no (close)
River Bend 12	McLennan	31.61572	-97.17166	Alluvium	4.47	0.14	yes
River Bend 11	McLennan	31.61613	-97.17190	Alluvium	3.97	0.39	no (close)
River Bend 10	McLennan	31.61655	-97.17215	Alluvium	5.09	0.53	no (close)
River Bend 9	McLennan	31.61694	-97.17242	Alluvium	4.84	0.39	no
River Bend 8	McLennan	31.61733	-97.17270	Alluvium	4.91	0.44	no (close)
River Bend 7	McLennan	31.61772	-97.17296	Alluvium	5.63	0.48	no (close)
River Bend 6	McLennan	31.61810	-97.17322	Alluvium	5.25	0.24	yes
River Bend 5	McLennan	31.61849	-97.17350	Alluvium	4.66	0.73	no
River Bend 4	McLennan	31.61892	-97.17378	Alluvium	4.66	0.48	no

Table C.1. Passive Seismic (HVSR) Measurements

Site ID	County	Latitude	Longitude	Alluvium/Terrace	Peak Frequency (Hz)	Standard deviation (± Hz)	Passes SESAME?
River Bend 3	McLennan	31.61931	-97.17406	Alluvium	4.53	0.46	no
River Bend 2	McLennan	31.61967	-97.17433	Alluvium	4.88	1.21	no
RB 1/BC 1	McLennan	31.62004	-97.17456	Alluvium	4.06	0.84	no
Buster Chatam 2	McLennan	31.62028	-97.17412	Alluvium	4.88	0.18	yes
Buster Chatam 3	McLennan	31.62053	-97.17368	Alluvium	4.84	0.64	no
Buster Chatam 4	McLennan	31.62077	-97.17323	Alluvium	4.66	0.17	yes
Buster Chatam 5	McLennan	31.62101	-97.17279	Alluvium	3.97	0.14	yes
Buster Chatam 6	McLennan	31.62127	-97.17235	Alluvium	4.47	0.37	no
Buster Chatam 7	McLennan	31.62152	-97.17187	Alluvium	6.44	0.43	no (close)
Buster Chatam 8	McLennan	31.62175	-97.17143	Alluvium	5.66	0.88	no
Buster Chatam 9	McLennan	31.62200	-97.17102	Alluvium	5.72	0.32	no
Buster Chatam 10	McLennan	31.62228	-97.17058	Alluvium	6.16	0.17	no
Buster Chatam 11	McLennan	31.62251	-97.17015	Alluvium	6.09	1.26	no
Buster Chatam 12	McLennan	31.62273	-97.16970	Alluvium	5.84	0.37	no (close)
Buster Chatam 13	McLennan	31.62298	-97.16921	Alluvium	4.69	0.44	no
Buster Chatam 14	McLennan	31.62320	-97.16879	Alluvium	5.75	0.18	yes
Buster Chatam 15	McLennan	31.62345	-97.16836	Alluvium	5.84	0.59	no
Buster Chatam 16	McLennan	31.62368	-97.16791	Alluvium	5.59	0.14	yes
Buster Chatam 17	McLennan	31.62395	-97.16748	Alluvium	4.22	0.86	no
Buster Chatam 18	McLennan	31.62418	-97.16702	Alluvium	5.06	0.44	no
Buster Chatam 19	McLennan	31.62440	-97.16655	Alluvium	No Clear Peak	N/A	N/A

Table C.1. Passive Seismic (HVSR) Measurements

Site ID	County	Latitude	Longitude	Alluvium/Terrace	Peak Frequency (Hz)	Standard deviation (± Hz)	Passes SESAME?
Buster Chatam 20	McLennan	31.62466	-97.16613	Alluvium	No Clear Peak	N/A	N/A
Buster Chatam 21	McLennan	31.62490	-97.16568	Alluvium	5.69	1.34	no
Buster Chatam 22	McLennan	31.62514	-97.16520	Alluvium	4.88	0.58	no
Buster Chatam 23	McLennan	31.62786	-97.16013	Alluvium	8.56	0.08	yes
Buster Chatam 24	McLennan	31.63027	-97.15578	Alluvium	11.72	1.07	no
Buster Chatam 25	McLennan	31.63265	-97.15132	Alluvium	7.03	0.21	yes
Buster Chatam 26	McLennan	31.63509	-97.14680	Alluvium/bedrock	9.38	1.3	no
ArcFalls1	Falls	31.38906	-97.02798	Alluvium	No Clear Peak	N/A	N/A
ArcFalls2	Falls	31.38911	-97.02866	Alluvium	5.59	0.4	No (close)
ArcFalls3	Falls	31.38918	-97.02950	Alluvium	5.38	0.16	Yes
ArcFalls4	Falls	31.38925	-97.03033	Alluvium	4.94	0.31	No (close)
ArcFalls5	Falls	31.38933	-97.03117	Alluvium	5	0.25	No, really close
ArcFalls6	Falls	31.38940	-97.03201	Alluvium	4.28	0.56	No (close)
ArcFalls7	Falls	31.38947	-97.03285	Alluvium	4.69	0.08	Yes
ArcFalls8	Falls	31.38955	-97.03389	Alluvium	4.38	0.07	Yes
ArcFalls9	Falls	31.38335	-97.01690	Alluvium	No Clear Peak	N/A	N/A
ArcFalls10	Falls	31.38381	-97.01755	Alluvium	6.47	0.19	Yes
ArcFalls11	Falls	31.38439	-97.01836	Alluvium	5.84	0.06	Yes
ArcFalls12	Falls	31.38485	-97.01900	Alluvium	6.38	0.14	Yes
ArcFalls13	Falls	31.38531	-97.01965	Alluvium	7.19	0.12	Yes
ArcFalls14	Falls	31.38589	-97.02046	Alluvium	6.22	2.64	No
ArcFalls15	Falls	31.38635	-97.02110	Alluvium	6.56	1.15	No
ArcFalls16	Falls	31.38690	-97.02195	Alluvium	6.63	0.19	Yes
ArcFalls17	Falls	31.38739	-97.02256	Alluvium	6	0.5	No
ArcFalls18	Falls	31.38779	-97.02326	Alluvium	6.13	0.2	Yes
ArcFalls19	Falls	31.38832	-97.02385	Alluvium	6.25	0.2	Yes
ArcFalls20	Falls	31.38889	-97.02466	Alluvium	5.84	0.2	Yes
ArcFalls21	Falls	31.38934	-97.02529	Alluvium	6.25	0.12	Yes
MLK & LaSalle	McLennan	31.55518	-97.10336	Alluvium	3.47	0.2	No, close
MLK 2	McLennan	31.55715	-97.10876	Alluvium	4.19	0.04	Yes

Table C.1. Passive Seismic (HVSR) Measurements

Site ID	County	Latitude	Longitude	Alluvium/Terrace	Peak Frequency (Hz)	Standard deviation (± Hz)	Passes SESAME?
MLK 3	McLennan	31.55886	-97.11208	Alluvium	4.97	0.08	Yes
MLK 4	McLennan	31.55976	-97.11644	Alluvium	5.09	0.2	Yes
MLK 5	McLennan	31.56406	-97.13009	Alluvium	4.69	0.25	No, close
MLK 6	McLennan	31.56622	-97.13391	Alluvium	4.97	0.5	No, close
MLK 7	McLennan	31.57200	-97.14118	Alluvium	4.69	0.06	Yes
MLK 8	McLennan	31.58298	-97.14993	Alluvium	4.25	0.21	Yes
MLK 9	McLennan	31.58922	-97.15326	Alluvium	5.25	0.19	Yes
MLK 10	McLennan	31.59311	-97.15316	Alluvium	10	0.21	Yes
JJ Flewellen Bend	McLennan	31.59184	-97.14190	Alluvium	11.25	0.08	Yes
JJ Flewellen Dripping Springs	McLennan	31.58650	-97.13693	Alluvium	10	0.09	Yes
Law School	McLennan	31.55330	-97.11550	Alluvium	No Clear Peak	N/A	N/A
BSB Field	McLennan	31.54914	-97.11067	Alluvium	5.84	0.07	Yes
RiverCrest	McLennan	31.54741	-97.10726	Alluvium	4.53	0.34	No
IM Field	McLennan	31.54889	-97.10155	Alluvium	4.38	0.07	Yes
Soccer Practice Field	McLennan	31.55117	-97.10929	Alluvium	3.94	0.07	Yes
Simpson Cal Pt	McLennan	31.55121	-97.11249	Alluvium	No Clear Peak	N/A	N/A
Dunlap Terrace	McLennan	31.50167	-97.01450	Terrace	6.56	12.5	No
Mt. Moriah #1	McLennan	31.48275	-96.98594	Terrace	5.38	0.16	Yes

APPENDIX D

Table D.1. Gravity Measurements

Station	Latitude	Longitude	Elevation (m above MSL)	Observed Gravity (mGal)	Bouguer Gravity Anomaly (μGal)	Standard Deviation (μGal)
Hirsch 1	31.51859	-97.05078	115.91	3511.687	119.8	15.1
Hirsch 1	31.51859	-97.05078	115.91	3511.681	114.0	20.3
Hirsch 1	31.51859	-97.05078	115.91	3511.655	119.9	16.9
Hirsch 2	31.51852	-97.05093	116.61	3511.476	107.9	22.0
Hirsch 3	31.51845	-97.05107	116.67	3511.405	80.2	22.2
Hirsch 4	31.51838	-97.05122	116.60	3511.398	84.3	24.4
Hirsch 5	31.51831	-97.05137	116.51	3511.42	111.2	26.6
Hirsch 6	31.51824	-97.05151	116.09	3511.477	93.8	22.4
Hirsch 7	31.51817	-97.05166	115.76	3511.519	81.7	15.9
Hirsch 8	31.51809	-97.05181	115.59	3511.527	77.9	20.8
Hirsch 9	31.51802	-97.05195	115.68	3511.485	84.5	17.5
Hirsch 10	31.51795	-97.05210	115.54	3511.507	101.0	18.9
Hirsch 11	31.51788	-97.05225	115.38	3511.498	79.9	14.9
Hirsch 12	31.51781	-97.05239	115.19	3511.488	51.0	15.7
Hirsch 13	31.51774	-97.05254	115.25	3511.471	77.7	15.3
Hirsch 14	31.51767	-97.05269	115.27	3511.387	27.4	12.8
Hirsch 15	31.51762	-97.05285	115.29	3511.337	7.3	24.9
Hirsch 16	31.51753	-97.05298	115.21	3511.36	40.3	21.6
Hirsch 17	31.51746	-97.05313	115.16	3511.341	36.7	13.8
Hirsch 18	31.51738	-97.05327	114.78	3511.401	29.3	17.1
Hirsch 19	31.51731	-97.05342	114.55	3511.425	26.7	14.6
Hirsch 20	31.51727	-97.05352	114.54	3511.44	58.5	24.4
Hirsch 21	31.51717	-97.05381	115.03	3511.211	0.0	27.5
Hirsch 22	31.51710	-97.05386	115.46	3511.142	50.0	25.3
Hirsch 23	31.51703	-97.05401	115.46	3511.113	49.8	18.7
Hirsch 24	31.51696	-97.05415	115.45	3511.104	66.4	25.8
Hirsch 25	31.51689	-97.05430	115.57	3511.031	50.5	12.6
Hirsch 26	31.51682	-97.05445	115.59	3511.016	66.1	59.1

Table D.1. Gravity Measurements

Station	Latitude	Longitude	Elevation (m above MSL)	Observed Gravity (mGal)	Bouguer Gravity Anomaly (μGal)	Standard Deviation (μGal)
Hirsch 27	31.51675	-97.05459	115.69	3510.981	84.0	17.9
Hirsch 28	31.51667	-97.05474	115.94	3510.857	49.8	12.2
Hirsch 29	31.51660	-97.05489	115.71	3510.878	42.5	16.8
Hirsch 30	31.51653	-97.05503	115.53	3510.941	90.5	13.5
Hirsch 31	31.51646	-97.05518	115.37	3510.967	103.1	13.4
Hirsch 32	31.51640	-97.05533	115.09	3510.988	84.3	25.2
Hirsch 33	31.51633	-97.05548	114.98	3510.999	94.5	28.3
Hirsch 34	31.51627	-97.05563	114.91	3510.998	104.0	18.3
Hirsch 35	31.51618	-97.05577	114.72	3510.994	83.2	33.1
Hirsch 36	31.51611	-97.05591	114.68	3510.985	92.0	13.5
Hirsch 37	31.51604	-97.05606	114.47	3511.043	127.2	12.5
Hirsch 38	31.51598	-97.05621	114.34	3510.978	57.5	20.2
Hirsch 39	31.51591	-97.05636	114.35	3510.977	86.4	21.1
Hirsch 40	31.51584	-97.05651	114.34	3510.943	76.4	20.2
Hirsch 41	31.51576	-97.05665	114.50	3510.847	48.9	16.0
Hirsch 42	31.51569	-97.05680	114.59	3510.842	95.0	13.0
Hirsch 43	31.51561	-97.05697	114.69	3510.807	121.3	12.7
Hirsch 44	31.51554	-97.05709	114.75	3510.739	92.1	15.2
Hirsch 45	31.51547	-97.05723	114.78	3510.693	81.7	19.2
Hirsch 46	31.51540	-97.05738	114.92	3510.62	70.7	32.7
Hirsch 47	31.51537	-97.05743	115.22	3510.539	89.7	21.5
MCC NW Corner	31.65490	-97.20370	128.14	3492.523	53.2	17.9
MCC NW Corner	31.65488	-97.20361	128.14	3492.536	53.2	65.8
MCC 5	31.65486	-97.20352	128.28	3492.533	90.1	20.1
MCC 6	31.65484	-97.20343	128.12	3492.533	47.4	25.2
MCC 7	31.65482	-97.20333	128.11	3492.563	71.5	33.1
MCC 8	31.65480	-97.20324	128.17	3492.578	95.8	34.9
MCC 9	31.65478	-97.20315	128.11	3492.543	43.5	16.8
MCC 11	31.65476	-97.20306	128.10	3492.587	76.5	29.7
MCC 12	31.65474	-97.20297	128.07	3492.583	62.0	20.3

Table D.1. Gravity Measurements

Station	Latitude	Longitude	Elevation (m above MSL)	Observed Gravity (mGal)	Bouguer Gravity Anomaly (μGal)	Standard Deviation (μGal)
MCC 13	31.65472	-97.20287	128.06	3492.578	49.5	94.5
MCC 14	31.65470	-97.20278	128.04	3492.599	61.7	28.0
MCC 15	31.65468	-97.20269	128.07	3492.611	76.9	27.1
MCC 16	31.65466	-97.20260	128.11	3492.605	76.9	24.2
MCC 17	31.65464	-97.20251	128.18	3492.609	93.4	21.3
MCC 18	31.65462	-97.20241	128.19	3492.606	88.5	33.5
MCC 19	31.65460	-97.20232	128.15	3492.587	57.3	35.4
MCC 20	31.65458	-97.20223	128.11	3492.609	64.6	30.5
MCC 21	31.65456	-97.20214	128.09	3492.619	66.5	17.7
MCC 22	31.65454	-97.20204	128.06	3492.64	77.3	20.4
MCC 23	31.65452	-97.20195	128.15	3492.636	89.5	128.4
MCC 24	31.65450	-97.20186	128.37	3492.636	138.3	37.6
MCC 25	31.65448	-97.20177	128.64	3492.572	136.0	21.3
MCC 26	31.65446	-97.20168	128.44	3492.528	39.6	26.6
MCC 27	31.65444	-97.20158	128.48	3492.573	91.6	62.2
MCC 28	31.65442	-97.20149	128.31	3492.578	51.2	30.1
MCC 29	31.65440	-97.20140	128.29	3492.593	56.2	104.9
MCC 30	31.65438	-97.20131	128.34	3492.644	114.8	17.6
MCC 31	31.65436	-97.20122	128.42	3492.631	118.6	24.2
MCC 33	31.65434	-97.20112	128.07	3492.667	61.4	18.5
MCC 34	31.65433	-97.20103	128.05	3492.706	92.8	35.1
MCC 35	31.65431	-97.20094	127.98	3492.693	58.2	22.8
MCC 36	31.65429	-97.20085	127.89	3492.723	61.7	24.1
MCC 37	31.65427	-97.20076	127.90	3492.752	90.0	22.6
MCC 38	31.65425	-97.20066	128.12	3492.777	163.9	48.0
MCC 39	31.65423	-97.20057	128.26	3492.723	139.4	15.3
MCC 40	31.65421	-97.20048	128.36	3492.687	123.2	29.1
MCC 41	31.65419	-97.20039	128.52	3492.681	152.5	17.7
MCC 42	31.65417	-97.20030	128.51	3492.639	105.8	88.1
MCC 43	31.65415	-97.20020	128.49	3492.653	110.3	17.1
MCC 44	31.65413	-97.20011	128.38	3492.648	75.1	47.9
MCC 45	31.65411	-97.20002	128.11	3492.674	32.3	16.5

Table D.1. Gravity Measurements

Station	Latitude	Longitude	Elevation (m above MSL)	Observed Gravity (mGal)	Bouguer Gravity Anomaly (μGal)	Standard Deviation (μGal)
MCC 46	31.65409	-97.19993	127.67	3492.752	0.0	23.9
MCC 47	31.65407	-97.19984	127.33	3492.849	10.2	19.3
MCC 48	31.65405	-97.19974	127.04	3492.941	28.4	57.5
MCC 49	31.65403	-97.19965	126.78	3493.048	68.6	22.6
MCC 50	31.65401	-97.19956	126.54	3493.101	59.2	20.1
MCC 51	31.65399	-97.19947	126.20	3493.173	45.9	39.1
MCC 52	31.65397	-97.19938	126.10	3493.23	74.7	41.3
MCC 53	31.65395	-97.19928	125.80	3493.243	12.5	70.2
MCC 54	31.65393	-97.19919	125.90	3493.322	111.0	32.2
MCC NE Corner	31.65391	-97.19910	129.58	3492.552	52.5	19.5
MCC NE Corner	31.65390	-97.19904	129.58	3492.583	52.5	14.8
MCC 55	31.65647	-97.20072	129.24	3492.618	47.1	15.4
MCC 56	31.65638	-97.20074	129.24	3492.581	24.8	11.2
MCC 57	31.65628	-97.20078	129.22	3492.588	37.1	18.6
MCC 58	31.65619	-97.20080	129.18	3492.586	37.9	11.2
MCC 59	31.65611	-97.20083	129.27	3492.551	34.4	12.1
MCC 60	31.65602	-97.20086	129.32	3492.526	32.9	13.2
MCC 61	31.65593	-97.20088	129.43	3492.545	88.8	13.2
MCC 62	31.65585	-97.20091	129.45	3492.468	26.8	10.9
MCC 63	31.65576	-97.20093	129.32	3492.485	23.6	26.2
MCC 64	31.65567	-97.20096	129.03	3492.571	51.3	19.1
MCC 65	31.65558	-97.20098	129.07	3492.553	53.7	13.2
MCC 66	31.65549	-97.20101	129.23	3492.477	28.6	16.0
MCC 67	31.65541	-97.20103	129.32	3492.491	76.6	15.3
MCC 68	31.65532	-97.20106	129.26	3492.505	85.1	14.2
MCC 69	31.65523	-97.20108	129.06	3492.526	69.5	11.1
MCC 70	31.65514	-97.20111	128.97	3492.518	50.4	11.3
MCC 71	31.65506	-97.20113	128.89	3492.543	66.7	20.9
MCC 72	31.65497	-97.20116	128.87	3492.549	79.1	9.8
MCC 73	31.65488	-97.20118	128.98	3492.476	45.2	13.6

Table D.1. Gravity Measurements

Station	Latitude	Longitude	Elevation (m above MSL)	Observed Gravity (mGal)	Bouguer Gravity Anomaly (μGal)	Standard Deviation (μGal)
MCC 74	31.65479	-97.20121	129.21	3492.461	95.5	14.9
MCC 75	31.65471	-97.20124	128.79	3492.511	55.9	22.8
MCC 76	31.65462	-97.20126	128.59	3492.534	42.7	20.9
MCC 77	31.65453	-97.20129	128.32	3492.576	30.7	20.6
MCC 78	31.65444	-97.20131	128.25	3492.601	47.4	31.5
MCC 79	31.65436	-97.20134	128.05	3492.6	10.5	22.9
MCC 80	31.65427	-97.20136	127.78	3492.697	53.3	18.5
MCC 81	31.65418	-97.20139	127.46	3492.761	50.8	26.5
MCC 82	31.65409	-97.20142	127.19	3492.764	0.0	19.2
MCC 83	31.65401	-97.20144	127.14	3492.791	27.3	14.3
MCC 84	31.65392	-97.20147	127.00	3492.806	18.1	16.5
MCC 85	31.65383	-97.20149	126.91	3492.821	22.1	13.8
MCC 86	31.65374	-97.20152	126.87	3492.83	32.9	32.8
MCC 86	31.65366	-97.20154	126.77	3492.819	9.0	18.3
MCC 87	31.65357	-97.20157	126.76	3492.838	38.6	20.7
MCC 88	31.65348	-97.20159	126.88	3492.847	85.4	18.4
MCC 89	31.65339	-97.20162	126.92	3492.836	97.2	16.8
MCC 90	31.65331	-97.20164	126.83	3492.802	52.7	15.7
MCC 91	31.65322	-97.20167	126.83	3492.793	53.4	11.9
MCC 92	31.65313	-97.20170	126.85	3492.811	87.8	14.4
MCC 93	31.65304	-97.20172	126.76	3492.779	45.2	16.5
MCC 94	31.65296	-97.20175	126.53	3492.791	12.6	19.2
MCC 95	31.65287	-97.20177	126.44	3492.814	24.3	15.2
MCC 96	31.65278	-97.20180	126.33	3492.846	40.7	14.7
MCC 97	31.65269	-97.20182	126.32	3492.817	20.7	23.4
MCC SWCorner	31.65261	-97.20185	126.37	3492.829	54.6	24.0
MCC SW Corner	31.65261	-97.20185	126.37	3492.878	102.9	22.2
MR Station 1	31.32260	-97.02513	107.60	3506.502	121.6	30.3

Table D.1. Gravity Measurements

Station	Latitude	Longitude	Elevation (m above MSL)	Observed Gravity (mGal)	Bouguer Gravity Anomaly (μGal)	Standard Deviation (μGal)
MR Station 1	31.32260	-97.02513	107.60	3505.389	121.6	17.1
MR Station 1	31.32263	-97.02506	107.60	3506.483	121.6	29.7
MR Station 2	31.32265	-97.02500	111.97	3505.39	367.0	17.3
MR Station 3	31.32268	-97.02493	111.41	3505.524	343.6	31.2
MR Station 4	31.32271	-97.02487	110.86	3505.649	316.7	12.4
MR Station 5	31.32273	-97.02480	110.43	3505.77	313.4	26.0
MR Station 6	31.32276	-97.02473	109.89	3505.869	259.9	16.9
MR Station 7	31.32279	-97.02467	109.28	3505.991	213.4	23.7
MR Station 8	31.32282	-97.02460	108.75	3506.108	164.5	13.9
MR Station 9	31.32284	-97.02453	108.45	3506.218	183.8	20.5
MR Station 10	31.32287	-97.02447	108.25	3506.274	171.6	14.9
MR Station 11	31.32290	-97.02440	108.08	3506.309	147.9	11.9
MR Station 12	31.32292	-97.02433	107.93	3506.35	134.2	22.3
MR Station 13	31.32295	-97.02427	107.79	3506.422	154.7	20.0
MR Station 14	31.32300	-97.02416	107.72	3506.418	103.9	24.3
MR Station 15	31.32300	-97.02415	107.60	3506.481	137.4	21.8

Table D.1. Gravity Measurements

Station	Latitude	Longitude	Elevation (m above MSL)	Observed Gravity (mGal)	Bouguer Gravity Anomaly (μGal)	Standard Deviation (μGal)
MR Station 16	31.32305	-97.02404	107.60	3506.496	121.6	29.7
MR Station 18	31.32310	-97.02392	107.51	3506.52	92.8	14.4
MR Station 19	31.32315	-97.02380	107.41	3506.555	70.7	31.9
MR Station 20	31.32320	-97.02369	107.26	3506.635	83.2	19.4
MR Station 21	31.32326	-97.02357	107.20	3506.674	77.2	15.5
MR Station 22	31.32331	-97.02345	107.21	3506.693	66.9	38.0
MR Station 23	31.32336	-97.02334	107.14	3506.744	69.2	15.1
MR Station 24	31.32341	-97.02322	107.08	3506.756	35.2	19.9
MR Station 25	31.32346	-97.02310	106.98	3506.845	68.8	20.1
MR Station 26	31.32352	-97.02299	106.92	3506.875	52.9	11.3
MR Station 27	31.32357	-97.02287	106.85	3506.899	29.1	17.0
MR Station 28	31.32362	-97.02276	106.80	3506.927	12.3	14.9
MR Station 29	31.32367	-97.02264	106.73	3506.981	16.8	19.0
MR Station 30	31.32372	-97.02252	106.71	3507.024	24.1	18.7
MR Station 31	31.32377	-97.02240	106.64	3507.075	28.4	36.6
MR Station 32	31.32383	-97.02229	106.48	3507.131	14.0	14.8

Table D.1. Gravity Measurements

Station	Latitude	Longitude	Elevation (m above MSL)	Observed Gravity (mGal)	Bouguer Gravity Anomaly (μGal)	Standard Deviation (μGal)
MR Station 33	31.32388	-97.02217	106.45	3507.196	38.8	15.9
MR Station 34	31.32393	-97.02205	106.38	3507.205	0.4	19.6
MR Station 35	31.32398	-97.02194	106.28	3507.261	0.0	4.3
MR Station 36	31.32403	-97.02182	106.25	3507.314	13.5	25.8
MR Station 37	31.32408	-97.02170	106.22	3507.351	13.3	28.9
MR Station 38	31.32414	-97.02159	106.19	3507.41	33.5	13.5
MR Station 39	31.32419	-97.02147	106.13	3507.485	63.0	28.4
MR Station 40	31.32419	-97.02146	106.16	3507.466	50.1	29.3
MR Station 41	31.32428	-97.02128	106.51	3507.428	50.5	23.3
MR Station 42	31.32436	-97.02110	107.22	3507.298	48.9	15.3
MR Station 43	31.32457	-97.02063	108.52	3506.614	-439.4	40.8
MR Station 44	31.32469	-97.02036	107.81	3507.381	78.4	13.3
MR Station 45	31.32478	-97.02017	107.16	3507.537	22.5	27.4
MR Station 46	31.32486	-97.01998	106.71	3507.753	76.1	30.1
MR Station 47	31.32495	-97.01980	106.59	3507.814	59.1	18.1
MR Station 48	31.32497	-97.01957	106.36	3507.928	65.5	50.5

Table D.1. Gravity Measurements

Station	Latitude	Longitude	Elevation (m above MSL)	Observed Gravity (mGal)	Bouguer Gravity Anomaly (μGal)	Standard Deviation (μGal)
MR Station 49	31.32499	-97.01935	106.29	3508.013	82.8	49.2
MR Station 49	31.32501	-97.01913	106.29	3508.104	123.4	22.7
MR Station 50	31.32503	-97.01890	106.25	3508.145	104.9	51.9
BustChat 2	31.62004	-97.17456	123.35	3488.239	67.6	32.6
BustChat 2	31.62004	-97.17456	123.35	3488.271	99.7	26.2
BustChat 3	31.62016	-97.17434	122.76	3488.387	42.0	23.5
BustChat 3	31.62016	-97.17434	122.76	3488.358	12.6	25.4
BustChat 4	31.62028	-97.17412	122.96	3488.412	88.9	20.2
BustChat 5	31.62040	-97.17390	122.84	3488.452	69.8	21.9
BustChat 6	31.62053	-97.17368	123.02	3488.444	77.1	22.2
BustChat 7	31.62066	-97.17347	123.01	3488.441	43.8	25.5
BustChat 8	31.62077	-97.17323	122.94	3488.482	38.0	21.9
BustChat 9	31.62089	-97.17301	122.73	3488.576	51.1	22.9
BustChat 10	31.62101	-97.17279	122.75	3488.547	0.0	39.5
BustChat 10	31.62101	-97.17279	122.75	3488.584	37.3	68.6
BustChat 11	31.62113	-97.17256	122.77	3488.611	39.2	66.8

Table D.1. Gravity Measurements

Station	Latitude	Longitude	Elevation (m above MSL)	Observed Gravity (mGal)	Bouguer Gravity Anomaly (μGal)	Standard Deviation (μGal)
BustChat 11	31.62113	-97.17256	122.77	3488.605	33.1	49.3
BustChat 12	31.62127	-97.17235	122.63	3488.666	31.3	27.0
BustChat 13	31.62139	-97.17213	122.77	3488.707	79.9	19.7
BustChat 14	31.62152	-97.17187	122.22	3488.814	20.3	24.3
BustChat 14	31.62152	-97.17187	122.22	3488.808	13.4	26.6
BustChat 15	31.62163	-97.17168	122.13	3488.846	4.7	23.1
BustChat 16	31.62175	-97.17143	122.53	3488.838	61.3	24.7
BustChat 17	31.62187	-97.17122	123.19	3488.696	55.2	26.7
BustChat 18	31.62200	-97.17102	123.43	3488.698	86.5	38.5
BustChat 19	31.62214	-97.17082	123.94	3488.624	110.3	30.3
BustChat 20	31.62228	-97.17058	125.06	3488.356	82.4	30.4
BustChat 21	31.62239	-97.17038	125.53	3488.265	78.9	38.4
BustChat 22	31.62251	-97.17015	125.34	3488.349	88.5	23.9
BustChat 23	31.62261	-97.16992	125.24	3488.393	83.6	26.5
BustChat 23	31.62261	-97.16992	125.24	3488.386	77.0	24.3
BustChat 23	31.62261	-97.16992	125.24	3488.377	68.0	22.5

Table D.1. Gravity Measurements

Station	Latitude	Longitude	Elevation (m above MSL)	Observed Gravity (mGal)	Bouguer Gravity Anomaly (μGal)	Standard Deviation (μGal)
BustChat 23	31.62261	-97.16992	125.24	3488.421	111.8	29.0
BustChat 24	31.62273	-97.16970	125.10	3488.44	65.9	24.5
BustChat 25	31.62283	-97.16946	125.02	3488.494	73.5	23.2
BustChat 26	31.62298	-97.16921	125.25	3488.458	60.3	23.8
BustChat 27	31.62309	-97.16902	125.00	3488.54	57.4	26.2
BustChat 28	31.62320	-97.16879	124.88	3488.604	64.3	20.1
BustChat 29	31.62332	-97.16857	124.70	3488.649	36.3	26.4
BustChat 29	31.62332	-97.16857	124.70	3488.717	103.9	21.3
BustChat 30	31.62345	-97.16836	124.88	3488.702	104.3	21.1
BustChat 31	31.62356	-97.16812	124.69	3488.743	70.1	23.4
BustChat 32	31.62368	-97.16791	124.74	3488.731	41.9	22.9
BustChat 33	31.62381	-97.16769	124.76	3488.757	43.5	20.3
BustChat 34	31.62395	-97.16748	124.71	3488.843	90.9	23.2
BustChat 35	31.62407	-97.16725	124.55	3488.865	43.5	22.8
BustChat 36	31.62418	-97.16702	124.74	3488.86	57.6	21.2
BustChat 37	31.62430	-97.16680	124.83	3488.87	60.4	26.3

Table D.1. Gravity Measurements

Station	Latitude	Longitude	Elevation (m above MSL)	Observed Gravity (mGal)	Bouguer Gravity Anomaly (μGal)	Standard Deviation (μGal)
BustChat 38	31.62440	-97.16655	124.76	3488.908	49.3	22.8
BustChat 39	31.62454	-97.16636	124.65	3488.949	37.8	19.3
BustChat 40	31.62466	-97.16613	124.55	3489	36.7	26.6
BustChat 41	31.62478	-97.16590	124.62	3489.059	82.0	32.4
BustChat 41	31.62478	-97.16590	124.62	3489.055	78.1	37.4
BustChat 42	31.62490	-97.16568	124.44	3489.102	52.8	40.1
BustChat 43	31.62502	-97.16546	124.28	3489.164	47.0	17.0
BustChat 44	31.62514	-97.16520	124.15	3489.216	35.9	26.5
BustChat 45	31.62525	-97.16501	124.26	3489.222	44.7	24.0
BustChat 1	31.62539	-97.16477	124.49	3489.213	37.9	21.2
BustChat 1	31.62539	-97.16477	124.49	3489.192	37.9	30.6
BustChat 1	31.62539	-97.16477	124.49	3489.192	37.9	23.8
BustChat 46	31.61527	-97.17145	121.64	3488.487	N/A	N/A
BustChat 46	31.61527	-97.17145	121.64	3488.476	N/A	N/A
BustChat 47	31.62748	-97.16103	124.80	3489.666	N/A	N/A
BustChat 48	31.63183	-97.15263	131.53	3489.365	N/A	N/A

Table D.1. Gravity Measurements

Station	Latitude	Longitude	Elevation (m above MSL)	Observed Gravity (mGal)	Bouguer Gravity Anomaly (μGal)	Standard Deviation (μGal)
AF1 W end transect 1 (Grav 2)	31.38955	-97.03389	110.20	3504.185	39.3	19.4
AF1 Grav 3	31.38954	-97.03368	110.27	3504.165	12.9	24.2
AF1 Grav 4	31.38952	-97.03347	110.20	3504.214	21.3	19.3
AF1 Grav 5	31.38950	-97.03326	110.15	3504.25	17.5	19.1
AF1 Grav 6	31.38948	-97.03305	110.08	3504.286	13.5	18.3
AF1 Grav 7	31.38947	-97.03285	109.92	3504.279	6.0	19.4
AF1 Grav 7	31.38945	-97.03264	109.92	3504.362	59.0	18.2
AF1 Grav 8	31.38943	-97.03243	109.96	3504.387	36.1	21.3
AF1 Grav 9	31.38941	-97.03222	109.95	3504.452	72.5	18.0
AF1 Grav 9	31.38940	-97.03201	109.95	3504.475	94.6	18.9
AF1 Grav 10	31.38938	-97.03180	109.91	3504.491	77.7	24.7
AF1 Grav 11	31.38936	-97.03159	109.93	3504.509	77.6	18.6
AF1 Grav 12	31.38934	-97.03138	109.80	3504.598	107.3	16.8
AF1 Grav 13	31.38933	-97.03117	109.81	3504.63	117.7	63.9
AF1 Grav 14	31.38931	-97.03096	109.82	3504.637	102.8	17.6

Table D.1. Gravity Measurements

Station	Latitude	Longitude	Elevation (m above MSL)	Observed Gravity (mGal)	Bouguer Gravity Anomaly (μGal)	Standard Deviation (μGal)
AF1 Grav 15	31.38929	-97.03075	109.76	3504.624	51.9	19.9
AF1 Grav 16	31.38927	-97.03054	109.73	3504.655	50.2	24.5
AF1 Grav 17	31.38925	-97.03033	109.82	3504.651	45.6	25.3
AF1 Grav 18	31.38924	-97.03012	109.84	3504.666	40.6	21.9
AF1 Grav 19	31.38922	-97.02992	109.95	3504.707	85.6	21.8
AF1 Grav 20	31.38920	-97.02971	109.75	3504.738	41.5	16.2
AF1 Grav 21	31.38918	-97.02950	109.63	3504.799	48.8	20.3
AF1 Grav 22	31.38917	-97.02929	109.62	3504.816	38.9	19.8
AF1 Grav 24	31.38915	-97.02908	109.56	3504.855	37.6	23.0
AF1 Grav 25	31.38913	-97.02887	109.56	3504.879	37.4	17.0
AF1 Grav 26	31.38911	-97.02866	109.77	3504.846	33.9	24.9
AF1 Grav 27	31.38910	-97.02845	109.80	3504.864	33.9	22.7
AF1 Grav 28	31.38908	-97.02824	109.85	3504.908	68.1	23.3
AF1 Grav 29	31.38908	-97.02824	109.85	3504.865	0.0	24.5
AF1 Grav 30	31.38908	-97.02824	109.96	3504.919	58.8	23.0
AF1 E end	31.38906	-97.02798	110.05	3504.918	74.6	22.6

Table D.1. Gravity Measurements

Station	Latitude	Longitude	Elevation (m above MSL)	Observed Gravity (mGal)	Bouguer Gravity Anomaly (μGal)	Standard Deviation (μGal)
Transect 1 (Grav 1) AF1 E end						
Transect 1 (Grav 1)	31.38906	-97.02798	110.05	3504.891	21.5	27.0
AF2 31	31.38335	-97.01690	108.31	3506.174	110.7	29.6
AF2 31	31.38335	-97.01690	108.31	3506.142	55.8	24.0
AF2 32	31.38346	-97.01707	108.33	3506.142	73.5	19.1
AF2 33	31.38358	-97.01723	108.32	3506.146	86.1	24.2
AF2 34	31.38369	-97.01739	108.27	3506.139	80.4	20.8
AF2 35	31.38381	-97.01755	108.31	3506.135	98.8	17.5
AF2 36	31.38392	-97.01771	108.29	3506.12	91.8	16.7
AF2 37	31.38404	-97.01787	108.22	3506.099	67.1	25.7
AF2 38	31.38416	-97.01803	108.23	3506.126	107.4	19.5
AF2 39	31.38427	-97.01820	108.17	3506.098	77.4	19.1
AF2 40	31.38439	-97.01836	108.19	3506.07	68.3	21.4
AF2 40	31.38450	-97.01852	108.19	3506.082	80.4	23.7
AF2 41	31.38462	-97.01868	108.29	3506.007	43.7	25.0
AF2 42	31.38473	-97.01884	108.41	3505.968	45.6	21.7
AF2 43	31.38485	-97.01900	108.60	3505.895	33.5	20.3
AF2 44	31.38496	-97.01916	108.79	3505.867	64.9	18.1
AF2 45	31.38508	-97.01933	108.77	3505.822	29.1	20.1
AF2 46	31.38520	-97.01949	108.77	3505.78	0.0	22.8
AF2 47	31.38531	-97.01965	108.91	3505.783	49.3	17.0
AF2 48	31.38554	-97.01997	108.84	3505.802	63.4	27.6
AF2 49	31.38566	-97.02013	109.00	3505.757	84.4	69.8
AF2 50	31.38577	-97.02030	108.26	3505.906	61.5	22.3
AF2 51	31.38589	-97.02046	108.96	3505.759	102.1	21.0
AF2 52	31.38600	-97.02062	109.10	3505.681	71.5	17.3
AF2 53	31.38624	-97.02094	108.02	3505.951	85.2	31.5
AF2 54	31.38635	-97.02110	109.11	3505.633	63.3	24.2

Table D.1. Gravity Measurements

Station	Latitude	Longitude	Elevation (m above MSL)	Observed Gravity (mGal)	Bouguer Gravity Anomaly (μGal)	Standard Deviation (μGal)
AF2 55	31.38650	-97.02123	108.75	3505.72	72.5	35.6
AF2 56	31.38670	-97.02159	108.45	3505.774	64.5	46.0
AF2 57	31.38690	-97.02195	107.83	3505.891	53.8	32.6
AF2 58	31.38704	-97.02207	107.87	3505.874	70.8	32.6
AF2 59	31.38716	-97.02223	107.87	3505.837	46.2	28.1
AF2 60	31.38727	-97.02239	107.96	3505.792	38.2	30.0
AF2 62	31.38739	-97.02256	107.78	3505.812	38.3	22.4
AF2 63	31.38751	-97.02272	107.92	3505.761	33.5	27.6
AF2 64	31.38762	-97.02288	108.22	3505.698	64.0	20.1
AF2 65	31.38773	-97.02304	108.35	3505.66	69.2	18.0
AF2 66	31.38779	-97.02326	108.19	3505.626	8.1	39.6
AF2 67	31.38797	-97.02336	108.33	3505.651	80.6	20.3
AF2 68	31.38808	-97.02353	108.43	3505.601	68.3	22.8
AF2 69	31.38820	-97.02369	108.48	3505.547	39.4	21.9
AF2 70	31.38832	-97.02385	108.47	3505.561	63.9	28.0
AF2 71	31.38843	-97.02401	108.51	3505.535	58.7	20.7
AF2 72	31.38855	-97.02417	108.41	3505.566	78.0	23.3
AF2 73	31.38866	-97.02433	108.43	3505.551	81.0	29.0
AF2 74	31.38878	-97.02449	108.49	3505.499	57.7	24.8
AF2 75	31.38889	-97.02466	108.44	3505.572	129.1	16.8
AF2 76	31.38901	-97.02482	108.56	3505.494	96.3	20.1
AF2 77	31.38912	-97.02498	108.57	3505.453	70.1	31.3
AF2 78	31.38924	-97.02514	108.61	3505.47	108.0	22.6
AF2 NW end (Grav 79)	31.38934	-97.02529	108.53	3505.486	91.6	23.4

BIBLIOGRAPHY

Bankey, V., 2006, Texas magnetic and gravity maps and data: A website for distribution of data. U.S. Geological Survey Data Series Report 232. https://pubs.usgs.gov/ds/2006/232/texas_boug.htm

Barnes, V.E., 1979, Geologic atlas of Texas, Waco sheet: Lloyd William Stephenson memorial edition, The University of Texas at Austin Bureau of Economic Geology.

Beall, A.O., 1964, Stratigraphy of the Taylor (Upper Cretaceous), East-Central Texas: Baylor Geological Studies Bulletin No. 6, p. 1-33.

Bignardi, S., 2017, The uncertainty of estimating the thickness of soft-sediments with the HVSR method: A computational point of view on weak lateral variations. *J of Applied Geophysics* 145, 28-38.

Blake, D.R. and Nash, T.A., 2018, Mapping bedrock topography and drift thickness of the preglacial Teays River within the Anna Seismic Zone, Ohio: Columbus, Ohio Department of Natural Resources, Division of Geological Survey Open-File Report 2018-2, p. 1-18

Bohidar, R.N., Sullivan, J.P. and Hermance, J.F., 2001, Delineating depth to bedrock beneath shallow unconfined aquifers: A gravity transect across the Palmer River Basin. *Ground Water* 39.5, 729-736.

Bradley R.G., 2008, GTA aquifer assessment 07-05mag. Texas Water Development Board: Groundwater Technical Assistance Section. https://www.twdb.texas.gov/groundwater/docs/AA/AA07-05_MAG.pdf

Cannata, S., 1987, A seismic refraction and electric resistivity study over different lithologic scenarios with emphasis on detecting the water table: Baylor University, unpublished student paper.

Carmichael, R. S. 1989, *Practical Handbook of Physical Properties of Rocks and Minerals*. Boca Raton, FL: CRC Press.

Carmichael, R. S. and Henry Jr., G., 1977, Gravity exploration for groundwater and bedrock topography in glaciated areas. *Geophysics* 42.4, 850-859.

Chandler, V.W. and Lively., R.S., 2016, Utility of the horizontal-to-vertical spectral ratio passive seismic method for estimating thickness of Quaternary sediments in Minnesota and adjacent parts of Wisconsin. *Interpretation* 4.3, SH71-SH90.

Cronin, J.G. and Wilson, C.A., 1967, Ground water in the flood-plain alluvium of the Brazos River, Whitney Dam to vicinity of Richmond, Texas: Texas Water Development Board Report 41.

Delgado, J., Lopez Casado, C., Giner, J., Estévez, A., Cuenca, A. and Molina, S., 2000, Microtremors as a geophysical exploration tool: applications and limitations. *Pure and Applied Geophysics* 157, 1445–1462.

Driscoll, F.G., 1986, *Groundwater and Wells*. St. Paul, MN: Johnson Division.

Epps, L.W., 1973, A geologic history of the Brazos River. Baylor Geological Studies Bulletin No. 24, p. 1-44.

Ewing, J.E., Harding, J.J., and Jones, T.L., 2016, Final conceptual model report for the Brazos River Alluvium Aquifer groundwater availability model. Texas Water Development Board: Austin, TX. p. 1-514

Ewing, J.E., and Jigmond, M., 2016, Final numerical model report for the Brazos River Alluvium Aquifer groundwater availability model. p. 1-357.

Feldpausch, S.A., 2017, Gravity and passive seismic methods used jointly for understanding the subsurface in a glaciated terrain: Dowling and Maple Grove quadrangles, Barry County, Michigan: Western Michigan University, unpublished Master thesis.

Goforth, T., and Hayward, C., 1992, Seismic reflection investigations of a bedrock surface buried under alluvium. *Geophysics* 57.9, 1217-1227.

Haefner, R.J., Sheets, R.A. and Andrews, R.E., 2010, Evaluation of the horizontal-to-vertical spectral ratio (HVSR) seismic method to determine sediment thickness in the vicinity of the South Well Field, Franklin County, OH. *The Ohio Journal of Science* 110.4, 77-85.

Harlan, S.K., 1985, Hydrogeological assessment of the Brazos River Alluvial Aquifer Waco-Marlin, Texas: Baylor University, unpublished Bachelor thesis.

Harlan, S.K., 1990, Hydrogeologic assessment of the Brazos River Alluvial Aquifer Waco to Marlin, Texas: Baylor University, unpublished Master thesis.

Hinze, W. J., von Frese, R.R.B, and Saad, A.H., 2013, *Gravity and Magnetic Exploration: Principles, Practices, and Applications*. Cambridge: Cambridge University Press.

Ibrahim, A. and Hinze, W.J., 1972, Mapping buried bedrock topography with gravity, *Ground Water* 10.3, 18-23.

Ibs-von Seht, M. and Wohlenberg, J., 1999, Microtremor measurements used to map thickness of soft sediments, *Bulletin of the Seismological Society of America*; 89.1, 250-259.

Jarvis, J.C., 2019, Compartmentalization in the Northern Segment of the Brazos River Alluvium Aquifer: Baylor University, unpublished Master thesis.

Johnson, C.D., and Lane, J.W., 2016, Statistical comparison of methods for estimating sediment thickness from horizontal-to-vertical spectral ratio (HVSR) seismic methods: An example from Tylerville, Connecticut, USA. *Symposium on the Application of Geophysics to Engineering and Environmental Problems*, Denver, CO, Proceedings. p. 1-7

Ju, D.H., 2014, Aquifer framework restoration (AFR) in an alluvial aquifer, Central Texas: Baylor University, unpublished Master thesis.

Leica SmartNet, 2016, *UK & Ireland Network RTK User Guide*. Leica Geosystems Limited. Milton Keynes, UK. https://surveyequipment.com/assets/index/download/id/142/

Langerman Foster LLC, 2020, Engineering properties database of bedrock and sediments in McLennan County. Accessed January 2020.

Micromed S.P.A., 2009, The short Tromino how to, Version 1.1. Treviso, Italy.

Micromed S.P.A., 2018, Grilla version 8.0, spectral and HVSR analysis. Treviso, Italy.

Montgomery, E.L., 1971, Determination of coefficient of storage by use of gravity measurements*:* University of Arizona, unpublished Doctoral dissertation.

Mucciarelli, M., Gallipoli, M.R., Giacomo, D.D., Nota, F.D. and Nino, E., 2005, The influence of wind on measurements of seismic noise. *Geophysical Journal International* 161.2, 303-308.

Nakamura, Y., 1989, A method for dynamic characteristics estimation of subsurface using microtremor on the ground surface, *Quarterly Report Railway Technical Research Institute* 30.1, 25–33.

Natural Resources Conservation Service, 2019, Web Soil Survey. Bulk density, one-third bar—McLennan County, Texas. Accessed April 25, 2020.

Noonan, E.P., 2019, Salinity in the Northern Segment of the Brazos River Alluvium Aquifer: A hydro-forensic approach: Baylor University, unpublished Master thesis.

Pinkus, J.R., 1987, Hydrogeologic assessment of three solid waste disposal sites in the Brazos River Alluvium Aquifer: Baylor University, unpublished Master thesis.

Pool, D.R. and Eychaner, J.H., 1995, Measurements of aquifer-storage change and specific yield using gravity surveys. *Ground Water* 33.3, 425-432.

Scintrix LTD, 2017, CG-6 R16 Autograv survey gravity meter brochure. Scintrex LTD: Ontario, Canada https://scintrexltd.com/wp-content/uploads/2017/07/CG-6-brochure_R16.pdf

Shah, S.D., Houston, N.A. and Braun, C.L., 2007, Hydrogeologic characterization of the Brazos River Alluvium Aquifer, Bosque County to Fort Bend County, Texas. U.S. Geological Survey Scientific Investigation Map 2989.

Shi, J., Bradley, R.G., Wade, S.C., Jones, I.C., Anaya, R. and Seiter-Weatherford, C., 2014, GAM Task 13-031: Total estimated recoverable storage for aquifers in Groundwater Management Area 8: Texas Water Development Board: Groundwater Resources Division. https://www.twdb.texas.gov/groundwater/docs/GAMruns/Task13-031.pdf

Site Effects Assessment using Ambient Excitations (SESAME), 2004, Guidelines for the implementation of the H/V spectral ratio technique on ambient vibrations: measurements, processing and interpretation. SESAME European Research Project WP12. European Commission – Research General Directorate Project No. EVG1-CT-2000-0026.

Solis, R.S., Kemp, J.J., Connell, T., McEwen, T., and Brock, N., 2012, Volumetric and sedimentation survey of Waco lake: May 2011 survey: Texas Water Development Board: Surface Water Resources Division. https://www.twdb.texas.gov/surfacewater/surveys/completed/list/index.asp#waco

Southern Trinity Groundwater Conservation District, 2015, *Slideshow for Well-Owners Part II: Managing our Groundwater*. https://southerntrinitygcd.org/wp-content/uploads/2015/03/STGCD-slideshow-for-well-owners-P2.pdf

Stricklin, F.L.,1961, Degradational stream deposits of the Brazos River, Central Texas: Geological Society of America Bulletin 72.1, 19-36.

Van der Baan, M., 2009, The origin of *SH*-wave resonance frequencies in sedimentary layers. *Geophysical Journal International* 178, 1587-1596.

WaveMetrics, Inc, 2019, Igor Pro 8. 64-bit. Academic License. Lake Oswego, OR.

Wenzel, H.G., 1994, Earth tide data processing package ETERNA 3.20. *International Center for Earth Tides Bulletin* 120, 9019-9022.

Wong, S.S., 2012, Developing a geospatial model for analysis of a dynamic, heterogeneous aquifer: The Brazos River Alluvium Aquifer, Central Texas: Baylor University, unpublished Master thesis.

Wong, S.S, Yelderman, J.C., and Byars, B., 2013, Developing a geospatial model for analysis of a dynamic, heterogeneous aquifer: The Brazos River Alluvium Aquifer, Central Texas. Gulf Coast Association of Geological Societies: *Transactions* 62, 653-660.